Structural Health Monitoring of Aircraft Structures: Development of a Phased Array System

by

Bruno Filipe Ferreira Graça Rocha
Licenciatura Aerospace Engineering, IST – Instituto Superior Técnico, 1997

A Thesis Submitted in Partial Fulfillment
of the Requirements for the Degree of

MASTER OF APPLIED SCIENCE

in the Department of Mechanical Engineering

Supervisory Committee

Structural Health Monitoring of Aircraft Structures: Development of a Phased Array System

by

Bruno Filipe Ferreira Graça Rocha
Licenciatura Aerospace Engineering, IST – Instituto Superior Técnico, 1997

Supervisory Committee

Dr. Afzal Suleman, Department of Mechanical Engineering
Supervisor

Dr. Yang Shi, Department of Mechanical Engineering
Departmental Member

Dr. Nikitas Dimopoulos, Department of Electrical and Computer Engineering
Outside Member

Abstract

Supervisory Committee
Dr. Afzal Suleman, Department of Mechanical Engineering
Supervisor
Dr. Yang Shi, Department of Mechanical Engineering
Departmental Member
Dr. Nikitas Dimopoulos, Department of Electrical and Computer Engineering
Outside Member

This work consisted in the research and development of a phased array embedded system for Structural Health Monitoring (SHM) of aircraft structures. This system is based on piezoelectric (PZT) transducers to excite fast propagating first symmetric Lamb wave mode (S_0) wavefronts. The intent of this research is to contribute for an increasing safety and efficient operation of aircraft.

Currently applied ultrasound inspections to aircraft structures in operation, as a conventional Non Destructive Tests and Evaluations (NDT&E) technique, were reviewed. Such and the previous development of a Lamb wave based SHM system using PZT transducers in a network configuration served as the basis and for comparison to the phased array SHM system developed. Lamb waves' propagation behaviour was carefully analyzed and a linear PZT phased array SHM system was developed and experimentally tested. The PZT phased array was applied to representative aircraft structural aluminum panels, considering also the existence of structural reinforcements and joints. New techniques, hardware and software, leading to automated damage detection and location, were researched, developed and implemented.

Tests for damage detection and location were performed, with the introduction of damages into the specimens being simulated by surface and through the thickness holes and cuts. Damages with a maximum dimension of 1mm applied cumulatively to the specimens subject to different boundary conditions were successfully detected and located.

Table of Contents

List of Figures

Acronyms

2D-FFT	*Two-Dimensional Fast Fourier Transform*
AE	*Acoustic Emissions*
AGS	*Advanced Grid Structure*
CFRP	*Carbon Fiber Reinforced Polymer*
CLoVER	*Composite Long-range Variable-direction Emitting Radar*
D2A	*Digital to Analog converter*
DAC	*Distance to Amplitude Correlation*
EMAT	*Electro-Magnetic Acoustic Transducers*
EMI	*Electro-Magnetic Interference*
FBG	*Fibre Bragg Grating*
FEM	*Finite Element Model*
FFT	*Fast Fourier Transform*
FT	*Fourier Transform*
GA	*Genetic Algorithms*
IDT	*Inter-Digital Transducer*
MCU	*Micro Controller Unit*
MEMS	*Micro-Electro-Mechanical System*
NN	*Neural Networks*
NDT&E	*Non Destructive Tests and Evaluations*
PoD	*Probability of Detection*
PZT	*Lead Zirconate Titanate Piezoelectric*
RMS	*Root Mean Square*
SNR	*Signal to Noise Ratio*
SHM	*Structural Health Monitoring*
ToF	*Time of Flight*
VI	*Virtual Instrument*
WT	*Wavelet Transform*

Acknowledgments

This work was only possible with the supervision of Dr. Afzal Suleman. I am thankful to Dr. Suleman for exposing me to the leading edge research currently being performed in Structural Health Monitoring (SHM), for his advice and for all resources made available for the execution of this work. During this work I met Captain Carlos Silva of the Portuguese Air Force Academy while performing his Ph.D at the University of Victoria (UVic). I am grateful to Carlos for his precious support in this work, for all the coding he did and help on performing the experimental part of this work.

I want to mention also Art Makosinski, Pat Chang and Ian Soutar from UVic for their help and valuable comments in very important stages of development of the SHM system. Furthermore, I want to acknowledge all the Applied Vehicle Technologies team at UVic for their support, help, friendship and useful conversations, Sandra Makosinski for her valuable work in all administrative tasks and laboratory organization and the personnel from the Aeronautical Laboratory of the Portuguese Air Force Academy for their help in implementing the experimental setup. I am thankful to UVic for giving me the opportunity to perform this research.

My recognition goes to my parents and grandparents and all my family and friends from my childhood, to university, to my professional life, if it wasn't for all of them I wouldn't be who I am.

I dedicate this work to my daughter Helena that, without knowing, gives me all her patience, gives me my strength and everything I need, and to my wife Joana for her patience and support.

Dedication

To my daughter Helena,
my wife Joana,
my family and friends.

Chapter 1

Introduction

Inspections for structural condition assessment are of the utmost importance for safe and efficient operation of current aircraft. Aircraft structures operate in harsh conditions, sustaining high loads, fatigue cycles and extreme temperature swings. Characteristics of aircraft operation, at altitude and both high speeds in air and on the ground (at take-off and landing), usually lead to catastrophic consequences in terms of life loss and economically, when failure of a primary aircraft structure occurs. To achieve lighter structures, damages are allowed to exist in aircraft structures in operation, as long as they are within predetermined, deemed safe dimensions. Aircraft structures are then designed according to a damage tolerant philosophy. Also to reduce structural weight, newer materials, such as composites, have been considered. These present radically different characteristics than (the extensively known from) isotropic materials widely used (ex. aluminum) in aircraft, for instance in terms of response to damage existence or stress concentrations. Furthermore, current aircraft fleets are rapidly ageing, while aircraft travelling is considerably increasing, with aircraft structures being introduced in operation presenting increased capacity and complexity. These characteristics are driving required research being presently developed to increase reliability and simplify the application of structural inspections.

Non Destructive Tests and Evaluations (NDT&E) developed in the last decades and currently applied to assess the health of aircraft structures in operation, suffer from localized damage detection capabilities, i.e., are able to detect damage uniquely in limited areas around their application region. Such requires repetitive execution of inspections in different areas of the structure, with necessary direct access to structural areas to be inspected. This involves complicated, time consuming and consequently expensive operations, particularly disassembling and assembling procedures, forcing aircraft

grounding. Being grounded and intervened, and not in operation, the aircraft is not profitable and in fact represents a cost for the operator (maintenance, hangar time, leasing, etc). Structural inspections and maintenance are then performed in a scheduled manner, with increasing pressure from aircraft fleet operators to reduce inspection and maintenance time and extend intervals in between consecutive interventions. This increases risk of damage existence and growth in between inspection operations, for instance due to unpredicted flight severity, or foreign object impacts. Also damage might exist and grow in regions not inspected. All of these disadvantages are related with the fact that there is no persistent, integrated, real time and global structural integrity evaluation system. Examples of aircraft accidents and potential damages are shown in Figs. 1.1 to 1.5.

Figure 1.1: Aloha Airlines Boeing 737-297 (tail #N73711), flight 243, Hilo to Honolulu, Hawaii, landed on Kahului Airport on Maui, April 28, 1988 - multi-site fatigue-corrosion crack damage in non predicted locations in the fuselage skin panel joints – ageing structure aggravated by commuting service with frequent short flights with take-off, compression-decompression cycles and landings [1].

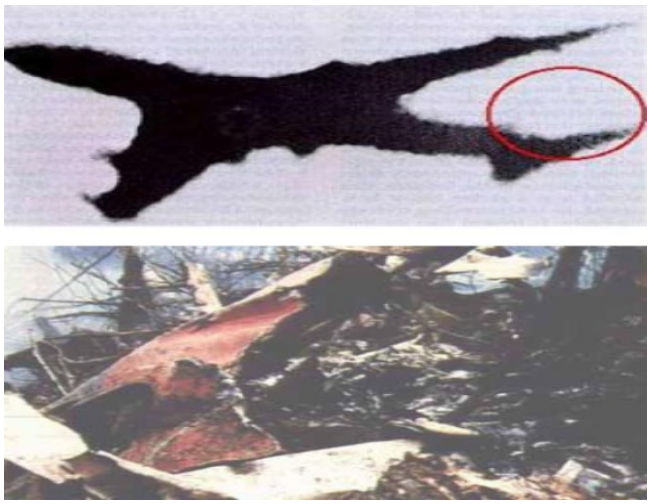

Figure 1.2: Japan Air Lines (JAL) Boeing 747-SR46 (tail # JA8119), flight 123, from Tokyo to Osaka, Japan, August 12, 1985 - tail structure loss due to a scheduled maintenance error on the rear pressure bulkhead – the single aircraft worst accident in history with 520 casualties [2].

Figure 1.3: Hawkins & Powers Aviation C-130A fire fighter (Tail#N130HP), Walker, California, June 17, 2002 - fatigue cracks in the wing structure [3].

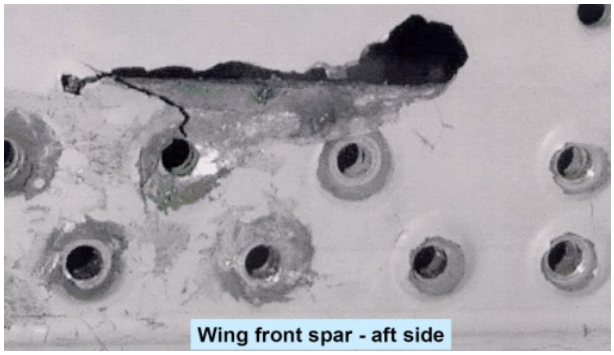

Figure 1.4: Fatigue crack developed by corrosion in wing front spar joint.

Figure 1.5: Impact damage.

Furthermore, structural inspections might be performed without detection of any damage, incurring costs that could have been avoided. On the other hand, structural components are sometimes replaced when identified damages approach their design maximum dimension, without, however, having reached their operational limit. It is less expensive to replace such components immediately while the structure is accessible, in the same scheduled inspection, as soon as defects were identified with dimensions approaching allowed maximums. If components were not replaced, the interval for next scheduled maintenance would most probably be reduced (with again grounding/non operation of aircraft, expensive and long maintenance procedures required, disassembling and assembling procedures, etc). Moreover, maintenance operations also involve certain dangers on potentially creating additional damage to the aircraft structure, without any awareness for such fact - this, besides manufacture imperfections, impact damage, corrosion, fatigue related damage, for instance due to pressurization cycles, excessive loads, unavoidable stress concentration locations in design, etc.

The difficulties posed by the present application of NDT&E techniques in aircraft structures in operation are responsible for the development of Structural Health Monitoring (SHM) methods and subsequent Structural Health Management. SHM techniques are currently being intensively researched. Initial important developments on SHM techniques emerged in the beginning of the last decade, enabled by advances in electronics and computation. SHM systems are intended to be embedded into the structure, assessing structural condition in real time or near real time, in a more global way. In such manner, inspections can be performed during operation, without requiring direct access to the structure to be inspected and then with no operation downtime and

required long and expensive disassembling and assembling procedures. Maintenance would then be performed when required, i.e., it would be condition based.

Reliable SHM systems can potentially identify damage earlier, and then in earlier stages of development, particularly if they allow for a reduction of the minimum damage dimension to be detected. One of the advantages of this specific aspect is that design safety factors could be decreased - particularly in areas of stress concentration and prone to fatigue, as for instance in riveted joints, where design safety factors are increased and structural reinforcement is required. The decrease of design structural safety factors, without deteriorating safety of operation, and subsequent reduction of required structural reinforcements and structural weight will have a direct impact in increasing available payload weight. Alternatively, the reduced weight will require a reduced lift, reducing generated drag, required thrust and then fuel consumption (economic benefits) and emissions (achieving a more environmentally friendly aircraft), reducing again aircraft weight, even more. Since aircraft design is a cyclic process, these reductions (even if small in the beginning of the process) are greatly amplified during the design cycle.

With SHM techniques embedded into aircraft structures and enabling real time or near real time damage detection, pilots could restrict flight severity depending on warnings. Subsequently, current and future operation of the aircraft could be tailored, based on damage severity. Similarly to what is applied presently with NDT&E in aircraft structures in operation, knowing the predetermined flight severity (flight loads spectrum) and having in mind that predictive algorithms for damage growth are established – Damage Prognosis -, the Remaining Useful Life (RUL) of the component could be estimated, but now in real time.

With the objective of detecting, locating and characterizing damage - identifying damage type, shape, dimensions, orientation, etc -, there are several SHM methodologies being actively researched and developed. These range from Eddy currents; to Acoustic Emission detection; to low frequency vibration characterization of the structure (both in undamaged and damaged states and subsequent comparison); to wave propagation based (interference of propagating waves with defects), and specifically to Lamb wave propagation based systems. For all SHM methods, it is fundamental the embedment of

transducers (actuators and/or sensors) into the structure under inspection. Transducer selection is strongly dependant on that aspect and on the technique to be applied.

In the research performed and described here, the development of a phased array SHM system, to apply Lamb waves, was carried out. The developed system can be applied to different phased array configurations, being particularly tested in a linear array configuration. Particularly, the implemented system excites fast propagating first Lamb wave mode (S_0) wave fronts and senses the resultant reflected S_0 waves (by boundaries, reinforcements, discontinuities and potential damages). The development of this system stemmed from the previous study and implementation of a transducer network, Lamb wave based SHM system [4, 5]. Such system was applied to plates made of aluminum and composite material and was successfully tested with the detection of defects as small as 1mm. The selection of a mechanical type of actuation system also emerged from previous work on low frequency aeroelastic vibration control and SHM of wing structures and the desire to condensate in a single system, SHM and aeroelastic control, and possibly vibration energy harvesting, in the future.

The decision to focus this research on Lamb wave systems was also based on the numerous references in literature to these systems as being a promising alternative to NDT&E, being capable of detecting smaller defects. Additionally, they represent a natural evolution from ultrasound based NDT&E systems, already widely used in aircraft structures in operation and considered a good inspection technique. These also do not require any special precautions in their application, for operator safety or to avoid damage to surrounding systems. Such is the case in the application of Eddy currents based methods, with electric currents passing through the host material to be inspected and electro-magnetic fields being generated, with possible Electro-Magnetic Interference (EMI) to surrounding systems. Furthermore, transducers considered for application of Lamb wave propagation based SHM methods can also be used for the implementation of all other SHM methodologies referred, except for Eddy currents based techniques.

The decision to develop a system based on the S_0 Lamb wave mode emerged from the high propagation velocity of such waves. These waves and their subsequent reflections generated by potential defects are then less prone to interference from slower propagating

waves (modes). S_0 waves are also more sensitive to internal structural damage, while presenting lower propagation amplitude damping. This aspect means that they are able to propagate in larger areas, increasing the potential inspection region. Their high propagation velocity has however the disadvantage of imposing more restrictive and demanding requirements into the development of actuation and acquisition systems, considering also their dispersive behaviour. This is in fact the reason for the inexistence in the literature of reports on the successful development of dedicated phased array systems for the activation of fast propagating S_0 wave fronts. This aspect is assessed by this work.

Specifically, Lead Zirconate Titanate piezoelectric (PZT) transducers were selected and applied in this phased array configuration, due to their capability of simultaneous high frequency actuation and sensing. This research comprised a study of Lamb waves and their propagation characteristics - based on the host material to be inspected – applied to the implementation of the phased array SHM system. Such study led to the selection of transducers to be employed and to the development of dedicated actuation, signal acquisition and data processing component systems. Tests for damage detection and location were performed on aluminum plates, representative of aircraft panels and wing spar webs.

Different boundary conditions were applied to the panels, from fully supported plates to simply supported in their edges. One of the main objectives accomplished in this work was to achieve a (reliably) detectable minimum damage dimension inferior to what is currently the standard for NDT&E techniques applied to aircraft structures in operation, independently from prescribed boundary conditions.

1.1 - Motivation and the need for NDT&E and SHM: Historical Perspective on Structural Integrity Assessment

Primarily due to safety, but also in some cases due to operational reasons, it is of the utmost importance a correct assessment of the health of structures in service. Most probably the first structures to be inspected were houses, followed by tools, weapons and transportation vehicles, such as wagons and vessels. First inspection methods were based

on visual inspections, of course with the limitations that might be inferred. Along history, other infrastructures became of importance in terms of required structural health assessment, due to potentially catastrophic consequences in case of their failure. Besides aircraft structures, buildings and bridges are presently the focus of great attention and recent developments in terms of their Structural Health Monitoring. For instance, bridges are being erected in more difficult places, with increasing complexity, dimensions, load capacity and human traffic across them. Consequences of their failure are severe as proved by the collapse of the I35W Mississippi River bridge, in the evening rush hour of August, 1st, 2007 [6] – Fig. 1.6.

Figure 1.6: Collapse of the I35W Mississippi River bridge [6].

The Industrial Revolution – with the development of factories, vessels and the railway-, further technology advancements in the XX century - with relevance for the aerospace domain - and higher safety concerns, brought the demand for more efficient and accurate structural condition inspection methods. The main objective of these methods is then the detection of potential catastrophic flaws in development, before the collapse of the structure, with the risk of loss of life and economic damage.

In the aerospace domain, the assessment of structural health condition, both for aircraft and space vehicles, is extremely important, since relatively small flaws might lead to the collapse of the much needed lightweight structures. Due to the nature of flight and aircraft operation on the ground - with relatively high speeds at landing and take-off -, the collapse of a primary structure of an aircraft usually has terrible consequences. Most important than the loss of the vehicle and consequent loss in operations, that, in a commercial aircraft, might result in the loss of many lives.

Flaws in an aircraft structure might be created during manufacturing, be impact related (foreign object impacts, operational impacts, such as in loading the aircraft, and sometimes even due to impacts occurring during maintenance operations), or emerge due to excessive loading - for instance when design flight envelope structural loads are exceeded due to unpredicted wind gusts or atmospheric turbulence. If not immediately catastrophic, the growth of such flaws, leading to structural collapse, is driven by fatigue due to operational loads variation (pressurization cycles, aeroelastic vibration, etc). Furthermore, fatigue cracks are prone to appear in stress concentration regions, which must be avoided, as possible, during structural design. Stress concentrations cannot, however, be totally eliminated. Required rivets and fasteners' holes to join different structural components are responsible for originating stress concentrations and consequently for the necessity to apply in those structural areas augmented design safety factors. These in turn result in the application of added structural material (reinforcements) in those areas, with one of the worst effects for aircraft design: increasing structural weight.

Aircraft operational loads that contribute to fatigue are: aerodynamic loads, on the ground, or in flight (aeroelastic loads induced vibration); ground reaction loads, impact and vibrations during take-off, landing and taxiing; ground operation loads; and pressurization cyclic loads (of the utmost importance for driving fatigue crack growth in aircraft fuselages). Aerodynamic loads are important in manoeuvres, in achieving a certain flight mission and flight path, when aircraft encounters atmospheric turbulence or wind gusts, inducing aeroelastic loads and vibration. They are also important in ground-air-ground transition flight phases, when counter balancing weight loads shift from ground reactions applied to the structure through landing gears to the wing generated lift, and vice versa. Aerodynamic loads affect fuselages, vertical and horizontal stabilizers and mainly wings and their connection to the fuselage. Ground operation loads have an important role in taxiing, take-off and landing, and ground handling operations. Examples of important loads in these phases are: aerodynamic and control loads in stabilizers; ground reactions, impacts, braking forces and vibrations in the landing gear and supporting structure; powerplant related forces (in acceleration at take off and thrust

reverse in landing); and forces and impacts applied in operations such as docking, loading and unloading the aircraft.

Inspection of aircraft structures becomes even more important with the evolution of aircraft structural design life concepts. In the early years of aviation, between 1920 and 1940, structures were designed according to an Infinite Life concept, i.e., so that they would be operated below their fatigue stress limit. Obviously, the application of such concept in design resulted in extremely heavy structures, considerably restricting aircraft performance, and was quickly abandoned. It must be remembered that increasing aircraft weight must be counterbalanced by increasing generated lift, leading to an increase in either wing area, or wing loading, and consequently increasing again (wing) structural weight. Increasing lift generation also increases drag generation that in turn must be counterbalanced by increasing thrust. This forces the use of powerful and probably bigger and heavier powerplants, with increased fuel consumption, leading again to the increase of overall weight (powerplant weight, structural weight to support heavier powerplants and added fuel weight). Moreover, higher structural weight, for a certain lift generated, decreases payload weight available (passenger and cargo capacity), manoeuvring capabilities and aircraft performance such as endurance and range, since available fuel weight is reduced.

A Safe Life structural design and operation approach was then adopted. In this concept a finite service life was established, within which the probability of fatigue cracks to initiate and develop was extremely remote. The derivation process to determine structural life span was therefore based on the crack initiation stage of the fatigue failure process. This concept was applied in structural design during several years. However, it did not account for rogue flaws generated in manufacture, with no provision also for other forms of damage, which reduce structural life, like corrosion or accidental damage. Furthermore, several times, service loads exceeded, were not from the same type and had different application points than the ones considered in structural design. Damage models and stress analysis were also often inaccurate and inadequate. These mistakes led to multiple accidents, like those of the five DeHavilland COMET, between May 1952 and January 1954 [7]. In the last accident, the aircraft had only about 1000 flights, while its flight simulation tests predicted an operational life of 3060 flights.

Additionally, in the Safe Life concept, the detection of defects in one component was automatically a cause for its removal from service. In the early 1970's, the development of inspection technology, in particular the ability to detect smaller flaws, led to an increasing number of parts being rejected.

At that time, advances in the discipline of fracture mechanics enabled the prediction of whether a crack of a given size would induce the collapse of a component under a particular load, if particular material properties and fracture resistance were known. Models were developed to predict the growth rate of cracks subject to cyclic loads (fatigue). It became possible to have structures in service with existing defects, as long as their existence and their dimensions were known and smaller than calculated maximum damage dimensions, determined to lead to structural collapse.

A Fail Safe structural design and operation concept was then in place. Here, a structure is designed to be capable of retaining required residual strength for a period of unrepaired service, after sustaining a failure or partial failure of a primary structural element. An example of a wing-fuselage connection, steel Fail Safe plate, is presented in Fig. 1.7.

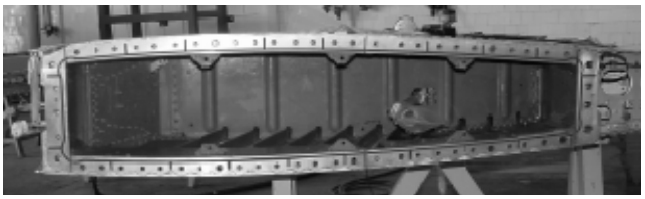

Figure 1.7: Steel Fail Safe plate, on the wing box to fuselage connection.

Structures designed according to this concept present multiple load paths and use crack stoppers, so that stress levels after crack initiation are kept low, providing controlled and slow crack growth rates. Simultaneously, structural design is performed to assure a high probability of crack detection before strength is reduced below limit load capabilities.

The Fail Safe structural design and life concept evolved to the establishment of the Damage Tolerance philosophy. In this concept worst case scenario assumptions of initial manufacturing defects are considered. Also, details on sensitivity of inspection techniques (minimum detectable damage dimensions and other limitations, such as imposed by structure’s geometry, potential locations and characteristics of damages to detect, their orientation, etc), to be applied for in service crack detection, are accounted

for. A service life before next inspection and structural repair is then predicted, based on quantitative calculations of crack growth rates and predicted flight loads severity. A regime of repeated inspections is defined to ensure a high probability of crack detection prior to catastrophic failure, i.e., a scheduled based inspection and maintenance is established [8].

The evolution in terms of structural design life concepts and in materials applied to aircraft structures lead to the required development of more efficient, reliable and accurate inspection methods to assess structural health condition. Such required developments are also justified by other current and important problems, as for instance, ageing aircraft fleets, with aluminum structures, surpassing by much their designed life flight hours. In the last years, there have been an increasing number of accidents related to ageing aircraft. Several accidents involved older cargo aircraft converted from passenger commercial jets, with extensive flight hours [9]. Fortunately in terms of passenger aircraft, the number of accidents was considerably lower. Minor accidents were proved to be related with unaccounted or undetected damage involving ageing aircraft, with the loss of wing and fuselage panels in flight – for example in 2008, three Boeing 757 performing domestic flights over US lost wing root panels [10].

Ageing aircraft fleets are presently a topic of concern. Even if fortunately there were no major accidents up to now, it is predicted that the continuous use of aircraft fleets reaching their limit design flight hours, without predicted replacements in the near future, is going to result in an increasing number of accidents, with possible loss of life. Due to economic considerations, fleet operators try to prolong the service life of aircraft, while scheduled maintenance is less expensive, at least in the short term, than removing the aircraft from operation and replacing it by a new one. The problem is aggravated since newer aircraft models, presenting increased efficiencies in terms of fuel burn and then environment and economic footprint are only predicted to come into service not before 2015, to replace existing fleets. Besides this, with new requirements in terms of dramatic increase in aircraft efficiency, due to environmental and economic reasons, new configurations are in development to be introduced in service in the next decade. This anticipated dramatic change in aircraft design and consequent changes in operation has aircraft operators delaying their decisions on replacing existing fleets.

Inspection and maintenance of ageing aircraft fleets becomes a difficult, lengthy and expensive task without guaranteeing total safety of operation [11]. Damage in unusual areas, commonly not inspected in the normal operational life of aircraft, may occur. These areas have not been considered previously, since they were determined to be damage free during the designed operational life span of the aircraft. Furthermore, since the designed operational life has been surpassed, there is no extensive information about these new locations where damages may develop. Unpredicted operational damage might also occur, such as impact damage, due to excessive loading (in flight or in ground operation), or even maintenance related damage. Also related with the localized capabilities of present inspection methods applied to aircraft structures in operation, to maintain safety levels, lengthy and costly major operations of disassembling and inspection in broader areas of the structure must be performed. An example of an operation related damage that occurred in flight, was the explosion of an oxygen gas tank in the cargo bay of a Qantas Boeing 747, in July, 25th, 2008, with the rupture of fuselage panels. Pilots had to make a decision of alternating the flight and limit manoeuvring loads based on the few amount of information they had, since they could not assess the true nature, reason, dimensions and possible consequences of damage [12].

US Air Force (USAF), for instance, has been assessing the economic consequences of inspection and maintenance of their ageing aircraft fleets, compared to removing from operation and replacing existing aircraft, for the same or newly designed aircraft models. Examples of USAF ageing fleets are the B-52 and F-14 fleets, in service for more than 45 years. The first conclusion is that, before totally new designs come into service, presenting dramatic improvements in efficiency, what is predicted only to happen in the next decade, it is not yet economically viable to replace existing ageing fleets. Such is related with the costly removal of an aircraft from operation that still performs well enough the missions it is intended to. However, it is not also acceptable to USAF the economic burden of current inspection procedures and maintenance operations [13, 14].

As referred previously, the evolution in aircraft structures' materials and specifically the introduction of composite materials (presently widely applied), replacing aluminum, in aircraft structural design is also an important factor for the development of damage inspection techniques. Composite materials are extremely interesting for application in

aircraft structures since they present high strength to weight ratios and good corrosion resistance. Furthermore, the application of composites enables the fabrication of structural components with more complex geometries and with increasing dimensions (reducing joints). However, when compared to aluminum, composites also present a worth behaviour in the presence of flaws – cracks and delaminations. Also, the application of composites poses difficulties in their connection to other materials and on how to connect different composite structural components. These problems are related to a worse response in the presence of localized stress concentrations – in the joints these are due to rivets holes, contact required to other materials, such as aluminum and steel rivets, screws and required sleeves, etc. Stress concentration in crack tips and delamination boundaries usually result in abrupt failure of the component, even sometimes when these damages have just appeared and still present small dimensions, i.e., just after a small and rapid growth.

Also, as referred, stress concentrations exist near required rivet and fasteners' holes for connection to other parts. In fact this is the reason for reducing the connection points and so to reduce the number of parts in a composite structure. The parts have then increased dimensions and are more geometrically complex, what is allowed by the intrinsic manufacturing characteristics of composite materials [15]. Since the structure consists of a smaller number of components with increased dimensions and geometrically more complex - Fig. 1.8 -, augmented difficulties are also introduced for the execution of an accurate structural inspection applying traditional techniques.

The recent boom in the application of composite materials in primary aircraft structures lead to important developments in the manufacturing methods, such as Resin Transfer Molding (RTM). However, some minor but relevant manufacture defects still emerge, requiring some engineering thinking and attention. Examples are the defects (air bubbles) detected in the first tail cone structural prototypes, integrally made of Carbon Fiber Reinforced Polymers (CFRP), for the Boeing 787 Dreamliner [16].

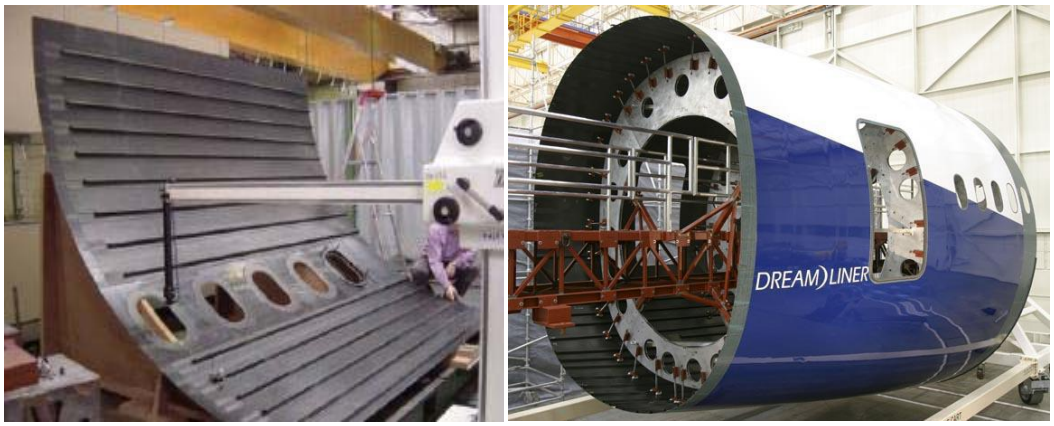

Figure 1.8: CFRP fuselage skin panel and fuselage section being assembled of the Boeing787 Dreamliner.

These manufacturing defects lead to the inspection of components right after manufacture, usually through the application of ultrasound C scans. Being local detection methods and the components to inspect bigger and more complex, inspection procedures are lengthy and costly. To assess this problem, newer techniques, such as “the squirter”, are being developed. Midas NDT is developing this method for the inspection of the main wing spar of the Airbus A400M military aircraft [17].

The sensitiveness of the mechanical properties of composites (such as Young modulus, yield strength, etc) to the manufacturing process – fiber directions, fiber to resin ratio, pressure and temperature applied during the curing process, solvent release, resin injection process, etc – led also to increased difficulties in inspection procedures. Usually sample structural prototypes are manufactured for mechanical testing, to validate mechanical properties of the manufactured composite materials.

The motivation driving this research effort is the desire to contribute for an increasing safety in aircraft operation, achieving simultaneously a reduction of structural complexity and weight. This last aspect leads to increasing economical efficiency in operation and to more environmentally friendly aircraft. To achieve such objectives, the intent is to develop structural inspection systems that will solve the previously referred difficulties and shortcomes posed by the application of current NDT&E methods to aircraft structures in operation. Those systems, falling into the SHM field of research, are embedded to the structure, allowing for real time or near real time and more global assessment of structural condition. They must be designed to be competitive to existing

systems, bearing in mind the requirements for their practical application in the near future, to real aircraft structures, and not uniquely as a laboratory application exercise. Moreover, the motivation is centered in developing such systems to achieve the detection of damage with dimensions inferior to what are currently detected by NDT&E applied in operation and SHM systems in research and development, reported in the literature.

The development of this system was based on the previously mentioned approach at the end of the introduction. This approach allowed the mitigation of some of the difficulties reported in SHM systems. The multiple actuation system developed enabled the excitation of wavefronts with consequently increased actuation amplitude. The data processing software developed applied multiple (parallel), concurrent methods. These were fundamental to achieve the final result of reliably detecting and locating damages with dimensions below 1mm.

1.2 – Thesis Outline

In Chapter 1, it is presented the introduction for this work. The requirements for inspection of aircraft structures are described and the motivation for the development of SHM systems and this work is explained.

A brief description of currently applied NDT&E methods into aircraft structures in operation is presented in Chapter 2. Particularly Sonic and Ultrasonic inspections are explained in more detail as the basis and for comparison to the SHM systems to be developed. From this insight into existing techniques to assess structural health and for damage detection, the need for the development of SHM systems is summarized and different techniques being presently researched for the application of SHM to aircraft structures are summarily explained.

Chapter 3 is focused in the explanation of Lamb waves. The dispersion behaviour of Lamb waves is explained, through the mathematical deduction of the equations that enable the calculation of Lamb wave propagation velocity dependency to their frequency. A review of the state of the art in Lamb wave based SHM systems is presented and the contributions of this work to this field are stated.

In Chapter 4, an analysis of the relevant characteristics of the Lamb wave dispersion behaviour, to be applied in the development of a phased array system, are determined. From such properties, the development of the phased actuation system is presented.

The experiments performed for the validation of the phased array system are explained in the beginning of Chapter 5. Afterwards, the developed damage detection algorithms are presented and the tests executed for inspection, i.e., for damage detection and location in a representative aluminum plate are described.

The conclusions retrieved from this work and the planned future work are summarized in Chapter 6.

Chapter 2

NDT&E and SHM

NDT&E are vital to ensure safe operation of aircraft. Particularly, corrosion detection, fatigue and impact crack detection capabilities are extremely important, even more in ageing aircraft and considering the current structural design (damage tolerant) philosophies. NDT&E is a generic name that covers all inspection techniques utilized in the examination of a structural component integrity, without causing any damage to it. The main objective of NDT&E techniques is to find if the structure is sound in accordance with associated standards, designs and specifications. NDT&E enable the detection and identification of the nature of damages, their location, dimensions, shape and orientation, and might also be used to assess mechanical properties of the host material.

There are several NDT&E techniques [18 - 20]. Traditionally NDT&E consist of systems external to the structure to be inspected and present capabilities to detect damage only locally. Conventional inspection methods can be classified according to the following categories:

- Mechanical-Optical (Visual Inspections)
- Chemical-Analytical (Liquid Penetrant Inspections)
- Electromagnetic-Electronic (Magnetic Particle Inspections, Eddy Current Inspections)
- Penetrating Radiation (Radiographic Inspections)
- Thermal and Infrared (Infrared Thermography)
- Sonic-Ultrasonic Inspections

It is not reasonable to infer the superiority of one method, since the appropriate technique to be applied depends on the type of material and component geometry, as well

as type of defect to be searched for. However, it is reasonable to compare the Probability of Detection (PoD) of a crack with certain dimensions, in a parameterized plate, for the application of different techniques.

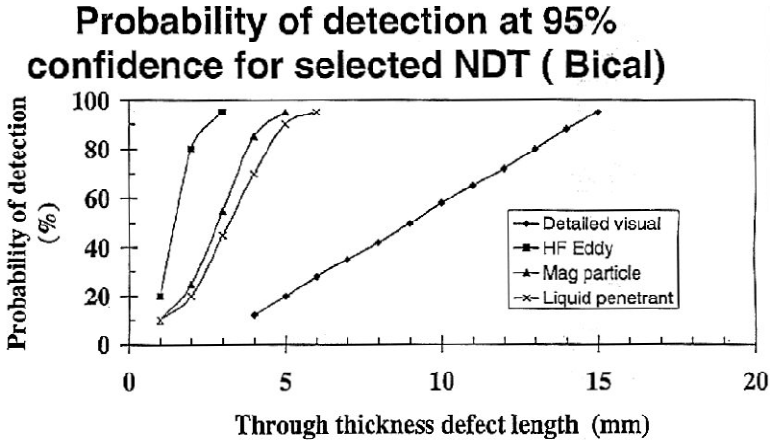

Figure 2.1: Probability of Detection for different NDT&E techniques [21].

In fact such a comparison and specifically the PoD depicted in Fig. 2.1, for the different NDT&E techniques and detectable damage dimensions, is of extreme importance for the present research. The SHM system in research should be able to detect defects with smaller dimensions than the NDT&E systems, with a certain PoD, to be reliably considered competitive and an improving alternative for their replacement. From observation of Fig. 2.1, the SHM system developed should be able to detect damages of 1mm in dimension (or smaller) with a PoD exceeding 50%. The successful detection of small damages is also important regarding potential damage growth monitoring. Minimum detectable damage dimension is related with the minimum difference in damage dimensions that the system will be able to detect during damage growth.

Lamb wave based SHM methods can be regarded as an evolution of sonic-ultrasonic inspections. Some of the principles applied in such conventional NDT&E techniques are also the basis for part of the development on the application of Lamb waves. A brief description of sonic-ultrasonic inspections is then introduced.

2.1 - Sonic and Ultrasonic Inspection

Sonic/ultrasonic inspection is a widely applied NDT&E technique, particularly to aircraft structures. This inspection method is based on the generation and propagation of sound waves in solids. These mechanical elastic deformation waves are generated whenever there is a mechanical deformation imposed to the structure's material [22]. The displacement waves travel through the structure at certain velocities, related with their frequency [23, 24].

Sound waves are reflected by any discontinuity or interfaces in the tested materials. Density or geometric discontinuities, such as boundaries, reinforcements, or, more importantly, internal flaws in the form of cracks, or inclusions can then be detected [25]. The interaction between waves and smaller discontinuities can be more clearly observed when smaller wavelengths are applied. Through the relation:

$$\lambda = \frac{c}{f} \tag{2.1}$$

where λ is the wavelength (m), c is the wave propagation velocity (m/s) and f is the wave frequency (Hz), the higher the frequency of the wave for a certain propagation velocity, the smaller the wavelength and the smaller are defects prone to be detected. Therefore, the waves used in this method usually present a frequency in the range of 0.1 to 25MHz.

The method is usually based on a pulse-echo technique, introducing a sound pulse in the host material with the objective of sensing echoes (reflections). Knowing the mechanical properties of the host material, such as Young modulus and density, and the dimensions of the component being inspected, the sound speed can be determined for the wave frequency of interest [26]. The time interval between pulse and echoes can then be translated into distances in the component under inspection, locating all reflection sources. After identifying reflections coming from boundaries and other intrinsic geometric and material features of the component being monitored, possible flaw reflections can be assessed.

Traditionally this inspection method is based primarily in body waves – longitudinal (pressure waves) and/or shear (transverse) waves -, propagating through the thickness of the component to be inspected – Fig. 2.2.

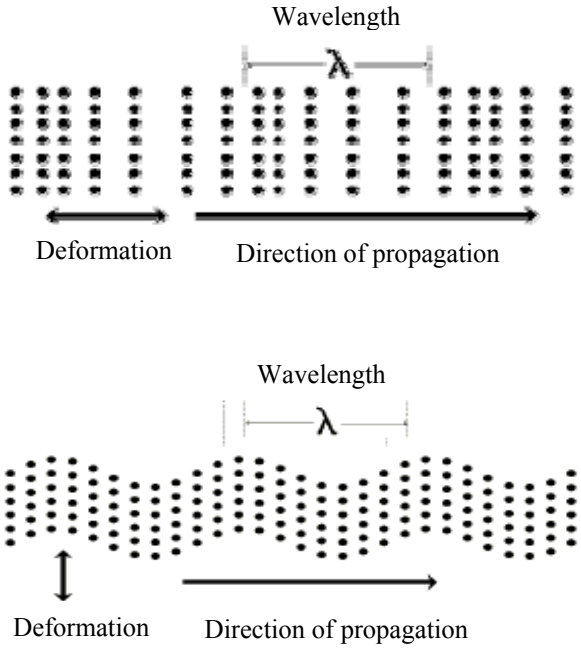

Figure 2.2: Longitudinal and transverse waves.

The use of body waves is a natural limitation derived from the fact that the transducers employed in this technique, used to generate and sense the waves, are external to the structure. The main difficulties in the application of this technique, and hence its limitation to only being capable to effectively detect, locate and allow for the characterization of damage in small regions around the deployment of the transducers probe (localized inspection), emerges exactly from the type of waves selected for its application and their generation, or actuation type (transducers external to the structure). Body waves present a highly scattered behaviour and are greatly attenuated in the host material, being only able to propagate to small distances, before their amplitude is reduced to undetectable levels.

Both straight beam and angle beam probes external to the structure can be used. In these probes, PZT elements are connected to a straight or angled wedge crystal and damping material, for interface, protection, delay and matching of the actuation with the host material [27, 28]. There have been reports of research being developed also on

generating sound waves from lasers and non contacting transducers. More recently it has been reported the development and application of PZT arrays, applied to the material under inspection with only a viscous elastic material layer separating both – without the application of a wedge [29].

Arrays are used to amplify actuation through the generation of a beam front, by promoting constructive interference between the different waves generated by each element in the array [29, 30]. The use of phased arrays is common in medical imaging. The array is fixed and generated beam front direction angle (or beam focus) is varied by introducing and modifying delays, or phase differences, in between the actuation signals for the different actuators. By promoting the generation of a beam front with higher amplitude (with relation to a single generated wave from a single actuator) the reflected waves and correspondent signals, potentially generated from a defect, also present higher amplitudes, improving Signal to Noise Ratio (SNR) and detectability. Also, using the resulting signals sensed by the different transducers improves sensing capabilities with relation to a single transducer configuration – either by superposition of the different waveforms (with the subtraction of the relative delays), or through the analysis of the multiple signals, instead of just one. Basically, this technique is similar to conventional angle beam inspection, except that the beam sweeps through a range of angles rather than just a single angle determined by a wedge, with the need to modify the probe's position, or wedge. This is very useful for defect visualization and increases probability of detection, especially with respect to randomly oriented defects, as many inspection angles can be assessed at once, without moving the probe with potential positioning errors.

Both in single and multiple transducer configurations, PZTs are excited by electrical discharges (with an extremely short duration in time) to generate the sound wave pulses in the interface and then host material [31]. Afterwards the same probes are used to sense the reflection waves, which ultimately cause the PZT element to deform and generate an electrical signal – examples are presented in Fig. 2.3. The probe is acoustically coupled to the surface of the test object with a liquid or coupling paste so that sound waves from the probe are transmitted to the test object.

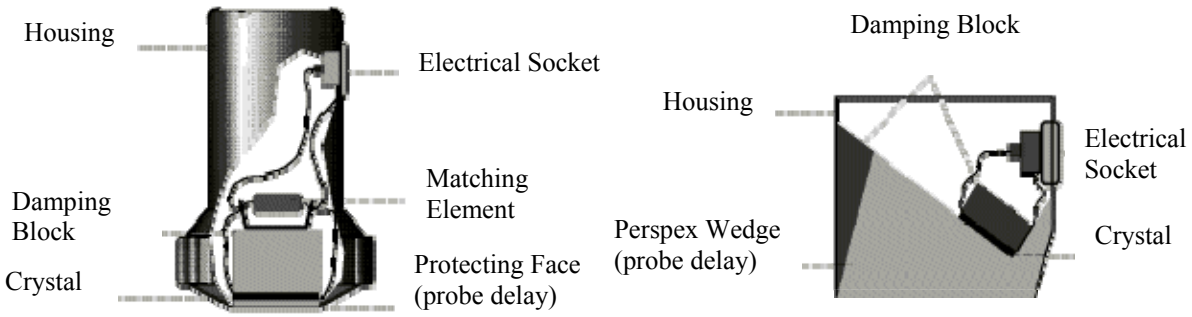

Figure 2.3: Straight beam probe and angle beam probe - ASTM E1065.

The sound waves only cover a defined area of the test object, i.e., the sound beam only travels in a delimited region – often to focus the beam to the area of interest, to inspect. A sound beam can be roughly divided into a convergent (focusing) area, the near field, and a divergent part, the far field, as shown in Fig. 2.4. The length of the near field (N) and the divergence angle (γ) depend on the diameter of the element (transducer(s)/probe), its frequency of actuation (equal to generated wave frequency) and the corresponding velocity of sound in the material to be tested. The centre of the beam is termed the acoustic axis.

To successfully and confidently detect damage with this method or to assure that no damage exists in the structure under inspection, the operator has to perform repeatedly scans from different directions. This procedure is allowed and limited respectively by the external nature of the inspection method equipment and by the geometry of the component under inspection. Such requirement results from: the highly damped characteristic of body waves; the referred aspects related with the sound beam; and the fact that beyond the intrinsic scattering behaviour of the body waves, these and their subsequent reflections are even more scattered by the defects to be detected while presenting significantly lower amplitudes. The scattering behaviour of damage reflections is highly dependent on damage shape/morphology. The natural consequence of such behaviour is that only part, or even none, of the reflected waves will be directed and sensed by the deployed transducers probe. The possibilities of detection increase when the discontinuity is oriented at a right angle to the sound beam.

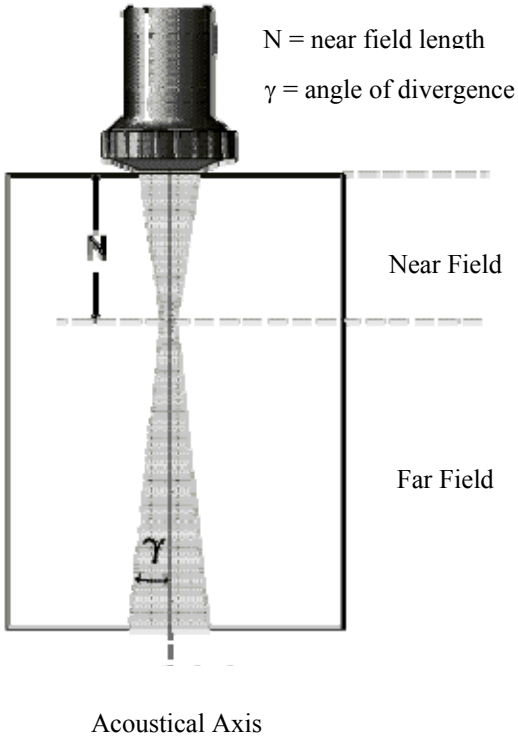

$$N = (D^2 - \lambda^2)/4\lambda$$

$$\mathrm{Sin}\gamma_{db} = k_{db}\,(\lambda/D)$$

D = diameter of flat circular oscillator
λ = wavelength
k = constant based on dB drop from centre max.

Figure 2.4: Sound field - ASTM E1065.

2.1.1 - Equipment

Usually actuation and sensed signals are displayed in an oscilloscope based instrument, measuring time with a high precision. Besides the displaying element, the basic components of the systems based on this NDT&E technique are: a pulse (signal) generator; a precise timer to control the entire system; amplifiers, to amplify the electrical pulses coming from the signal generation module to the actuators and also the electrical signal from the sensors to the acquisition module, to increase their original small amplitude; and transducers (actuation and sensing) probe. To note that the timer precision is extremely important in the determination of the time delay between actuation and arrival time of reflections, so that with the known propagation velocity their origin and potential defect location/distance can be precisely determined. It should be emphasized that sound waves propagate at high speeds, so that a small error in the determination of the time referred before will result in a considerable error in the determination of the defect location. Also, in the application of PZT arrays the timer is responsible for creating

the actuation delay between the different PZT elements in the transducers probe, to form and direct the sound beam into the intended direction. Such delays are considerably small and must be created with significant precision, otherwise the sound beam might be directed not to the intended locale, or even destroyed, since no constructive interference between waves generated from the different elements is promoted. Furthermore, as referred before the wave propagation velocity is dependent on the wave frequency (equal to generation signal frequency) and so the actuation signal must be generated precisely, with the intended frequency.

The capability to modify the actuation signal (and then generated wave) frequency and waveform is not offered by most systems. This results from a lack of understanding about the dispersive behaviour of sound waves (present still the focus of research and one of the topics focused in the research reported in this thesis) and amplifies their scattering and damped behaviour. This is in fact one other reason for these methods to be only applied and able to detect damages locally and mainly through the thickness of components to inspect.

2.1.2 - Probe selection

The use of straight beam probes is important when through the thickness transmission is considered, i.e., transmitting probe in one of the surfaces of the component under inspection and sensing probe in the opposite surface. However, straight beam probes present disadvantages that can be minored with the use of angle beam probes [32]. Since straight beam probes assess the regions straight beneath their surface position and require a smooth surface for their reliable application (with a limited inspection region due to the fast amplitude decay of body waves and a loss in precision of the method due to their scattering behaviour), they are not ideal to inspect structural components connection elements, such as welds or rivets. Also, due to the time length of the actuation (and thus the requirement of having a short actuation in time, besides the involved high frequencies and small wavelengths), there is an area close to the probe that is not inspected (dead zone – Fig. 2.5). Transducers cannot be used as sensors to detect any potential reflection generated from defects in that area close to the probe, while they are being used as actuators. Straight beam probes are not capable to detect near surface defects. This is

even more critical since the components under inspection do not usually present a considerable thickness – with then a considerable part of it not being inspected.

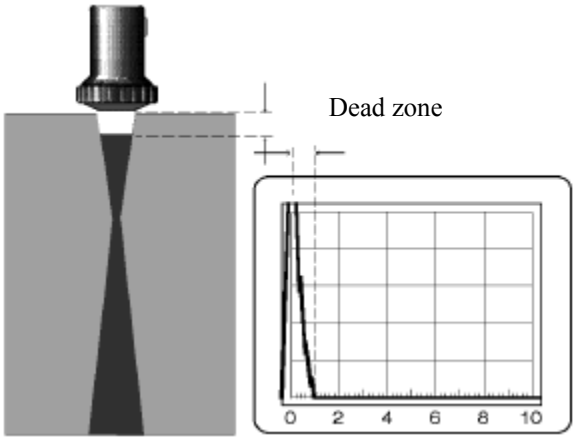

Figure 2.5: Dead zone - ASTM E1065.

Applying the angle beam probes - Fig. 2.6 -, potential defects departing from welds and connecting elements can be assessed, by directing the sound waves through the cross section of the component under inspection, laterally with respect to the welds, etc. Also, the reflections generated by the opposite component surface (now diagonally), relatively to the surface where the probe is being applied, can be used in the assessment. Since the applied waves are now at an angle with relation to the surfaces and thickness of the host material, the percentage of the dead zone when compared to the distance covered by these waves is now smaller.

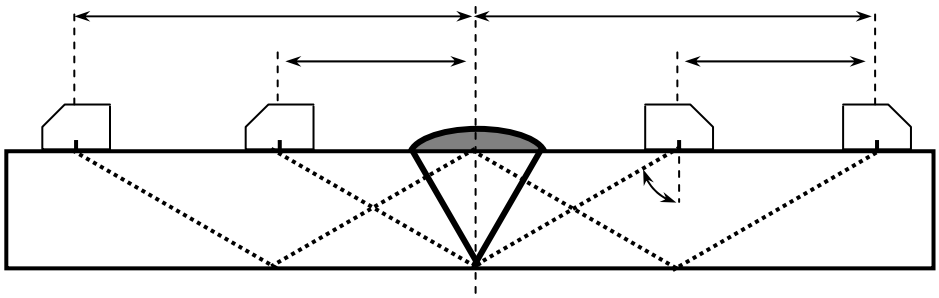

Figure 2.6: Inspection of weld with angle beam probe.

Scan patterns for manual weld inspections are usually in zigzag with some overlap to ensure 100% coverage. As a check and for reliability, the test should be repeated from the opposite side of the weld because flaws are indicated more favourably if irradiated from one direction rather than from other.

It must be noted the fundamental role of the Perspex crystal wedge in the angle beam probes. This wedge is designed so that the inclination in its boundaries is such that the generation of the sound wave in the host material is focused in a single mode and single direction. Through the application of Snell's law to the boundaries of the wedge, the transmitting wave is passed onto the host material and the reflected wave propagates along the wedge's boundary and not into the host material. Multiple wave generation in the material under inspection would compromise the detection capabilities of the method – increased complexity in signals with multiple waves present.

In addition to this, transverse waves propagate at lower velocities than longitudinal waves in the same material. Such is an advantage considering the precision and particularly time and frequency definition and sampling rate required in actuation and signal acquisition electronic systems.

2.1.3 - Evaluation of imperfections

In order to evaluate whether the dimensions of imperfections are within acceptable limits for the component being inspected, Distance to Amplitude Correlations (DACs) are used. A DAC relates the amplitude of propagating waves with the distance travelled, accounting for material damping of the wave amplitude. Since through the detection system the distance to the defect is known, the amplitude of the damage generated reflection waves can be analyzed to assess damage dimensions and orientation. For a certain distance, reflection wave amplitude will be proportional to the projection of the dimension of damage in the direction perpendicular to that of the impacting wave propagation. The amplitude of the sensed damage reflections can then be compared to the ones obtained in previous and regulated experiments, applying the same detection method and predefined damages (shapes, types, dimensions and orientations). Damage dimensions and orientation can then be determined through such comparisons [33 - 37].

2.1.4 - Visualization

The signals resulting from a scan can be presented in different forms: A, B, C or S scans, or even in a format combining some or all the previous forms. In an A scan, only the actuation and sensed signal waveforms are presented, in terms of amplitude vs. time. These allow the determination of the time delay between actuation and reflection arrival. Consequently, since sound propagation velocity is known, the distance from the probe to defect can be determined. B scans also relate the depth correspondent to determined reflections to the position of the probe in the component. Optionally, data contained in A scans for the different positions can be recorded and post processed. C scans present a planar view of the component under inspection (similarly to an x-ray image), with the possible defects (and their positions) represented. To obtain a C scan, the position of the probe is varied and recorded from scan to scan (or alternatively, with transducer arrays, the generated beam angle is recorded). For each position (and possibly beam angle) the waveforms and depths/distances corresponding to reflections are also recorded. An S scan is an enhanced version of a C scan with embedded A scans, to be applied when arrays are employed. Specifically, an A scan is recorded for each beam angle and the information is also presented in a cross section image of the component (usually in real time).

2.1.5 - Summary

As a summary of the advantages and disadvantages of this type of inspections, it must be mentioned that they are sensitive to both surface and subsurface discontinuities. The depth of inspection is superior to other NDT&E methods. Access is required to only one side of a component when the pulse-echo technique is used. This technique is highly accurate in determining defect positions (origin of reflections) and estimating their orientation, size and shape. Minimal part preparation is required. Electronic equipment provides instantaneous results and detailed images can be produced with automated systems. As with all NDT&E methods, the surface of the structures to inspect must be accessible. Components that present a rough surface, irregularities in shape, small size (particularly thickness), or inhomogenities are difficult to inspect. Cast iron and other coarse grained materials are difficult to inspect due to low sound transmission and high

signal noise [38]. Linear defects oriented parallel to the sound beam may not be detected. Reference standards are required for both equipment calibration and the characterization of flaws.

It is important to refer that these methods, all the techniques applied within them, the knowledge database originated with them and all their aspects including their shortcomings are the basis for research and development of SHM systems based on wave propagation. It was of the utmost importance to thoroughly understand sonic-ultrasonic conventional NDT&E techniques for the research developed and hereby reported. The parallelism to the application of Lamb wave propagation was assessed, not in all, but in multiple aspects of these techniques.

2.2 - The need for Structural Health Monitoring

The need for inspection of aircraft structures to achieve safe and economically efficient operation has been demonstrated and justified by, among others: risks involved in aircraft operation; current structural design damage tolerant philosophies; ageing aircraft; and introduction of composites into primary aircraft structures. NDT&E techniques presently applied to aircraft structures in operation are unable to assess structural condition either reliably and persistently or on a global level. The research, development and implementation of SHM techniques, as embedded, real time and more global assessment methods, is justified by the characteristics of current NDT&E. With the application of conventional NDT&E methods for aircraft structural condition assessment, higher safety levels while maintaining good economical performance will hardly be achieved. This is due to:

- the consequent lengthy and costly inspection operations (involving profuse disassembling and assembling procedures), with the aircraft not in operation for longer periods (and therefore not profitable);
- the increased safety factors included during the design of the damage tolerant structures to overcome the deficiencies of the current NDT&E methods. The minimum damage dimensions that can be reliably detected are still considerable.

Therefore requiring structural reinforcement and then increasing structural weight, reducing available payload weight, or increasing required power, fuel burn and emissions.

2.3 - SHM Techniques under Research

SHM involves assessing structural integrity through different damage diagnosis levels: detection, location, severity assessment (damage characterization, such as shape, type, orientation and dimensions) and finally damage prognosis, by assessing the remaining useful life [39].

There are different approaches to SHM of aircraft structures. Besides research on the application of Eddy current techniques, the majority of the emerging methods are based on mechanical excitation of the structure being inspected. These mechanical excitations vary from low to high frequencies and can be applied by an active SHM system, or by environmental loads.

2.3.1 - Low Frequency or Vibration Based SHM

Low frequency methods are based on static, quasi-static and/or vibration analysis of the structure to inspect. These methods assess deformation, curvature, vibration and damping changes - globally and/or locally -, natural frequencies (shifts, distortion, etc), vibration energy and changes in natural modes shape (their orthogonality, local curvatures, etc), due to damage existence. Changes in mass and rigidity of the structure, again globally and/or locally may indicate the existence of damage [40]. These methods are based on a comparison of damaged with undamaged data.

As an advantage, these methods can use, in some cases, the free vibration response of the structure, then without the need to apply actuation and related systems, power and actuators. If actuation is considered to be applied on the structure by the SHM system, actuators are usually required to have high actuation power, due to the considerable dimensions, mass and rigidity of the structures to inspect.

As an advantage, low frequency, or vibration based SHM systems can, theoretically, assess the structure condition globally. These techniques do not require complex and state of the art data acquisition systems with high sampling ratios and having to work at high frequencies. However they require high precision and definition on data acquisition. A wide range of transducer types can be considered, including widely applied and known strain gauges, PZTs and FBGs.

The disadvantage of these methods is that with a simple and direct approach, defects must present considerable dimensions to be reliably detected, i.e., their influence in mass and/or rigidity change must be substantial. Simultaneously, there are, possibly, particular locations in the structure (depending on the structure's geometry, material, etc), where certain changes in mass accompanied by certain changes in rigidity will not result in significant changes in the structure's natural frequencies or natural modes of vibration [41]. Vibration based SHM techniques are then ideal for structures designed to be capable of sustaining damages of significant dimensions before collapse and where damage growth monitoring is not required with a high definition.

To improve damage detection capabilities of low frequency methods, their precision and reliability, significant research has been performed in the development of data post processing techniques, data mining, etc. Data processing techniques being researched are also extremely interesting in terms of the application of their principles into high frequency methods. These techniques include Statistical Methods, Neural Networks (NN), application of Fuzzy Logic principles, signal filtering and signal Wavelet reconstruction, Genetic Algorithms (GA) for damage search, etc [42].

2.3.2 - High Frequency SHM

Higher frequency methods are based on acoustic wave propagation in the structural component under inspection and the influence of damages in their propagation pattern. They can be divided into three main groups.

The first group, impedance based methods, includes the application of burst actuations to the structure, usually involving more intermediate frequencies (as an evolution of sonic inspections) and in general, also without any regard for the types of waves/waveforms

being generated. These particular techniques assess structural condition and deal with damage detection based on impedance changes on the material due to damage existence [43]. Damage detection is ensured by sensors applied to the structure, based on electro-mechanical impedance effects. The more common applied sensors are PZTs The damage generated wave reflections, their amplitudes, wave velocity changes, among other characteristics of propagating waves, are monitored. As an example, the Time of Flight (ToF) of detected waves being reflected by a known end boundary condition is determined, i.e., the time between the burst actuation and sensing the reflected wave. Knowing the ToF and the distance travelled by the original generated wave and boundary reflection, the reference wave velocity can be determined. In the presence of damage, it is expected that a damage reflection will be sensed before the end boundary reflection. With the ToF of the damage reflection and since this wave will have the same propagation velocity as the original wave, the distance travelled by the original and damage reflected waves can be determined and damage position is then obtained [44]. Impedance assessment techniques still suffer from a lack of accuracy in damage detection. As a consequence, the dimension of reliably detected damages are in the order of several centimetres. Such is also related with the fact that, in general, actuation is not tuned to generate a particular type of sound wave. Due to this, sensors cannot be tuned *a priori* for a certain wave type or wavelength. To overcome these deficiencies, relatively powerful actuations are necessary to guarantee that propagating waves (generated and boundary and potential damage reflections) have sufficient amplitude to be detected. This technique is being widely researched for its application to beams [45]. Since they are not usually tuned for a particular wave, they are more prone to detect any type of wave being emitted. This is particularly important in beams, where geometrical constraints and the proximity of lateral boundaries introduce significant complexity in the wave propagation pattern. Waves propagating along the beam length and their corresponding sensed signal are highly affected by wave reflections being generated from the beam lateral boundaries. Moreover, since intermediate frequencies are considered in this type of applications and, normally, there is no tuning required *a priori* for the actuation signal, simpler actuation signals, such as steps and square waves can be applied. The requirements for the

actuation and data acquisition systems are also not as stringent with lower sample rates and frequencies. However, significant filtering of sensor signals is usually required.

Acoustic Emissions (AE) have also been researched for a long period of time [46 - 49] and are being explored for their application to SHM systems [50 - 52]. Their principle hinges on the fact that when a crack appears and grows in a component, sound waves are emitted. These are usually generated in the crack tip growth region, due to material deformation.. When such occurs, bursts of waves of different types are generated, propagating through the host material with different and undetermined frequencies, velocities and wavelengths. The different generated waves also present different amplitudes and propagation amplitude damping characteristics, depending on the wave type and frequency. Wave types and frequencies being generated with higher amplitudes and more prone to be detected, depend largely on the defect type, dimensions, orientation, and growth characteristics. In addition, AE usually present very small amplitudes and low SNR. Both the undetermined wavelengths and low SNR create substantial difficulties for the selection of the sensors (their type, dimensions and positions) which are able to reliably detect these waves and consequently the existence of damage and its growth. The development of data acquisition systems and the implementation of data post processing schemes is also a complex task, even more if the method is intended for a particular frequency. Previous work has been done on achieving optimum sensor selection, data acquisition and signal processing, for different, specific types of damage [52]. Regulations for AE testing have been developed [53 - 55], based on the results of benchmark experiments executed in certain materials. These results can be used for comparison during inspection. Such comparison allows the determination, or a better idea of damage existence and size. In those experiments, the AE of certain crack types, dimensions and growth rates, in certain host materials and parameterised component geometries, at certain distances from damage location, were matched to the ones being emitted when impact tools are used. Shapes, material of the impact tool and impact energy are parameterised. Furthermore, with AE being generated by an impact tool, , multiple components do not have to be damaged when executing benchmark tests of an AE system – what would represent a lengthy, complex and costly procedure. AE systems can be effortlessly embedded into the structure to be monitored. Persistent and

real time structural condition assessment is then possible by these passive systems. In the case of the application of piezoelectric sensors, no energy is consumed/necessary to power the sensors (only needed for data acquisition and signal processing). This is an important factor when longer endurance systems are being considered with persistent SHM and limited energy resources. FBG and strain gauge sensors can also be applied for inspections employing this technique. In AE systems, damage detection is related with the assessment of sensor signals and the detection of the corresponding crack appearance/growth generated sound waves. The determination of damage location involves the application of multiple sensors in different positions on the component and the implementation of triangulation schemes [52]. In some cases, sensor type and dimensions are previously selected to tune the system into a certain frequency, i.e., optimizing the system for detection of specific wave frequencies. This system will not be optimized to detect all types of defects. Defects will potentially exist in the component under inspection, whose appearance or growth will not generate AE in that frequency with sufficient amplitude to be reliably detected. For the host material properties, wave propagation velocities are known, so that a triangulation scheme can be applied if AE in a particular frequency are detected. Such scheme is based on the relative time delays between the arrival of AE to the different positions of the component under inspection, where sensors are deployed. When the system is not designed to be tuned to a certain frequency, filters and/or wavelet signal reconstruction can be applied to search for AE at different frequencies. After finding AE signals and their corresponding frequencies, again triangulation algorithms can be implemented.

The main high frequency SHM methods being researched can be regarded as an evolution of ultrasonic inspections and involve the direct activation and propagation of sound waves in solids. The application of sound waves for damage detection is based on their propagation characteristics and particularly on the fact that they are reflected by any discontinuity in the host material (potentially a defect and then allowing for damage detection). Similarly to the previously referred high frequency SHM systems, different wave types can be potentially considered: body waves, specifically longitudinal and/or shear/transverse; creep; Stonely; Love; Rayleigh waves; or Lamb waves. The main consideration for their application is the geometry of the component to be inspected.

Considering their applications in SHM systems, the main decisive aspects are related with:

- detection capability of defects with smaller dimensions, requiring the application of waves with smaller wavelength and higher frequencies. The frequency of the waves to be applied should however be maintained as lows as possible so as not to have stringent requirements in terms of the actuation and data acquisition systems;
- allowing transducer embedment;
- the intended capability to monitor larger areas of the structure with a single and simpler system. To achieve the latter, sound waves to be applied must be able to propagate farther with small amplitude attenuation (small propagation damping).

Besides a highly scattered behaviour, body wave amplitudes are highly damped along their propagation and this is the reason for their localized application in conventional NDT&E Sonic-Ultrasonic methods. Lamb waves, however, are able to propagate to longer distances without showing significant amplitude damping, being ideal for application in SHM systems. Their small propagation amplitude damping is related to the fact that Lamb waves propagate in plate like (or low curvature shell) structures with limited thickness. The two close-by parallel free boundaries (surfaces) decrease propagation damping. The majority of structural components can in fact be decomposed into plate like sections. This justifies the fact that they are main candidates to be applied in SHM methods to replace existing NDT&E [56, 57]. For all these reasons, the research and development of the SHM system reported in this thesis was based on Lamb wave propagation.

Chapter 3

Lamb Waves

In 1885, Lord Rayleigh developed his wave theory [58], based on which Horace Lamb mathematically proved, in 1917, the existence of a particular type of mechanical, elastic deformation waves in solids with two parallel and close free boundaries. Such waves were later named after him – Lamb waves [59]. These waves propagate in thin plate like, or small curvature shell like components, with two parallel free boundaries. Due to the low damping imposed by the two parallel free surfaces, Lamb waves are capable of propagating for longer distances with small amplitude attenuation. In 1960, Mindlin [60] completed a theoretical analysis of these types of waves. In 1961, Worlton [61] proposed the use of Lamb waves for damage detection and their potential application for NDT&E emerged. Frederik and Worlton, in 1962, conducted initial experimental studies [62].

Similarly to ultrasonic NDT&E, pulse-echo or pitch-catch scanning methods can be applied. Developments in electronics and computation in the last decades enabled the achievement of the required actuation, data acquisition systems and data post processing to allow the application of Lamb waves for SHM in reality.

The types of damage that are prone to be detected by this type of inspection were summarised by Rose [63]. Some of the emphasised advantages of these methods were:

- the fact that structures can be inspected while retaining coating and insulation;
- changing the structural health assessment system position during inspection is not required for accurate damage detection;
- the exceptional sensitivity to the detection of multiple defects, with high identification accuracy. The potential of Lamb wave based SHM methodologies to monitor large metallic aircraft surfaces was given further consideration by Dalton et al. [64].

3.1 - Lamb Wave Theory

In order to reliably and accurately apply Lamb waves in SHM, it is of extreme importance to thoroughly understand *a priori* their properties and propagation characteristics. A fundamental characteristic of Lamb waves that must be considered is their dispersion behaviour, i.e., the relationship between their propagation velocity - both phase and group velocities – and their frequency. Such relation is depicted by phase and group Dispersion curves.

Moreover, there are different modes of propagating Lamb waves. In Fig. 3.1 the stationary patterns of the first symmetric (S_0 wave) and anti-symmetric (A_0 wave) modes are depicted. Higher order Lamb wave modes can also exist and propagate in the host material, depending on certain material properties and frequency of excitation. These higher Lamb wave modes present inflection points in their corresponding deformation patterns along the thickness of the host material. The mode number, or order, is defined by the number of existing inflection points. The higher order Lamb waves are identified either as S_n or A_n waves, being n the number of inflection points (equal to the mode number/order). Again, S_n or A_n respectively represent waves that are symmetrical or anti-symmetrical, with respect to deformation along the thickness of the host material, with relation to its mid plan.

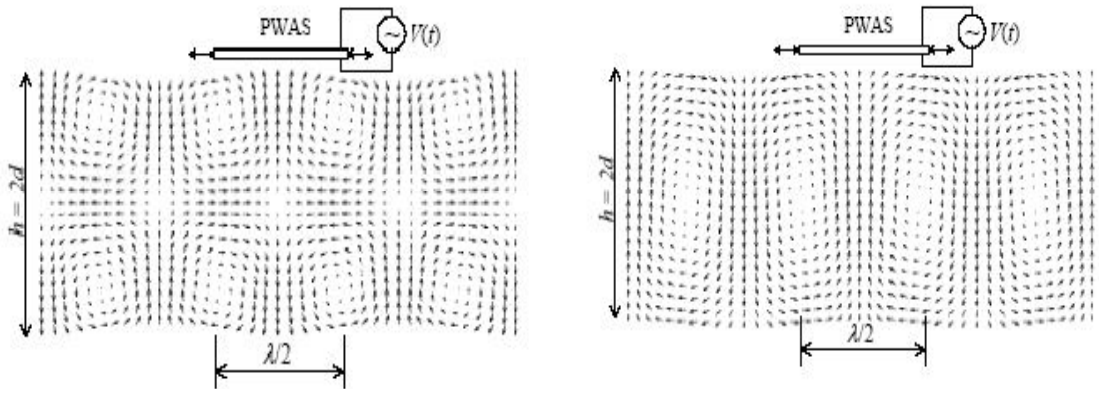

Figure 3.1: Symmetric wave (S_0) and anti-symmetric wave (A_0) [65].

The S_0 wave mode is essentially a longitudinal compression-traction mode, while the A_0 wave mode is a transverse, or bending mode, generating deformation mainly in the thickness direction, normal to wave propagation.

3.1.1 - Mathematical Model

The development of the mathematical model describing Lamb wave propagation is presented next. The intent of such an analytical analysis is to retrieve important characteristics of Lamb wave propagation. Since Lamb waves only propagate in plate like structures, a thin plate of thickness $2h$, as seen in Fig. 3.2, is considered.

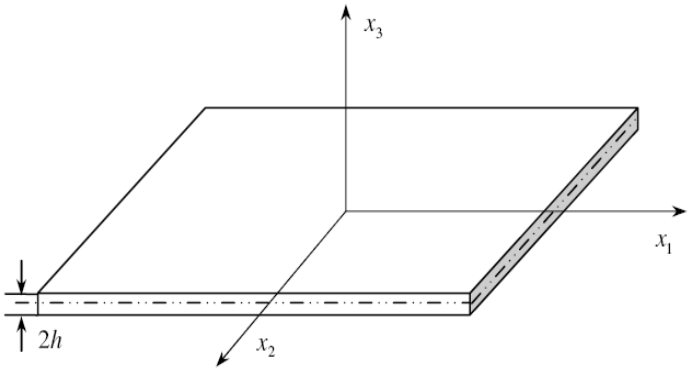

Figure 3.2: Plate element.

Assuming a continuum body with small deformations (or strains), Newton's second law can be written as:

$$\sigma_{ji,j} + F_i = \rho \frac{\partial^2 u_i}{\partial t^2}, \text{ with } i, j = 1, 2, 3 \tag{3.1}$$

where $\sigma_{ji,j}$ is the stress tensor divergence, F_i and u_i are respectively applied body forces and displacement in the direction x_i and ρ being the density.

The relation between deformations and strains is expressed by:

$$\varepsilon_{ij} = \frac{1}{2}(u_{j,i} + u_{i,j}) \tag{3.2}$$

Assuming that there are no plastic deformations, linear relations between the components of stress and strain can be considered. For elastic materials, constitutive equations - the general Hooke's law - have the form:

$$\sigma_{ij} = C_{ijkl}\varepsilon_{kl} \tag{3.3}$$

where C_{ijkl} is the elasticity tensor, being defined for an isotropic medium as:

$$C_{ijkl} = K\delta_{ij}\delta_{kl} + \mu(\delta_{ik}\delta_{jl} + \delta_{il}\delta_{jk} - \frac{2}{3}\delta_{ij}\delta_{kl}) \tag{3.4}$$

with δ_{ij} being the Kronecker delta, K the host material Bulk Modulus and μ the Shear Modulus, related to the material Young Modulus (E) and Poisson Coefficient (υ) by:

$$K = \frac{E}{3(1-2\upsilon)} = \frac{E\mu}{3(3\mu - E)} \tag{3.5}$$

$$\mu = \frac{E}{2(1+\upsilon)} \tag{3.6}$$

For a homogeneous medium (where material properties are constant and not a function of position), the material constitutive equation can now be written as:

$$\sigma_{ij} = K\delta_{ij}\varepsilon_{kk} + 2\mu(\varepsilon_{ij} - \frac{1}{3}\delta_{ij}\varepsilon_{kk}) \tag{3.7}$$

The previous expression can be simplified into:

$$\sigma_{ij} = \lambda_{Lame}\delta_{ij}\varepsilon_{kk} + 2\mu\varepsilon_{ij} \tag{3.8}$$

Here, λ_{Lame} is the Lamé first constant, defined by:

$$\lambda_{Lame} = \frac{2\mu\ \upsilon}{1-2\upsilon} \tag{3.9}$$

Substituting strains by displacements according to Eq. 3.2 in Eq. 3.8 and subsequently substituting the resultant equality in Eq. 3.1, the Rayleigh equation is derived, describing wave propagation in solids [66]:

$$\mu\ u_{i,jj} + \left(\lambda_{Lame} + \mu\right)\ u_{j,ij} + F_i = \rho\frac{\partial^2 u_i}{\partial t^2} \tag{3.10}$$

Following Helmholtz decomposition, Eq. 3.10 can be separated into longitudinal and transverse governing modes, respectively:

$$\frac{\partial^2\phi}{\partial x_1^2} + \frac{\partial^2\phi}{\partial x_3^2} = \frac{1}{C_P^2}\frac{\partial^2\phi}{\partial t^2} \tag{3.11}$$

$$\frac{\partial^2\psi}{\partial x_1^2} + \frac{\partial^2\psi}{\partial x_3^2} = \frac{1}{C_S^2}\frac{\partial^2\psi}{\partial t^2} \tag{3.12}$$

C_P and C_S are the longitudinal and transverse wave propagation velocities on the material, given by:

$$C_P = \sqrt{\frac{E(1-\upsilon)}{\rho(1+\upsilon)(1-2\upsilon)}} \tag{3.13}$$

$$C_S = \sqrt{\frac{\mu}{\rho}} \tag{3.14}$$

Solutions for Eqs. 3.11 and 3.12 have the form:

$$\phi = \left[A_1 \sin(px_3) + A_2 \cos(px_3)\right] e^{i(kx_1 - \omega t)} \tag{3.15}$$

$$\psi = \left[B_1 \sin(qx_3) + B_2 \cos(qx_3)\right] e^{i(kx_1 - \omega t)} \tag{3.16}$$

where:

$$p^2 = \frac{\omega^2}{C_P^2} - k^2 \tag{3.17}$$

$$q^2 = \frac{\omega^2}{C_S^2} - k^2 \tag{3.18}$$

$$k = \frac{2\pi}{\lambda} \tag{3.19}$$

A_1, A_2, B_1 and B_2 are determined by boundary conditions (including the free parallel upper and lower surfaces), k, ω and λ are respectively the wave number, circular frequency and wavelength.

Displacements in the wave propagation direction and its normal direction, for the plate, can be defined as:

$$u_1 = \frac{\partial \phi}{\partial x_1} + \frac{\partial \psi}{\partial x_3} \tag{3.20}$$

$$u_2 = 0 \tag{3.21}$$

$$u_3 = \frac{\partial \phi}{\partial x_3} - \frac{\partial \psi}{\partial x_1} \tag{3.22}$$

With stresses being given by:

$$\sigma_{31} = \mu\left(\frac{\partial u_3}{\partial x_1} + \frac{\partial u_1}{\partial x_3}\right) = \mu\left(2\frac{\partial^2 \phi}{\partial x_1 \partial x_3} - \frac{\partial^2 \psi}{\partial x_1^2} + \frac{\partial^2 \psi}{\partial x_3^2}\right) \tag{3.23}$$

$$\sigma_{33} = \lambda_{Lame}\left(\frac{\partial u_1}{\partial x_1} + \frac{\partial u_3}{\partial x_3}\right) + 2\mu\frac{\partial u_3}{\partial x_3} = \lambda_{Lame}\left(\frac{\partial^2 \phi}{\partial x_1^2} + \frac{\partial^2 \phi}{\partial x_3^2}\right) + 2\mu\left(\frac{\partial^2 \phi}{\partial x_3^2} - \frac{\partial^2 \psi}{\partial x_1 \partial x_3}\right) \tag{3.24}$$

For the plate presented in Fig. 3.2, applicable boundary conditions (plane strain) can be defined as:

$$u(x,t) = u_0(x,t) \tag{3.25}$$

$$t_i = \sigma_{ij} n_j \tag{3.26}$$

$$\sigma_{31} = \sigma_{33} = 0 \text{ for } x_3 = \pm h \tag{3.27}$$

After applying the previous boundary conditions with Eqs. 3.23 and 3.24 and performing the corresponding derivatives, the resultant equations can be separated in symmetric and anti-symmetric modes. In the symmetric mode u_1 is given by a combination of only cosine functions, i.e., even, or symmetric functions, while on the anti-symmetric mode it is given by a combination of sine functions (odd functions). Through Eqs. 3.15, 3.16, 3.20 and 3.22, A_1, A_2, B_1 and B_2, u_1 and u_3 can be determined for both modes (as $A_1 = B_2 = 0$ in the symmetric mode and $A_2 = B_1 = 0$ in the anti-symmetric mode). Using the resultant expressions with Eq. 3.27 and forcing a non trivial solution (the determinant of the solution matrix must be zero), Lamb waves' propagation velocity can then be obtained from the roots of the following equation – Rayleigh-Lamb equation, for both modes:

$$\frac{\tan(qh)}{\tan(ph)} = -\left(\frac{4k^2 qp\mu}{\left(\lambda_{Lame}k^2 + \lambda_{Lame}p^2 + 2\mu p^2\right)\left(k^2 - q^2\right)}\right)^{\pm 1} \tag{3.28}$$

Using Eqs. 3.6, 3.9, 3.13, 3.14 and 3.17 to 3.19, the previous equation can be separated in symmetric and anti-symmetric modes:

$$\frac{\tan(qh)}{\tan(ph)} = -\frac{4k^2qp}{\left(k^2-q^2\right)^2} \tag{3.29}$$

$$\frac{\tan(qh)}{\tan(ph)} = -\frac{\left(k^2-q^2\right)^2}{4k^2qp} \tag{3.30}$$

These equations can only be solved numerically.

3.1.2 - Dispersion Curves

Lamb wave phase velocity (C_L) is dependent on the frequency (equal to frequency of excitation). Such relation depends on host material properties (as can be observed from the previous equations) and thickness ($2h$). For a certain plate thickness and host material properties, Lamb wave phase velocities can be calculated for different frequencies and that relation can be illustrated graphically - dispersion curves. The dispersion curves also confirm the existence of multiple modes, for a given frequency. With the emitted waves being a complex combination of different modes, with different velocities, their propagation pattern becomes extremely difficult to evaluate.

Viktorov [67] developed the following methodology to solve Eqs. 3.29 and 3.30, with the objective of obtaining afterwards Lamb wave dispersion curves. First, transverse and longitudinal velocities, C_P and C_S are calculated by Eqs. 3.13 and 3.14. Afterwards, ξ, ζ and $\bar{d}$ are defined as:

$$\xi = \frac{C_S}{C_P} \tag{3.31}$$

$$\zeta = \frac{C_S}{C_L} \tag{3.32}$$

$$\bar{d} = \frac{\omega}{C_S}h \tag{3.33}$$

Substituting these equalities in Eqs. 3.29 and 3.30, the dispersion curves can be calculated by solving the new form of the Rayleigh-Lamb equations, for the symmetrical and anti-symmetrical modes:

$$\frac{\tan\left(\sqrt{1-\zeta^2}\ \bar{d}\right)}{\tan\left(\sqrt{\xi^2-\zeta^2}\ \bar{d}\right)} = 4\ \zeta^2\sqrt{1-\zeta^2}\ \frac{\sqrt{\xi^2-\zeta^2}}{\left(2\ \zeta^2-1\right)^2} \tag{3.34}$$

$$\frac{\tan\left(\sqrt{1-\zeta^2}\ \bar{d}\right)}{\tan\left(\sqrt{\xi^2-\zeta^2}\ \bar{d}\right)} = \frac{\left(2\ \zeta^2-1\right)^2}{4\ \zeta^2\sqrt{1-\zeta^2}\sqrt{\xi^2-\zeta^2}} \tag{3.35}$$

Both equations admit several roots, corresponding to several symmetric and anti-symmetric Lamb wave modes: S_0, A_0, S_1, A_1, etc.

Figure 3.3 depicts the numerically obtained solutions for the above equations, with the representation of the different symmetric and anti-symmetric modes.

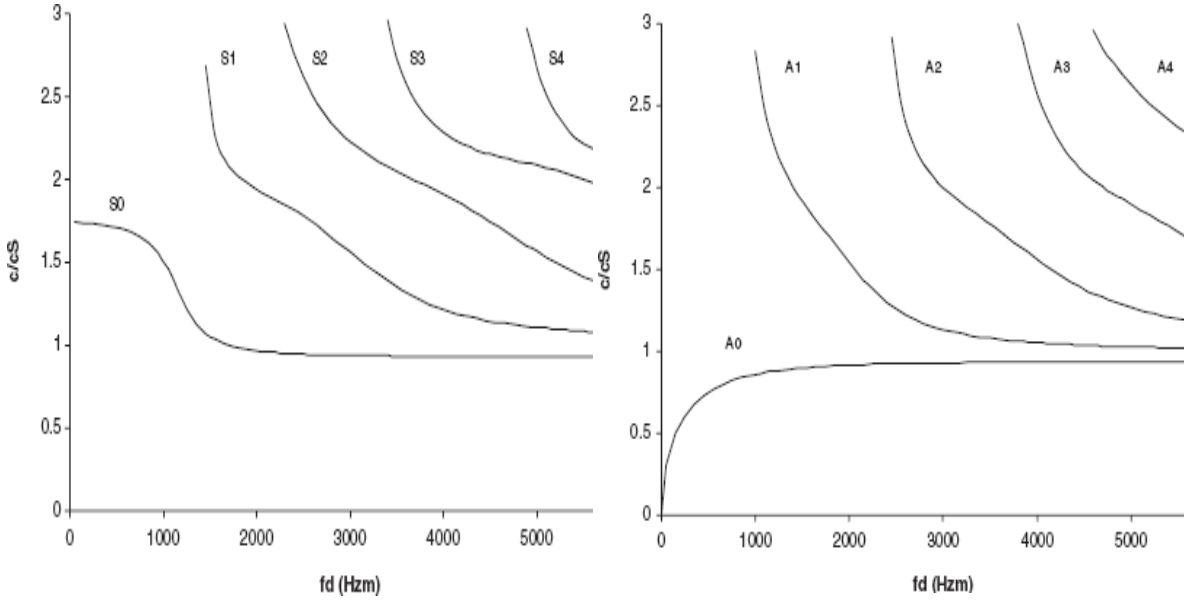

Figure 3.3: Dispersion curves for an aluminum (Al2024) plate.

Due to the pattern complexity of Lamb waves, propagating in multiple modes (and different velocities), and consequent difficulties in the evaluation of such patterns, the majority of Lamb wave based SHM applications are focused on the first symmetric and anti-symmetric modes. According to the dispersion curves presented in Fig. 3.3, to avoid generating Lamb wave modes other the first ones, excitation frequencies should be

inferior to a certain value. Observing Fig. 3.3, for an Al2024 plate and for a thickness range of 1 to 3mm, a safe upper limit for excitation frequency would be 500kHz.

Giurgiutiu and Bao [65] present the dispersion curves (for an Al2024 plate, 1.6mm thick) in terms of absolute values and only for the first symmetric and anti-symmetric modes (of interest for the implementation of a SHM system) – Fig. 3.4. At low frequencies (f <500kHz) the symmetric Lamb wave velocity approaches the longitudinal wave velocity (C_P), while the anti-symmetric Lamb wave velocity approaches zero. At high frequencies (f >2500kHz), the dispersion curves of these modes coalesce, approaching the transverse wave propagation velocity (C_S).

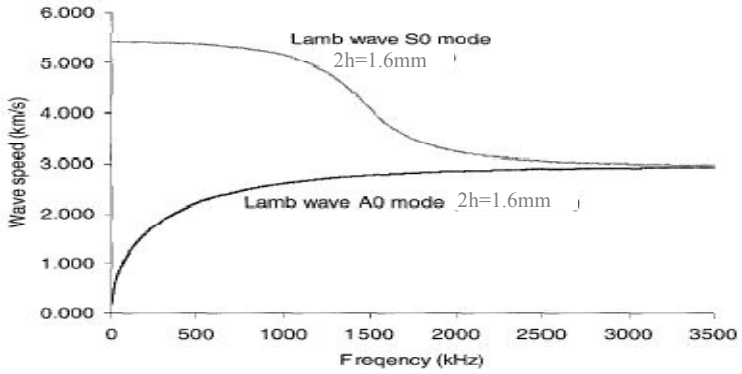

Figure 3.4: Lamb waves' phase propagation velocities [65].

It is important to refer that Lamb waves propagate in groups, with the group propagation velocity being different than the phase propagation velocity. It is then important to determine the Lamb wave group propagation velocity (C_g), defined by:

$$C_g = C_L^2 \left[C_L - (fd) \frac{d\,C_L}{d(fd)} \right]^{-1} \tag{3.36}$$

To simplify the calculation of C_g, it is reasonable to consider the following approximation:

$$\frac{d\,C_L}{d\,f} \approx \frac{\Delta\,C_L}{\Delta\,f} \tag{3.37}$$

A numerical method can then be employed to extract group velocities from phase velocities, for each frequency. The results are then plotted in a C_g vs. f curve – group dispersion curves, depicted on Fig. 3.5.

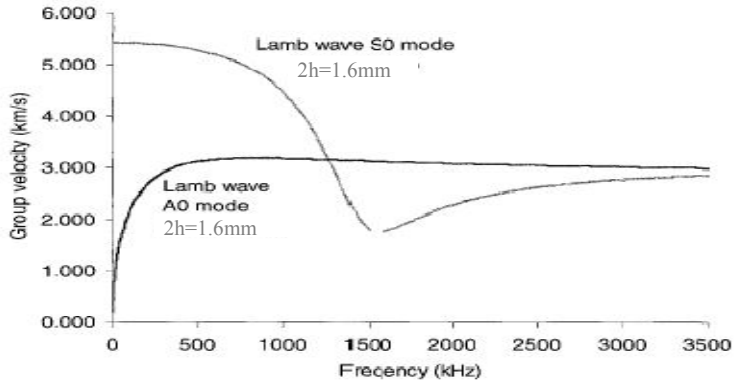

Figure 3.5: Lamb waves' group propagation velocities [65].

The importance of group velocities lies in the fact that these are the velocities that can be more accurately and effortlessly measured (as the average velocity of the group of waves, or the velocity of the mid-point).

A careful analysis of the dispersion curves is extremely important for the successful implementation of an SHM system. Frequency of the generated Lamb waves must be selected considering that:

- only the first modes are emitted, not to increase considerably the complexity of evaluation of the waves propagating pattern (and assessment of corresponding sensed signals);
- the group and phase velocities should be as close as possible, again to facilitate their evaluation and not to have a considerable spreading of the propagating group of waves in space and consequently in sensor signal time;
- the propagation velocities of the first symmetric and anti-symmetric modes should be as different as possible, so that the interference in between the two modes is minimized (since they will be propagating in totally different locations at the same time, or alternatively they will be sensed in different times at the same sensor location), decreasing the complexity in their evaluation;

- the variation of the propagation velocity with wave frequency is as small as possible in the selected frequency range, so that small errors in the generation frequency will not result in considerable differences of the propagation velocity, compromising the determination of defect locations;
- as it will be shown, the relation of wave frequency and velocity, and corresponding wavelength, is important for the selection of transducers, their working frequency and dimensions (to amplify their actuation and sensitiveness capabilities and not to implement transducers either incapable of correctly generate the desired waves, or sense them);
- resulting wavelength is also important if trying to minimize the detectable damage dimensions, bearing in mind that smaller wavelengths (and hence higher frequencies) are more prone to interference by smaller damages.

3.2 - State of the Art in Lamb Wave based SHM systems

Developments in electronics and computation enabled the intensive research that has been performed in the last two decades and is currently being developed in several fields related to the practical application of this SHM approach, namely:

- Numerical simulations, involving wave generation and propagation models, damage modelling and simulated damage detection and characterization;
- Factors which affect Lamb wave propagation such as geometric features, structural reinforcements, boundary conditions, temperature and damage existence, orientation and morphology;
- Transducer application, including investigation of different transducer types and dimensions, and their capabilities. In this field, transducer degradation and interface with host material are also two topics being addressed;
- Lamb wave mode and frequency selection, effects of actuation waveform profile selection and mode conversion;
- Implementation techniques through networks and arrays of transducers;

- Actuation, signal generation and data acquisition capabilities;
- Signal processing, in time and frequency domains, with the development of Statistical Methods, Neural Networks (NN), application of Fuzzy Logic principles, signal filters and signal Wavelet reconstruction, etc;
- Damage detection, localization and characterization algorithms.

Much of the work in this area involves more than one of the previously mentioned subjects, rather than focusing on a single aspect.

Concerning numerical simulations, Lee and Staszewski [68] presented an important review of the efforts and outcomes regarding numerical simulations of Lamb wave propagation and Lamb wave based damage identification. The Finite Element Method (FEM) and particularly spectral elements [69] have been widely used in these research efforts. Besides dedicated developed simulation code, commercial software packages, such as ANSYS® and PATRAN/NASTRAN® have been used. Furthermore, some of the research efforts involve purpose developed finite elements to be embedded in those commercial packages. Galan and Abascal [70], for instance, reported successful simulations of wave scattering in laminated plates using boundary elements. Using spectral finite elements, Ostachowicz [71] presented a method capable of robustly detecting damages with small dimensions despite artificially introduced measurement errors.

Due to high propagation velocities, high frequencies, small amplitudes and damping of Lamb waves, any minute errors in the measurements might result in a considerable error in damage detection and location by an SHM system. In the worst case scenario, these small errors, either introduced by the system itself (generation, acquisition, etc), or by environmental conditions, might incapacitate such a system – rendering it unable to even detect damage reflections and therefore damage existence, or completely missing the location of potential defects. Besides the external pressure, one of the important factors that might affect Lamb wave propagation is ambient temperature. Studies performed by Blaise and Chang [72, 73] indicate that Lamb wave amplitudes and propagation velocities suffer significant changes (of up to 50%) for temperature variations in cryogenic applications. Konstantinidis et al. [74] performed structural condition

assessment experiments with the successful detection of a 22mm damage. However, they concluded that in the long term detection capabilities were significantly decreased, considering drastic temperature variations in the range of what is to be expected during aircraft operation.

A straightforward conclusion is that, for an SHM system to be able to assess an aircraft structural integrity during operation, it will have to account for variations of the characteristics of Lamb waves propagating in the structure. Namely, in their amplitude and propagation velocity, with the objective of detecting potential defects. Besides imposed noise, vibration and stresses/loads in flight, such system would have to consider the variation of ambient pressure and temperature (and other secondary ambient characteristics, such as humidity, etc). One method to address this difficulty is to use a baseline subtraction method. Knowing the environmental conditions in which such inspection is to be performed, Lamb wave propagation characteristics can be corrected according to, and compared with the ones previously determined for similar conditions. Such baseline parameterized conditions must be included as a database for the SHM system.

However, if an SHM system is designed for almost real time operation, i.e., for ground on demand tests, the previously referred difficulties do not have to be considered. Here the deployment of such system is considered to occur, for instance, inside a hangar with some ambient temperature control, if severe climate/ambient conditions occur. Alternatively, it can be used in between passenger (and/or cargo) disembarking and embarking ground operations, in moderate wind and ambient conditions (temperatures) – removing all applied operation loads and reducing temperature effects. Such inspections can be performed in normal operation, or whenever it is suspected that the aircraft structure might have sustained a damage (for instance due to excessive loads or impacts), or a damage has grown to excessive dimensions (for instance due to accelerated fatigue). Even if used merely as a near real time inspection system, it presents significant advantages to what is current practice with conventional NDT&E systems. Increased safety is achieved by regular and just in time inspections and maintenance; and by more global inspections. Economically, this is achieved without necessary complicated and lengthy disassembling and assembling operations, tackling the issues raised by hard to

access areas - reducing significantly (costs and related) operation downtime (non operation, grounding time). In this case maintenance and repair of the structure is only applied if necessary (in these extraordinary events). To prove this capability, some works refer that for temperatures in the range of 20ºC to 40ºC do not affect the outcome of damage detection [75].

The majority of individual components in aerospace structures can be decomposed as several plate like or shell like parts (with small curvature), which promotes the application of Lamb wave based SHM methods. However, most of the components also present structural reinforcements, e.g. stiffeners, either integrated in the component in composite material parts, or with related rivet lines in metallic structures. One other field where intensive research is being developed is on the perception of how wave propagation pattern is altered due to the existence of such reinforcements: generated wave reflections; if waves are able to travel through such reinforcements; and what is their effect on wave amplitude attenuation. Zhao et al. [76] conducted several experiments on a representative reinforced aluminum aircraft panel with stringers, using the first symmetric Lamb wave mode (S_0). Experiments were conducted, employing eight PZT transducers' forming a network distributed in a 0.1m x 0.1m area of the panel, in between stringers (positions marked as x, for Case 1, in Fig. 3.6). Damages with dimensions of 3mm were detected. However it was verified that stringers imposed significant amplitude attenuation to propagating Lamb waves, through energy dissipation, wave reflection/scattering and mode conversion. This resulted in an inability to detect damage beyond stringers, with relation to the transducer network location. In order to study such amplitude damping, a different panel was used, and a PZT array was installed (positions marked as Δ, for Case 2, in Fig. 3.6). In this figure the sensed propagating Lamb waves are also depicted. It is clearly observable the wave amplitude damping imposed by each of the existing stringers along the wave propagation.

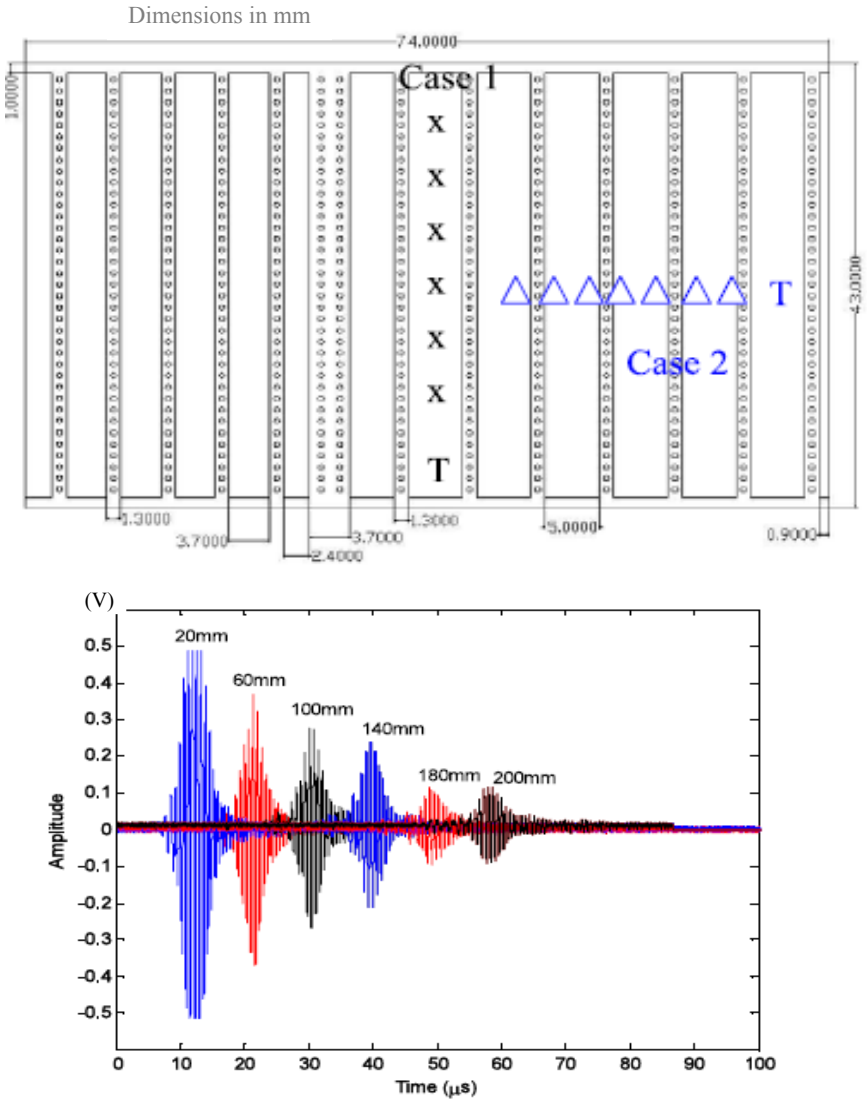

Figure 3.6: S_0 mode amplitude attenuation due to riveted stringers [76].

Monnier [77] tested a composite panel, also with multiple stringers. These experiments led to the conclusion that in the particular component under testing, the S_0 wave mode was able to travel along the panel, through the stringers positions. In Fig. 3.7 the composite panel tested and the S_0 energy attenuation (related with amplitude attenuation) along their propagation in the panel, through the stringers positions are presented.

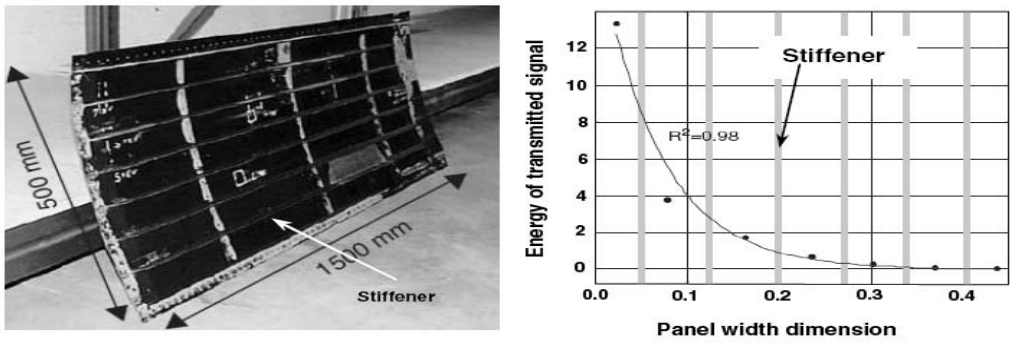

Figure 3.7: S_0 wave mode energy attenuation [77].

The existence of potential damages in the component being inspected, and their characteristics, such as their dimensions, type, orientation, distance to applied transducers and emitted wave reflections, influence Lamb waves' propagation pattern. The degree of changes in such pattern due to damage existence, and consequently damage detectability, significantly depends on the referred damage characteristics. Lu et al. [78] performed numerical simulations and experimental studies to determine the influence of imposed cracks' orientation on their generated reflected waves. Several sensors were bonded to the structure, around imposed 20mm and 40mm cracks. The main conclusion of this work is that damage generated wave reflections' amplitudes decrease and through wave transmission amplitude increase as the incident wave propagation direction is aligned with the length of the crack. Also, as the direction of the incident wave propagation is aligned with the crack's length, the number of reflections increases. Furthermore, when a crack's length increases, the acquired amplitude of damage generated reflection waves also increases, while the transmitted energy decreases. These results are in agreement with empirical expectations.

Jin et al. [79] used the first anti-symmetric Lamb wave mode (A_0) to inspect plates with cracks, with a length of around 50mm. In this study Inter-Digital Transducers (IDT) were applied. It was found that for this case, only the deployment of IDTs in particular positions allowed a correct assessment of crack location, size and shape – Fig. 3.8.

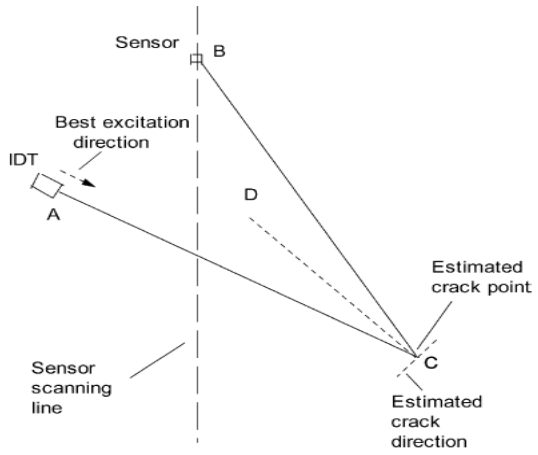

Figure 3.8: IDT damage interrogation example [79].

Several functional materials have been studied, developed and applied to transducers, for Lamb wave generation and sensing. From these, PZT transducers have been widely applied [80]. PZT transducers have the capability to translate mechanical deformations into electrical outputs and vice-versa (piezoelectricity), or respectively direct and reverse piezoelectric effect. One PZT transducer can then be used as an actuator and as a sensor, at different times. PZT transducers can be easily integrated into the structures to inspect, for instance by surface bonding. They can be used in a wide frequency bandwidth, are lightweight and do not require external power when used as sensors. Furthermore, they can be manufactured in almost every shape and size. The fact that PZT transducers provide both actuation and sensing capabilities has justified their systematic application in SHM systems [81, 82]. Size, shape, constitutive material and location must be selected in order to achieve optimum transducer performance [83]. Numerical simulations of the application of PZT transducers to SHM, along with experiments, have been performed by Nieuwenhuis et al. [84]. Giurgiutiu [85] also dedicated a great part of his research to this aspect. In particular, the relationship between PZT transducer dimensions and their actuation and sensing performances was studied. The amplitude of generated Lamb waves with a wavelength double of the PZT transducer planar dimension was enhanced. A relation in between optimum PZT transducers' dimensions, Lamb wave mode applied, its wavelength and actuation frequency can then be determined.

Particular developments on PZT transducers, involving directionality of actuation and sensing, and embedment of PZT films have also been investigated. Quek et al. [86]

established a performance comparison between these and conventional PZT transducers for damage location in aluminum plates. Both transducer types were able to detect cracks with 3mm of length, using the A_0 mode. The directionality of these transducers proved to be an advantage for the location of potential defects along their preferred direction, in detriment of all other locations. However, by application of particular networks with the transducers oriented along specific directions, such disadvantages could be diminished.

The application of optical fiber based transducers, for Lamb wave detection, has also been investigated with still preliminary, but promising results. Fiber optic based transducers can only be applied as sensors, so that they present a disadvantage with relation to PZT transducers in the sense that they are not capable of Lamb wave actuation. Another main disadvantage of this type of sensors is that they are also able to measure temperature, i.e., their deformation measurements corresponding signal output is highly affected by temperature changes [87].

Fiber optic sensors measure deformation directly, either statically or dynamically, enabling the subsequent determination of strains and stresses. PZT transducers, however, are only capable of measuring deformation dynamically, i.e., they are not able to directly sense absolute static deformations. Moreover, their impedance (electro mechanical capacitance and resistance) changes with frequency.

Until recently, the majority of applications of fibre optic sensors involved static or low frequency/vibration measurements [88]. Applications involving dynamic deformation acquisition at high frequencies, essential for Lamb wave based SHM, are presently being developed with the introduction of Fibre Bragg Gratings (FBGs). These sensors are based on the crystallization of multiple planar fibre cross sections along the fibre direction (gratings), according to a pre-determined spacing. The crystallization of such cross sections is achieved through the application of UV light through a mask. The crystallized planar cross sections reflect part of the light being transmitted through the fibre. Since these crystallized cross sections are spaced according to pre defined relative distances, the reflected light from, and transmitted light through these cross sections interfere. The resulting reflected light is then centered on a specific wavelength, which is reduced in the spectrum of the transmitted light. This wavelength is proportional to the spacing in

between the consecutive crystallized cross sections in the FBG sensors, according to Bragg's law:

$$\lambda_{light} = 2n\Lambda \tag{3.38}$$

Here, λ_{light} is the reflected light wavelength, or Bragg wavelength, n is the effective refractive index of the grating in the fibre core and Λ the distance/spacing in between consecutive crystallized cross section planes, or grating period.

The principle to sense deformation with FBGs is that the grating period and consequently the Bragg wavelength will change when deformation is applied to the sensor.

FBG sensors, being based on optical fibers, are extremely lightweight, what is a significant advantage for their application in aircraft. They are thin and above all, can be either bonded to the surface of the structure to inspect (either in metallic or composite structures), or embedded in the structure when composite components are considered, during their manufacture. Furthermore, these sensors are immune to Electro Magnetic Interference (EMI) and do not require recalibration during their service life (as for instance strain gauges do). They are, however, extremely fragile, requiring a careful application. Also, their sensitiveness to temperature requires that deformation measurements must be compensated. Another shortcoming of this type of sensors is their sensing directionality (similar to strain gauges), being sensitive to deformation along the fiber direction and much less sensitive to deformations applied perpendicularly to them.

Nonetheless, Betz et al. [89] performed damage location experiments using FBGs. An initial and very preliminary, and far from optimized, FBG filter and data acquisition systems were implemented – Fig. 3.9. By using rosettes, the incoming deformation waves could be sensed, independently of their propagation direction. Furthermore, such direction could be determined by the comparison of measured wave amplitudes in the sensed signals by the different FBGs in the rosette. The implemented SHM system was able to detect damages with dimensions as small as 12mm (through the thickness circular holes were imposed to simulate damage). Hongo et al. [90] and Frieden et al. [91] also reported experiments with high speed interrogation techniques, involving other filter configurations. Majumder et al. [92] presented a review of the applications of FBGs for

SHM, including Lamb wave based systems. Takeda et al. [93], Lam et al. [94] and Li et al. [95] applied some of these techniques for Lamb wave detection and SHM, with preliminary, but promising results.

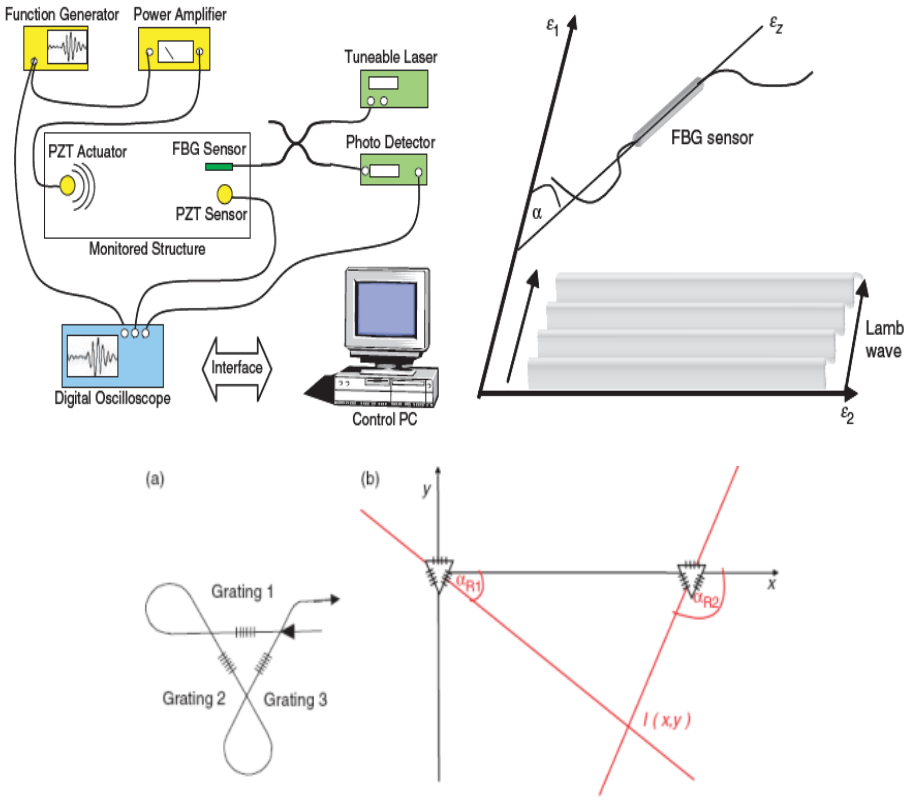

Figure 3.9: FBG system for Lamb wave based SHM [89].

Other promising transducers have been studied and developed for application in SHM systems, as for instance magnetostrictive sensors [96]. Research on the application of Micro Electro-Mechanical Systems (MEMS) with embedded transducers has also been reported [97, 98].

Research has also been performed to assess the optimum application of the different Lamb wave modes for damage assessment. It has been reported the proneness of the application of the S_0 mode to detect internal defects [99, 100], such as delaminations in composite material components, while the application of the A_0 wave proved to be more sensitive to surface damages. It must be referred, however, that both modes were sensitive to any type of damage. With relation to the second symmetric Lamb wave mode (S_1), Rose et al. [101] determined that while the application of the S_0 mode is more

adequate for internal damage detection, the S_1 mode was applied for surface damage detection more successfully. Su and Ye [102], by studying different sensor arrangements, confirmed that careful frequency selection can lead to better mode separation. Furthermore, when comparing A_0 with S_0 mode, it was verified that the latter mode presents also lower propagation amplitude attenuation than the first, with obvious advantages for their application to SHM. To refer that the excitation of either S_0 or A_0 modes can be enhanced by applying two actuators in the same planar position, on opposite surfaces of the component under inspection. By actuating them in phase the S_0 mode is enhanced with relation to A_0 mode, while if actuated in opposite phase, the A_0 mode is enhanced with relation to the S_0 mode. The tuning of the SHM system can also be performed to enhance S_0, or A_0 mode, based on frequency of excitation, corresponding wavelength and actuator dimensions. The best choice of actuation frequency is such that the actuator dimension selected corresponds to half of the wavelength of the wave mode to be enhanced and to a multiple of the wavelength of the mode to be attenuated.

Other studies are centered on the most adequate generation signal waveform for actuation of the desired Lamb wave mode. Through the observation of Lamb waves' dispersion curves, it is clear that if an actuation is applied, such that it is not centered as much as possible around a single frequency, multiple groups of Lamb waves with different frequencies will be generated and will propagate with different velocities. If attention is not dedicated to achieve correct signal generation, the wave propagation pattern can become so complex (with corresponding complexity in sensors' signals) that might compromise its correct assessment. Wilcox et al. [103] performed intensive research on this topic. Furthermore, the applied sensors and acquisition systems must be compatible with such signal generation and corresponding emitted waves.

Two main strategies for transducer positioning are presently being researched, namely, transducers' networks and arrays. Both strategies attempt to reduce the number of transducers to a minimum and maximize sensitivity and reliability on the detection of smaller and different types of damage, while increasing the inspected area covered by the SHM system. Important aspects in the implementation of these different strategies are transducers' types and dimensions to be applied, and relative positions and distances.

Furthermore, for damage location, triangulation algorithms are usually applied, requiring at least three sensors in three different positions.

There are various studies reported in the literature dedicated to optimization of transducers' networks, such as the research developed by Chakrabarty et al. [104]. The main objective of that study was to minimize a cost function which included coverage area and system cost. Staszewski and Worden [105] also studied the optimization of a transducers' network, seeking the best positions and number of sensors for a direct wave analysis damage assessment.

The phased array approach consists on applying a certain number of transducers, which may be aligned in various configurations, depending on the application (in linear, round, cross, star, diamond fashions, etc). By sequential activation, with a predetermined time delay introduced in between actuation of neighbouring transducers, beam forming is possible through constructive interference of the different propagating Lamb waves, generated by individual actuators. Through the variation of such time delay, the wave front can be emitted according to different predefined directions (steered). The time delays for a certain desired direction are determined knowing the wave propagation velocity of interest. Another possibility is to focus the wave front in a certain point (or region around a pre-determined point). For instance, in a damage detection scheme applying a phased array, first a scan is executed in a certain direction (with the wave front emitted and propagating in that direction). If the detection of a possible damage reflection occurs and it is suspected that damage exists in a certain direction, damage location is calculated (through Time of Flight of reflected wave). Afterwards, the wave front can be focused in that point, increasing even more the amplitude of incident beam and consequently of damage reflection. Such can be achieved by performing a single scan, introducing different time delays in between the actuation of consecutive transducers.

Similarly, the phased array principle can be applied to sensing, i.e., wave sensing and potential damage generated reflections sensing capabilities can be focused into a certain direction. This can be achieved by gathering the sensed signals from the different transducers after the execution of a scan (with an actuation either introduced by the phased array, or by any single actuator) and shifting neighbouring sensor signals by a

certain time delay. This time delay is equal to the difference in times at which an incoming wave from the selected direction would reach two consecutive transducers in the array. With this procedure, the reflection from a potential damage existing in that particular direction will appear in all sensor signals at the same time. Afterwards, the different shifted sensor signals are added, so that the potential damage reflection in the scanned direction will be enhanced with relation to the remaining sensor signal. Particularly, the detected reflection will be enhanced with relation to noise and other reflections, for instance from other damages in other directions, or boundaries. This is equivalent to assume a potential damage reflection as a beam, travelling through the different sensors. This approximation potentially enhances damage detection capabilities, since the resultant augmented reflected wave corresponding signal is prone to be detected. However, errors are introduced in the determination of damage location by assuming that the reflected wave is rectilinear (as a beam) and not curved as it is in reality. These errors are smaller if damage is distant from the phased array, since the damage reflected wave segment passing by the phased array will be more approximately rectilinear.

The first advantage of a phased array actuation, with relation to a transducer network configuration, is the amplification of the original mechanical deformation wave actuation. Such actuation enhancement is not based on electric or electronic amplification, which can be, however, optionally implemented. Usually electric, or electronic amplification also introduces additional noise in actuation and consequently in wave pattern frequency and propagation velocities, and subsequent sensing (possibly generating unwanted waves). Through amplification of actuated wave front, potential damage reflections will consequently present increased amplitude and then will be more prone to be detected. Detectable damage size might also be reduced. Even more importantly, the difficulties created due to damping of propagating waves, particularly when structural reinforcements exist, can be diminished.

A second advantage is the capability of scanning the component in all directions, through the execution of several scans in different directions, with the introduction of different time delays. With relation to transducer networks, phased arrays present the advantage of being capable to steer the generated wave front, i.e., to emit the enhanced

actuation in a determined direction, focusing inspection effort into a certain predetermined area.

One disadvantage of phased arrays is that the activated wave front originates always from the same point, or region, in the component under inspection. With the application of transducers' networks, in different scans, different transducers in different positions can be actuated. In the phased array approach, since the generated wave origin is always in the same location, the incident wave with relation to a potential damage will always come from the same direction and side, what is not true for transducers' networks. As a result, damages that present a detectable dimension at least in one direction, even if their dimensions in other directions are considerably small, are prone to be detected with a network. Such might not be true for phased arrays. A damage that presents a small dimension perpendicular to a radial direction with relation to the phased array, (considering the origin as the phased array position), might not be detected - even if it has considerable and detectable dimensions along that radial direction. This disadvantage is however diminished by the increased amplitudes introduced by the phased array, either in actuation and generated wave front, or in the resulting damage reflection corresponding sensed signal.

The principle applied to phased arrays is similar to what is applied in static radar arrays, medical imaging ultrasounds and conventional NDT&E ultrasonic inspection phased array systems [30]. The difficulty in the application of phased arrays to SHM, involving Lamb waves and their generation, is mainly related with the required phased actuation system. Due to the high propagation velocities of Lamb waves, such system must be capable of reliably and accurately introduce diminutive time delays involved in the phased array approach. Simultaneously, all the requirements related to Lamb wave generation must be considered. Particularly more complex generation signals are involved with required significant amplitude, time and specifically frequency definition. Such accuracy is even more important when the fast propagating S_0 wave is selected as the mode of interest to be activated by the phased array and to base the damage detection system on. For these reasons, the development of automated and dedicated phased array actuation systems, for S_0 Lamb wavefront emission, is not reported in literature.

Actuation systems for the applications referred in the beginning of the previous paragraph rely in their majority in the generation of bulk pulses or pulse trains. In the specific case of conventional NDT&E ultrasonic inspections, based on phased array systems involving high frequencies, such actuation waveforms degenerate in the actuation of the scattered bulk body waves. Application of a phased array reduces the difficulties created by such scattering, by promoting a wave front with relevant amplitude, propagating into a determined direction of inspection, i.e., focusing the inspection efforts into a determined region. Even though, those systems are only capable of localized damage detection and particularly through the thickness of the structure to be inspected (due to significant wave scattering, poor definition and propagation amplitude damping).

A phased array actuation system cannot be based, at least uniquely, in simple multiplexing techniques involving a single channel signal generation input and multiple outputs - one for each actuator. With such approach, the application of minimal time delays - corresponding to the generation of a wave front propagating in directions approaching the perpendicular to the phased array – would not be possible. The reason is that with such small delays, although phased, actuation will occur in different transducers at a certain time. To consider multiplexing, delay or repeater circuits must be employed in each channel output, for each actuator, usually at the cost of loosing signal definition. Not to consider multiplexing, a dedicated signal generation and actuation circuit must be developed and applied to each actuator. A precise master circuit must then be implemented to control time delays and the activation of each slave actuator circuit.

The application of multiple actuation circuits results in complex and costly systems. Currently, there are reported efforts in research, development and application of this type of systems for both conventional NDT&E ultrasonic inspection using phased arrays and SHM systems [29, 106, 107]. Accellent [106] developed a similar system that is now commercially available. However, besides an elevated cost, it does not allow a simple selection of generation signal waveform. At the same time, this system requires the application of a considerable number of transducers to achieve reliable damage detection. Furthermore, minimum damage detectable dimensions are in the order of centimetres. There are also reported efforts to adapt originally National Instruments [107] developed

boards for signal generation in multiple channels. During the research reported in this thesis, that system was also investigated. It was verified that the synchronizing time accuracy of the master system, necessary to apply the required precise time delays, was insufficient.

Due to the difficulties related to actuation of phased array Lamb wave based SHM systems, the majority of reported research involves uniquely the referred phased array principles in sensing. Bao [108] and Purekar [109] studied this approach applied to linear arrays. Bao [108] by means of simulation and experimental work, successfully detected and located a 19mm crack introduced in a 2mm thick Al2024 plate – Fig. 3.10.

More recently Pena et al. [110] and Malinowski et al. [111] reported the successful application of SHM Lamb wave based phased arrays for damage detection. These systems included also dedicated actuation systems developed by the authors. To decrease the complexity of such actuation systems, the authors selected to base the system and damage detection algorithm on the slower A_0 Lamb wave mode.

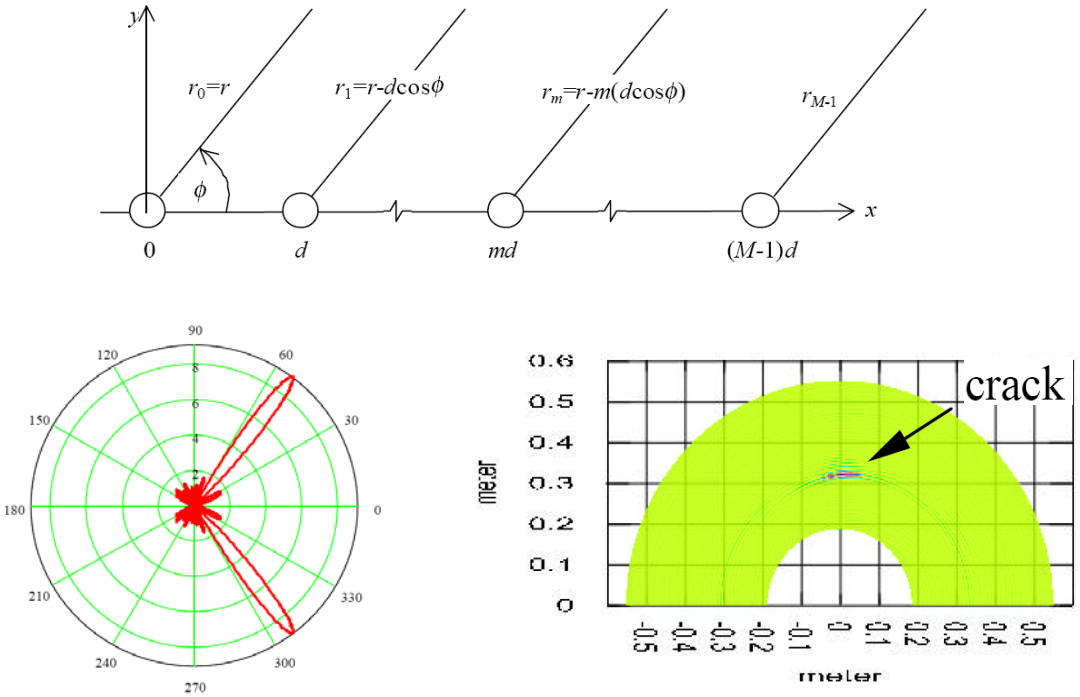

Figure 3.10: Implementation, wavefront steering and resulting damage scan image, from phased array system [108].

Salas and Cesnik [112] developed a new concept of PZT transducer fabrication meant to produce similar results as a phased array - CLoVER. In this particular case, one probe contains eight independent transducers, each one responsible for enquiring a determined azimuth – Fig. 3.11. Analytical studies and experimental damage detection scans, with the introduction of simulated damages, were performed successfully. Main advantages reported for the CLoVER were: its flexibility and conformability to curved shapes; its capability of generating multiple modes; and possibility of independent sensor/actuator function for each one of its individual transducers.

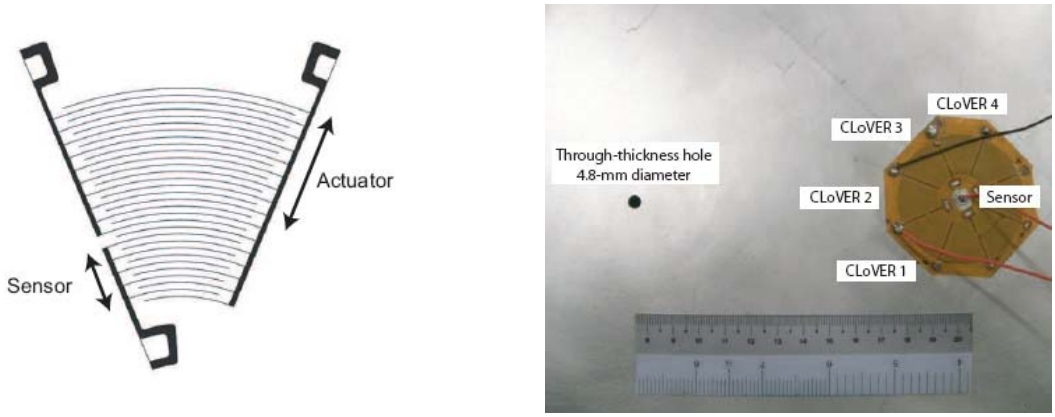

Figure 3.11: CLoVER transducer [112].

With relation to signal processing techniques, directly from sensors' signals, in amplitude vs. time, it is possible to extract corresponding wave modes' signals, their boundaries' reflections, Time of Flight and consequently propagation velocities. To improve accuracy on sensor data assessment, reducing noise influence, data post processing techniques must be applied. For instance, Bao [108] used the signal Root-Mean-Square (RMS) and energy densities by Hilbert transform with such objective. However, usually further data processing techniques must be applied to achieve an accurate damage detection based on the comparison between a baseline (corresponding reference or undamaged state signal) and the current, or damaged state signal. Usually, normalization and data shifting in time (tuning/aligning time origins) are necessary to synchronize both responses. Michaels and Michaels [113] used both normalization and data shifting during a damage detection experiment on an aluminum plate with a bonded transducer network of 4 elements. Using this approach and with damages introduced near sensors, 6.4mm holes, were successfully detected.

Time reversal is also used for damage location. The implementation of this technique does not require the previous knowledge of a baseline response for future comparison with inspection scan responses. However, the propagation velocity of the waves (and wave mode) of interest, to be employed in the algorithm, must be known. Time reversal is particularly interesting for passive sensing applications, i.e., when an actuation is not required. For instance time reversal can be applied in the implementation of Acoustic Emission detection methods [114]. Sohn et al. [115] also applied this method successfully for delamination detection on a composite panel, with a combined transducer actuation. On the delaminated plate, the sensed signals mismatched the original signals created by the actuator – Fig. 3.12. This approach was focused in assessing that feature, only for waves propagating in the direct path established between sensor and actuator. With this limitation, time reversal signal processing techniques became feasible only when relatively high density transducer networks were applied or in 1D specimens. Still, very small damages could be detected.

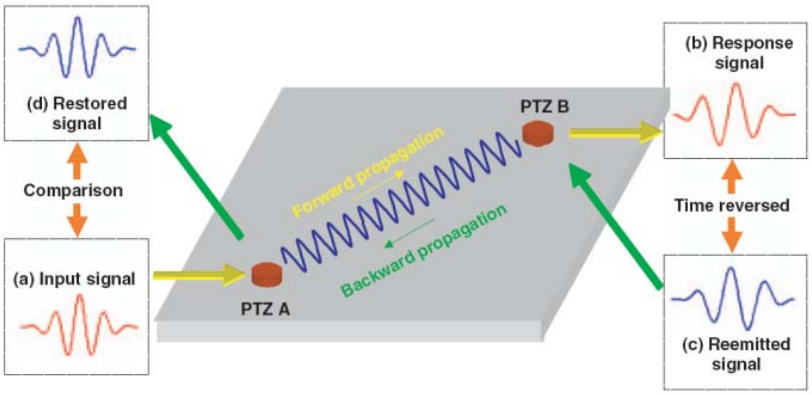

Figure 3.12: Time Reversal example [115].

Xu and Giurgiutiu [116] dedicated part of their research to assess the effects of mode selection, i.e., actuation wave tuning, on the application of time reversal post processing techniques. They concluded that system tuning for actuation (and posterior sensing) of a single wave mode is essential to enhance the method reliability.

Post processing techniques commonly considered for Lamb wave based SHM derived data include Fourier Transforms (FT), Fast Fourier Transforms (FFT) and two-dimensional FFT (2D-FFT). These techniques allow for posterior signal filtering, signal

reconstruction, noise reduction and ultimately to focus damage detection algorithms in the frequency of interest (of actuation). This last aspect is particularly interesting if care is not dedicated to achieve an accurate and efficient actuation, centered in a single frequency, with the consequent generation of multiple groups of waves with different frequencies and propagation velocities. In that case, these techniques enable the selection of the waves (frequencies) to be considered in the SHM inspection system. Interesting experimental results were attained by Gomez-Ullate et al. [117] using 2D-FFTs on data collected using a vibrometer. Gao et al. [118] performed similar experiments, with the implementation of referred techniques, using now laser actuation and sensing, on a copper plate. Based on identified waves and corresponding modes and properties – Fig. 3.13 -, the plate's mechanical properties were calculated.

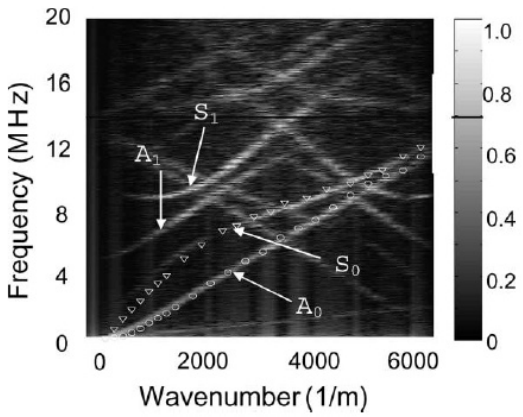

Figure 3.13: Lamb wave modes detected by Laser sensing and application of FFTs [118].

Joint time and frequency domain analysis can also be applied to sensor signals, for data post processing. These methods conjugate both phase and frequency variations along the time response. For such analysis, sensor signals (amplitude vs. time) are divided into different time segments. In a specific time range, the signal is then decomposed into several amplitude and phase components, for different frequencies. These methods promote a more accurate signal assessment in the time segments of interest, by either noise reduction, and/or allowing to assess uniquely one or more specific frequencies of interest. Two interesting techniques included in this particular type of data post processing are Short Time Fourier Transform (STFT) and Wavelet Transform (WT). Paget et al. [119] executed experimental impact tests on a composite panel, with the

application of Wavelet Transforms to decompose sensor data. Relative WT coefficients changed accordingly from a healthy condition to three different conditions of increasing levels of impact energy. This approach provided significant information for damage assessment.

In order to assess damage severity, damage indexes are also usually applied. Damage indexes are established from the comparison of certain features, extracted from sensor signals. One interesting damage index, usually established, is based on Distance to Amplitude Correlation (DAC) of the propagating waves, similarly to what is used in conventional NDT&E ultrasonic inspections. DACs are established based on propagation wave amplitude damping. This can also contribute for the determination of the distance in between sensors and damage. Damage indexes are based on the correspondence between damage generated reflections' amplitude and projected damage dimensions in a perpendicular direction to wave propagation, promoting the determination of damage severity. Basically, after damage detection and determination of damage location, and distance between damage and sensor, DACs can be applied to obtain damage reflection amplitude, at damage position, from the sensed reflections amplitude. Based on the corrected sensed reflections amplitude, through DACs, damage indexes can be established. Examples of the application of this feature are given by applying it to signal amplitude in time domain [120], to RMS magnitude in the time domain [121], or in frequency domain [77] and combined domains [122].

After signal acquisition and data post processing, qualitative and/or quantitative characteristic features related to damage existence can be extracted. Depending on transducers' disposition (networks or arrays) and on extracted features, different algorithms for damage location can be applied.

The application of Neural Networks (NN) [123] has also been and is still being actively investigated for fast and accurate data post processing in Lamb wave based SHM systems, with promising results. The implementation of Neural Networks is based on the consideration of different features of sensors' signals and optionally on the different sensors themselves. Neural Networks are based on multiple, individual decision making neurons which must be trained before to achieve a correct decision output. This is in fact

the main disadvantage of this technique: it is not readily available. Long learning periods and complex training are required. This technique can learn based on previous results obtained from the system (and structure, geometry, material, etc) to which is going to be applied. Such results might be obtained either experimentally or through system simulations. Considering damage detection systems, it is not time wise and cost wise practical the execution of multiple experiments, considering multiple damage types, positions, orientations, etc. For instance, if it is desirable to test one component with a single damage, varying that damage dimensions, or orientation, numerous test components would have to be damaged, one for each experiment to perform. The obvious solution is that NN must learn from simulation results. This justifies the development of numerical simulations discussed before. However, simulations are still not perfect and do not absolutely match reality. Difficulties in damage simulation, wave propagation pattern simulation, etc, still exist.

When transducers' networks are considered, there are two possible approaches for damage detection: pitch-catch, and pulse-echo. Pitch-catch is based on the detection of the scattered wave caused by damage existence in the direct path between an actuator and sensor pair. A relative high number of sensors is frequently needed in this case. The simplest approach implies creating a sufficient dense grid, established by numerous direct paths established between every transducer pair available. Ihn and Chang [124] tested successfully this principle on an Airbus aircraft panel – Fig. 3.14. Using two strips with eighteen PZT transducers each, damage indexes based on sensed wave energy were calculated. Cracks with dimensions as small as 4mm were detected, with damage length being linearly proportional to established damage indexes.

The application of time reversal techniques is also adequate for pitch-catch implementations. The intersection of at least two direct concurrent paths established by different pairs of transducers, whose reversibility failed, indicates damage location. The relationship between reversibility magnitudes detected can contribute to the determination of damage dimensions.

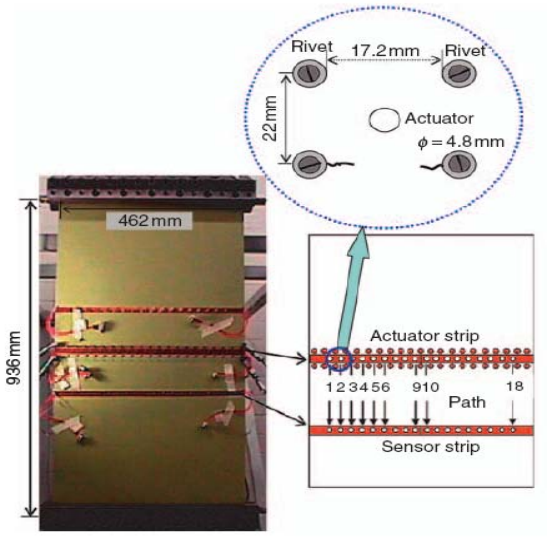

Figure 3.14: Pitch-catch test example [124].

Pulse-echo techniques rely on the fact that activated wave echoes produced by a damage can be captured by sensors in the network. This is an active approach requiring actuation and activation of waves. It totally depends on successful and reliable detection and assessment of potential damage reflected waves in corresponding sensed signals. A smaller number of sensors are required, in comparison with the previous approach. Disadvantages of this technique are also related to the smaller number of sensors employed and the possibility of active waves having to travel through longer distances with considerable amplitude attenuation to reach those sensors. If that occurs, the method will present inferior detectability and will be more prone to noise interference, with consequent information loss. Raghavan and Cesnik [125] performed tests for damage location using a transducer network – Fig. 3.15. Holes with diameters as small as 5mm were successfully detected and located applying the pulse-echo technique.

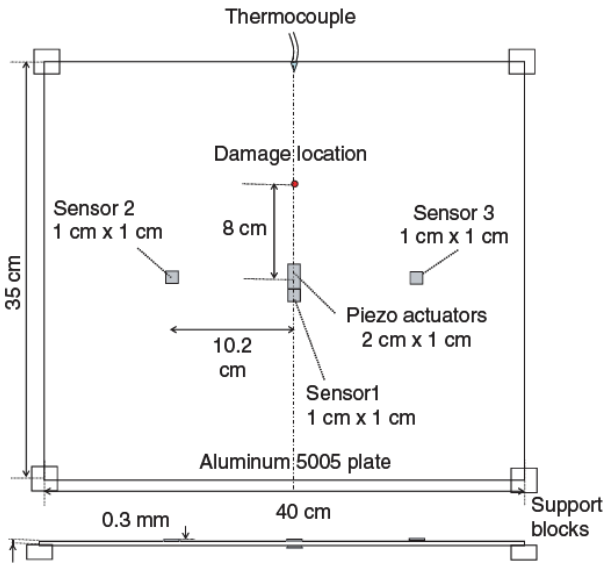

Figure 3.15: Network experiment setup [125].

During this study, temperature influence on the system was also analysed and the main conclusion states that both PZT transducers performance and bonding material can be affected. Basically small offset variations occur in sensor signals, in a temperature range of 20ºC to 80ºC. However, for higher temperatures (80ºC to 130ºC), activated wave peak amplitude is also significantly decreased. Furthermore, variations of host material Young modulus and wave phase velocities were also assessed – Fig. 3.16.

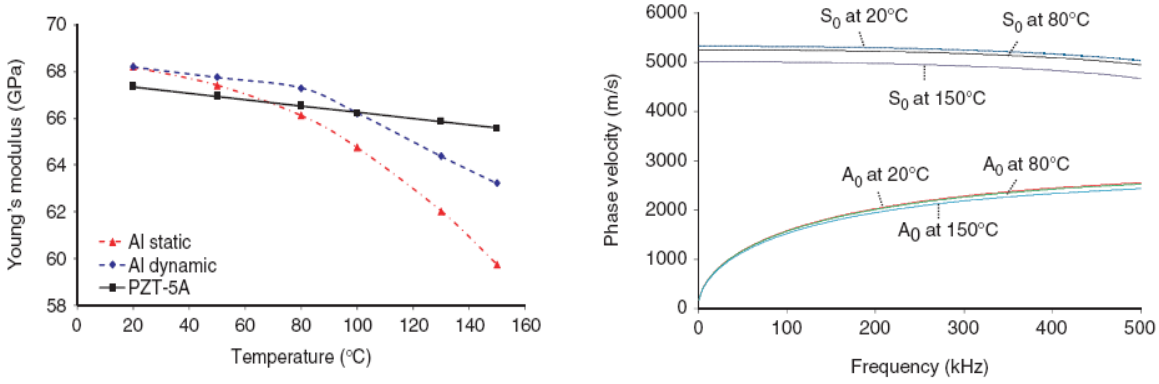

Figure 3.16: Host material Young modulus and wave phase velocity variations with temperature [125].

For both pitch-catch and pulse-echo approaches, waves' Time of Flight (ToF) is frequently used to determine potential defects' location, knowing the wave propagation velocity of interest. ToF consists in the time interval between the successful detection of

a (potential damage generated) wave reflection, in the corresponding sensor signal, and actuation, i.e., the propagation time of the original activated wave plus the propagation time of a (potential damage) wave reflection. For an accurate determination of a potential damage location, this time must be precisely established. For the particular case of pulse-echo, the application of at least three sensors enables the use of triangulation schemes.

Another available method is named migration technique. This approach does not require a baseline for comparison and is based on a geophysical method to detect seismic epicentres, in use for the last fifty years. Some research efforts have been dedicated to explore the viability of application of such method in Lamb wave based SHM. Wang and Yuang [126] studied its implementation to the inspection of a quasi-isotropic composite panel with two distinct delaminations. The active wave propagation pattern was calculated by time reversal of the sensed response in several time steps. Such resulted in the development of a step by step visualization technique – Fig. 3.17. On this particular case, the two 0.1m x 0.1m delaminations were successfully identified. Here, existing damages were treated as wave sources, according to Huygens' Principle.

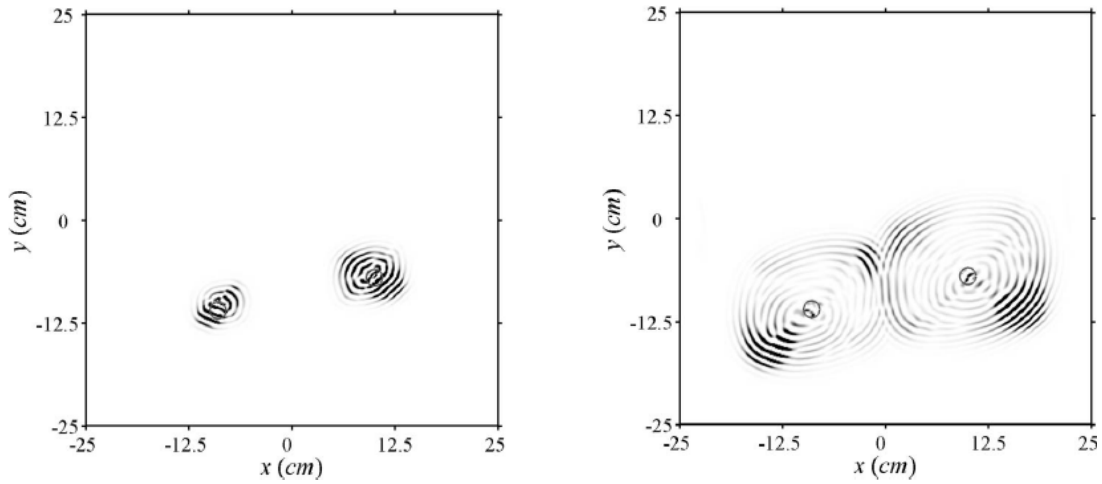

Figure 3.17: Migration techniques [126].

For phased arrays the pulse-echo technique is commonly applied. The main difference, with relation to the application of pulse-echo techniques with transducers networks, is based on the fact that the damage location azimuth is pre-determined by the phased array wave front steering. Thus, if the echo ToF is obtained for a determined scanned azimuth, knowing the wave propagation velocity of interest, damage location can be found.

Different phased array arrangements are currently being studied. Malinowski et al. [111] conducted a numerical study, with the use of spectral elements, to assess a star shaped array performance on damage detection, with encouraging results – Fig. 3.18. This shape is being considered as an attempt to overcome the difficulties related with application of linear phased arrays. Interference between transducers and generated waves from neighbouring transducers (or in the sensing mode, from transducers to the damage generated reflection wave), results in wave front amplitude damping when the wave front is steered along the linear phased array direction. Smaller wave front amplitudes result in smaller potential damage wave reflection amplitudes, more prone to noise influence and more difficult to detect in sensor signals - and then in a decreased damage detectability. The advantage of phased array inspections is compromised in those directions. Furthermore, linear arrays, if placed in the middle of a panel, generate two wave fronts propagating in opposite directions, such that if a damage reflection is detected there will be two possible damage positions.

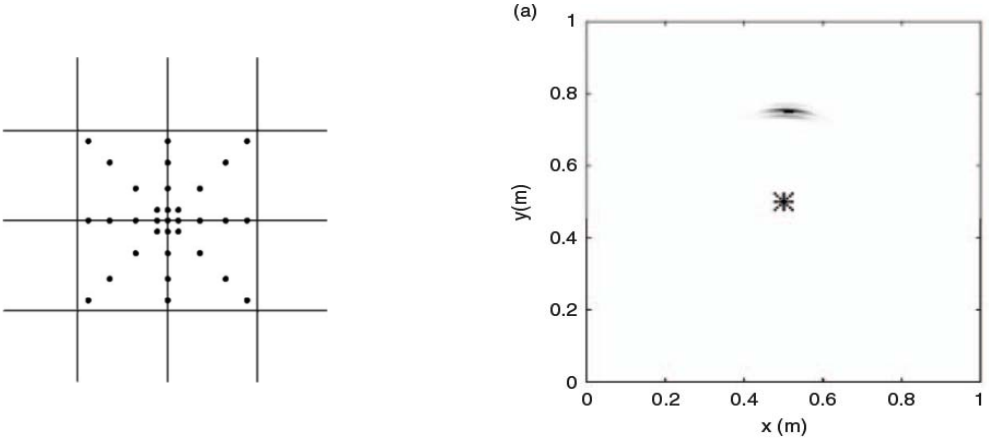

Figure 3.18: Star shaped array [111].

Finally, Yu et al. [127] summarized analytical and experimental work using PZT transducers for damage location in thin walled structures, both in isotropic and orthotropic (composites) host mediums. Results show that available techniques (networks and phased arrays) using different approaches (pulse-echo, pitch-catch and time reversal) are suitable for damage detection. Influence of operational and environmental characteristics variations and bonding materials reliability were also addressed. One of the conclusions is the required improvement in reliability of PZT transducers bonding.

Finally, the advantages of having transducers equipped with processing wireless units were also pointed.

Research efforts have been reported in 2010, related to the development of Lamb wave based SHM systems [128, 129], visualization algorithms [130] and specifically frequency tuning [131], in between others.

3.3 - Contributions

From the presented literature review it is understandable that most of independently developed research efforts are focused on a single, or on few aspects of the all complexity of this problematic – development and application of Lamb wave based SHM systems for reliable and accurate damage detection. On their majority, these research efforts are not focused in the broad integration of the different knowledge and aspects reported into a single SHM system. These are based on that such a SHM system is not yet mature enough to be adequate for a reliable practical application; so that most of research efforts can be seen as extremely important contributions to achieve such future integration.

A great part of the reported research is based on laboratory experimentation, with the inclusion of simplified boundary conditions, application of considerable number of sensors with near simulated damages and with the use of not fully automated actuation, or data acquisition and post processing systems. Just a small number of reported research efforts and system development is applied to and tested in real applications, or at least more close to reality.

Furthermore, to be competitive and then to be considered for replacement of current NDT&E methods applied to aircraft structures in operation, a SHM system must be capable to reliably detect defects with smaller dimensions. The term reliably meaning that a SHM system must be able to detect repeatedly damages with dimensions in the range of 0.5mm and with great confidence damages with dimensions of 1mm. Reported minimum detectable damage dimensions, across the literature, with no reliability considerations involved, are of the order of 3mm.

With relation to phased arrays, there are no reports on the development of dedicated automatic (low cost) systems for Lamb wave based SHM, involving accurate generation and application of fast propagating S_0 wave fronts. Previously several characteristics of the application of the S_0 mode, in comparison to the application of the A_0 mode, were referred. The former presents smaller propagation amplitude damping, while the latter presents a smaller wavelength (for the same frequency), being theoretically more prone to detect smaller damages. However, the deformation pattern imposed by the A_0 mode (as a transverse or bending wave) results in lesser interference with damages and consequent more difficult damage detection, particularly when interior damages are considered.

Nonetheless, the high propagation velocity of the S_0 wave mode introduces difficulties and related complexity in actuation and sensing systems. Accurate time definition is required to achieve correct actuation and implementation of damage detection and localization algorithms. Furthermore, when phased arrays are considered, accurate time definition is necessary to set precisely the small time delays in between actuation of consecutive transducers in the array, to correctly generate a wave front. However, one of the advantages of using S_0 Lamb wave mode, in detriment of A_0 mode, lies exactly in its high propagation velocity, being less prone to interference from the slower A_0 mode and its reflections. Oppositely, the slower propagating A_0 wave mode always appears after the S_0 mode, with the wave pattern of the former being prone to interference by the later, in particular by S_0 reflections, either damage or boundary originated. For these reasons, it was decided to develop the phased array SHM system based on the application of the S_0 Lamb wave mode.

The present work aim for the research, development and application of a SHM system considering in its design several different aspects reported in literature. For instance, the combined application of multiple data post processing techniques in a parallel fashion. Such enables superposition of results to enhance damage detection capabilities and reliability.

The objective of this research is to obtain a final, relatively simple and low cost system, capable for a near future reliable application in real aircraft structural components. It is, in fact, planned the application and testing of the developed system in real aircraft, in

operation, in the near future. The final system should be competitive for replacement of conventional NDT&E. Furthermore, such system will aim to be capable of detecting smaller damages in components with any boundary conditions, using a minimized number of sensors and with a wide inspection area coverage. The developed system will include phased arrays with a dedicated automatic system for the activation and use of S_0 wavefronts for accurate damage detection.

Chapter 4

Development of a Phased Array Actuation System

Previously, research was developed and experiments were performed with the implementation of a PZT network for SHM, applied to aluminum and composite material panels [4]. During that study it was verified the small amplitude of generated and consequently (boundaries and damages) reflected Lamb waves. Particularly, damage generated wave reflections were of extremely small amplitude and then prone to noise interference and more difficult to detect (in corresponding sensor signals). Aggravating this fact, damage reflection wave amplitude decrease considerably when smaller damages are considered, introducing paramount difficulties when trying to decrease the detectable minimum damage dimensions.

Such is related with the single actuation that occurs in a transducer network. A possible way to increase the amplitude of emitted waves would be the use of actuation signal amplification, with the use of amplifiers. This solution introduces, however, two main difficulties: inclusion and amplification of noise with relatively small improvements in SNR; and the fact that the actuation signal applied in the referred experiments (in the range of ±18V, permitted by the maximum output swing of the used signal generator) was already close to the maximum voltage and charge permitted by the PZT transducers used - previous experiments resulted in the depolarization and damage of the small transducers used, when the actuation signal was amplified to a range of ±21V.

The solution to increase amplitude levels of actuation and reflection waves (specifically of damage, when smaller sizes have to be considered in order to reduce detectable damage dimensions) was then to use multiple actuation. The objective is then to promote constructive interference in predetermined positions of the plate, between the waves excited by several single actuators (beam forming, or generation of a wavefront). Since actuators will have to be in different positions on the panels, a phased actuation is

necessary. The phased actuation implies that small time delays will be introduced in between the actuation of neighbouring transducers. The time delays to introduce are related with the (relative) positions at which transducers are applied on the plate (configuration of the array); distance in between them (considering a linear array, its pitch); the propagation velocity of waves to excite; and the propagation direction of the generated wavefront. By varying the time delays, the wavefront propagation direction can be modified (steered). Inspection can then be focused into predetermined regions of the component, while by modifying time delays in between different scans, the component can be entirely inspected.

In the PZT network experiments, a National Instruments (NI) PXI-5421, 100MS/s Arbitrary Waveform Generator, with 16 Bit resolution, 8MB of internal memory and a single output actuation channel was used for signal generation and actuation. Due to the high propagation velocities of Lamb waves to excite, in order to achieve successful constructive interference, time delays to be introduced will be extremely small. Such means that even when phased actuation is considered, at certain times multiple transducers will be actuating simultaneously. The implication of this fact is that a single actuation channel simply demultiplexed cannot be applied. Delay circuits would then have to be considered, with the introduction of noise and imprecision in the establishment of time delays. The conclusion is that multiple actuation channels are required. As stated before, besides presenting extremely high cost of acquisition, existing systems with multiple actuation channels commercially available, or under research, suffer either from:

- not offering enough precision in time definition for the correct establishment of smaller time delays required for the generation of fast propagating S_0 wavefronts – some of the commercial available systems are capable only to establish the correct actuation signal to generate S_0 waves in a single channel at a time; while phased array systems under research generate slower propagating A_0 wavefronts, relaxing the requirement of high definition in time, since to generate slower wavefronts, the time delays to introduce are higher;

- or not even being capable of the generation of the correct actuation signal for each individual actuator, in terms of time or (higher) frequency definition - or at least not offering the capability of the user to define such actuation signal (black/closed box systems), either in terms of waveform or frequency selection, restricting its application to certain conditions, materials and components.

The obvious conclusion is that a lower cost, dedicated multiple channel actuation system had to be developed. The system must be capable of a high time definition, to establish precisely: the required small time delays in between consecutive channels/transducers to be actuated, for the correct generation of the fast propagating S_0 wavefronts; and the correct actuation signal waveform and (high) frequency, for the generation of the single, fast S_0 waves, by each transducer.

For the reasons stated previously, PZT transducers were selected, to be applied in the phased array SHM system. This selection is based on the fact that a single PZT transducer can be used as an actuator and as a sensor. Furthermore, PZT transducers can be used in techniques involving high frequency generation and sensing. As the basis for a future development of arrays with different configurations (cross, star, circular shapes, etc), it was decided to implement a linear array to excite fast propagating S_0 wavefronts (the selection of this wave mode was based in the reasons stated before). A linear array presents advantages in terms of a simpler development. At the same time, different array configurations can be seen as a combination of multiple linear arrays, while solving the disadvantages in terms of inspections introduced by a single linear array (also referred before).

Also to simplify the implementation and testing of this phased array SHM system in development, it was considered its initial application to aluminum plates (isotropic materials, with homogeneous properties and then constant wave propagation velocities in all directions). However, in its development it was also considered its future application to panels made of composite materials (orthotropic), presenting different mechanical properties in different directions and then with wave propagation velocities depending on the direction considered. This fact became also important even for the experiments executed in aluminum panels, since, due to their manufacturing processes, mechanical

properties are not exactly the same in all directions. Small relative differences in properties exist, for instance due to the lamination direction in aluminum plates. These small relative differences are translated to considerable absolute values when the high values of Young modulus and wave propagation velocities are considered. In the previous experiments with the PZT network SHM system, differences around 200m/s (however less than 0.5%) were verified in the propagation velocity of the S_0 wave in aluminum plates, in different directions.

The development of the phased array SHM system accounted for its future implementation in real structural panel components, in the sense that it was considered, in its development, its experimentation in representative plates with more stringent boundary conditions. For instance, experiments with the plate totally supported (increasing wave propagation damping), with simply supported and riveted boundaries were considered.

Furthermore, experiments were considered to be performed in environmental conditions close to reality. Some experiments were considered to be executed in an aircraft maintenance hangar, without any surrounding sound/noise control and with limited temperature control.

4.1 - Dispersion Curves

As referred before, Lamb waves present a dispersive behaviour, i.e., their propagation velocity depends on their frequency. Such behaviour significantly influences the implementation of a SHM technique based in these waves and its consequent performance. It is extremely important to calculate and carefully analyse Lamb wave dispersion curves for the component (material and thickness) to be inspected, before designing and implementing a dedicated SHM system.

Considering the Young modulus, density and Poisson ratio for the Al2024 plate and plate thickness:

Young modulus (E)	70GPa
Density (ρ)	2700Kg/m^3
Poison ratio (υ)	0.35
Thickness (h)	0.002m

Longitudinal and transverse velocities were calculated using Eqs. 3.13 and 3.14:

$$C_P = 6450.05 m/s$$

$$C_S = 3098.70 m/s$$

Rayleigh-Lamb Eqs. 3.34 and 3.35 were numerically solved for frequency and Lamb wave phase propagation velocity. The phase dispersion curves for the first two Lamb wave modes, S_0 and A_0 waves, for frequencies up to 3.5MHz, were obtained – Fig. 4.1. The simple numerical procedure consisted in a solution search algorithm implemented in MATLAB®.

As it can be observed for frequencies higher than 700kHz, higher Lamb wave modes are excited (than uniquely the first symmetric and anti-symmetric modes). Initially, the interesting range of actuation frequency for the application of the SHM system becomes then limited by that upper value. As referred before, since higher Lamb wave modes do not propagate, complexity of wave pattern and corresponding sensed signal is decreased. Sensor signals can then be more effortlessly assessed with less interference in between different waves (modes).

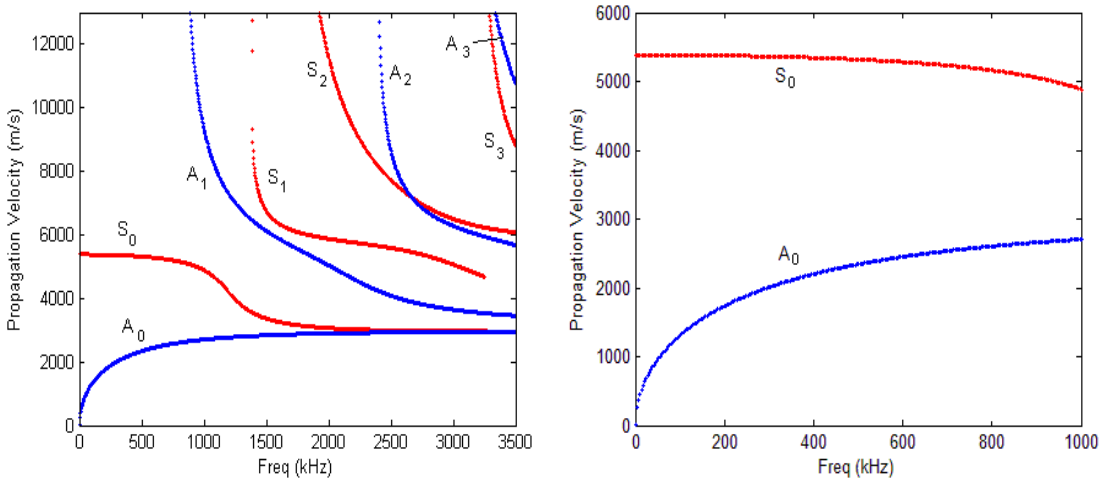

Figure 4.1: Phase dispersion curves.

Group velocity was then calculated and the corresponding dispersion curves determined – Fig. 4.2.

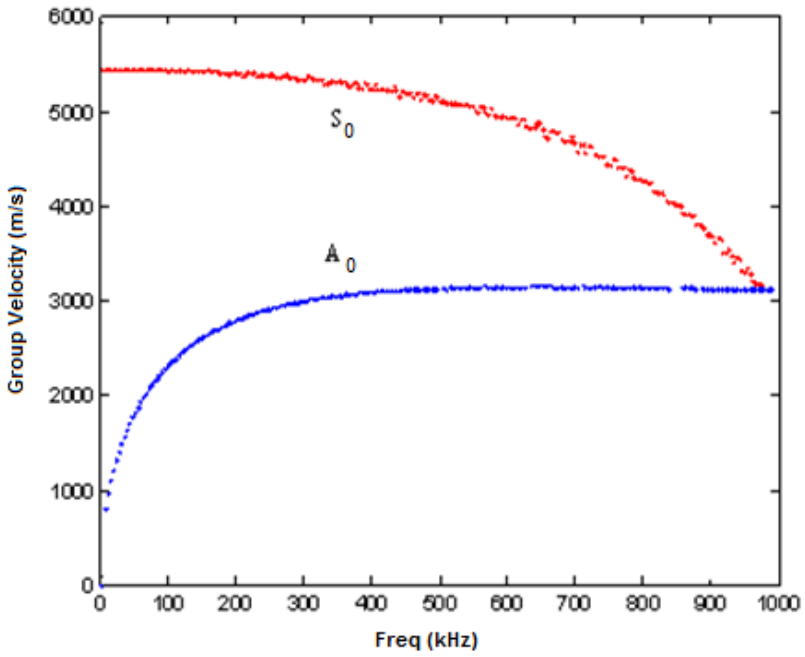

Figure 4.2: Group dispersion curves.

These curves were calculated also for frequencies up to 3.5MHz, however, they are presented only to frequencies up to 1MHz, for the reasons presented before.

It is observable that phase and group propagation velocities of the first modes are similar for frequencies up to 400kHz. Also, as referred, such is desirable to avoid the spreading of wave groups in space while propagating, and consequently in time, in corresponding sensed signal. In this frequency range the difference between propagation velocities of both modes is considerable, enabling a good separation in their propagation in space and consequently in time in corresponding sensor signals, again simplifying sensor signal assessment. This difference is decreased with increasing frequency, being reduced to zero for higher values. Furthermore, both S_0 phase and group propagation velocities do not considerably change in that frequency range. This is important since any small error introduced in their generation frequency will not result in considerable differences on S_0 propagation velocity and consequently in erroneous determination of potential damages' location, compromising the inspection method. Due to its high propagation velocity, any small error in between its real and considered propagation velocities would result in the inspection method missing the damage location considerably.

From this analysis it becomes evident that an activation frequency range up to 400kHz is optimum for application of Lamb waves for SHM, specifically for the aluminum plate considered.

With the dispersion curves, wavelength vs. frequency curves were determined – Fig. 4.3.

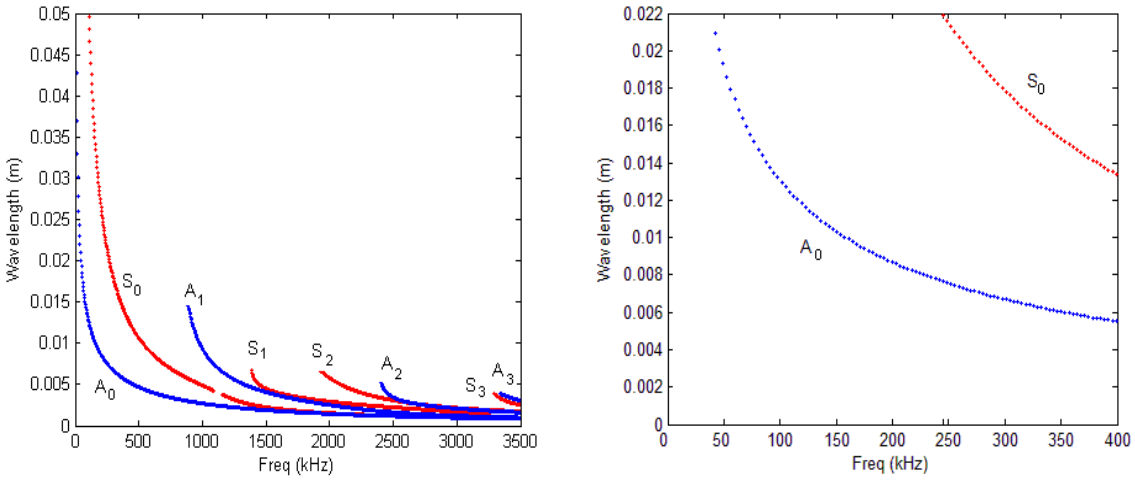

Figure 4.3: Lamb waves wavelength.

These curves are extremely important for the selection of optimum PZT transducers diameter and phased array pitch, for the frequencies to be applied. PZT transducers actuation and sensing capabilities are amplified when their diameter is closer to half of the wavelength to be emitted. At the same time it must be remembered that smaller damages are more prone to interfere with smaller wavelengths.

Regarding the implementation of phased arrays, so that undesirable side lobes are not generated, the phased array pitch should be less than, or equal to half of the wavelength to be excited [132]:

$$pitch \leq \frac{\lambda}{2} \tag{4.1}$$

Since the array pitch is equal to the dimension of one of its PZT transducers plus the spacing in between consecutive elements in the array, the tuning of such system (selection of excitation frequency and wavelength) should now be performed with relation to the array pitch and no longer with relation to the PZT element dimensions. However, it is still true that the amplitude of generated Lamb waves is increased when the dimension of the PZTs used approaches half wavelength of excited waves. The logical conclusion is that the array pitch should be equal to half of the wavelength of waves to be activated and the PZT transducer dimension should be as close as possible to the phased array pitch, reducing spacing in between consecutive elements to a minimum. Nonetheless, neighbouring elements should not be in contact (and not even their bonding material). If contact existed, the actuation of one element would be passed to the adjacent element, creating actuation noise and interference on the later PZT. To enforce this condition, while trying to minimize the spacing in between consecutive elements of the array, and due to practical aspects, it was considered a spacing of 3mm - to account for 1mm around each transducer to be potentially occupied by its bonding material and 1mm of effective spacing. This means that it was considered that the PZT elements have a diameter equal to the phased array pitch (equal to half of the wavelength to be excited) minus 3mm.

4.2 - Tuned Lamb Waves: Mode, Frequency, Array Pitch and Transducer Selection

Based on referred considerations, and as mentioned in the literature review, the inspection system can be tuned for application of a certain wave mode and frequency. Tuning means that the desired mode to be applied in the method (its generation and sensing) is enhanced, while decreasing the amplitude of the remaining mode. Such is achieved at specific frequencies, for corresponding wavelengths, array pitch and PZT transducers dimensions. To achieve Lamb wave tuning, observation of Fig. 4.3 is essential. Specifically, tuning the system for the S_0 wave can be achieved by selecting an activation frequency and correspondent array pitch (equal to half of S_0 wavelength to be excited, corresponding to the frequency selected), and PZT transducers diameter, such that the PZT diameter is a multiple of A_0 wavelength to be excited, again corresponding to the frequency selected (or at least as close as possible to a multiple). To refer that the higher that multiple is, the more the activated A_0 amplitude is decreased.

Based on the wavelength vs. frequency curves depicted in Fig. 4.3, for all frequencies, S_0 wavelength was halved, with these values being subtracted of 3mm (the spacing in between consecutive elements in the array) to obtain the optimum PZT dimensions (to excite and sense those S_0 wavelengths at their corresponding frequencies). The resulting values were then divided by the A_0 wavelengths excited at the same frequencies. Afterwards, the absolute values of the difference between such results and the nearest integers were analyzed. For an easier representation and assessment of those results, those differences were doubled and the results were subtracted to unity. In such manner, values close to one represent optimum conditions and values close to zero the worse cases. The resulting curve is presented in Fig. 4.4.

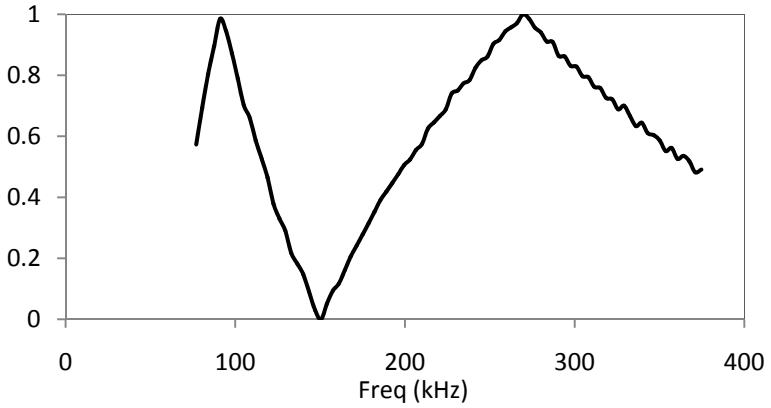

Figure 4.4: Lamb wave tuning.

According to this curve, activation frequencies around 150kHz (and correspondent wavelengths, array pitch and PZT transducers diameters) should be avoided, while frequencies around 100kHz and 275kHz give the best results. It must be remembered, however, that the application of smaller wavelengths is desirable for the detection of smaller damage dimensions, what is achieved at higher frequencies. The frequency of excitation should then be selected to be 275kHz. As a compromise between these considerations, based on the activation frequency range selected (up to 400kHz, as referred); in the application of S_0 as the elected wave mode to base the developed inspection system on; and availability of transducers, PZT discs with a diameter of 8mm were selected. Considering the spacing in between neighbouring elements in the array of 3mm, this corresponds to an array pitch of 11mm (what should be equal to half of the wavelength of the S_0 wave to excite). The corresponding actuation frequency, from Fig. 4.3, is then 245kHz, with the S_0 waves of that frequency presenting a propagation velocity of 5390m/s, in the considered aluminum plate.

Other aspects that must be considered in the definition of the PZT transducers, not yet referred, are related with their thickness and material. The selected PZT transducers have a disc shape with the piezoelectric material principal direction (of actuation and sensing - d_{33}) oriented through the disc thickness, so that a constant actuation and sensing capability is obtained, for all directions in the disc plane (constant radial d_{13}).

Density, mechanical stiffness, aging rate, temperature stability and relative permittivity are significant characteristics of piezoelectric materials. Besides these, some of the most

important piezoelectric material properties to be considered for this application and for transducer definition are:

- Charge constants (V/mm, or C/N), defining piezoelectricity capability, or (direct and reverse) piezoelectric effect capability of the material in the different directions – d_{33} and d_{13}. Here, direction 3 is the principal actuation/sensing direction (principal piezoelectric effect direction in the material), selected to be through the thickness of transducers, and 1 its perpendicular - radial direction for the transducer configuration selected; d_{33} defines the piezoelectric effect capability of the material with mechanical deformations and electrical fields applied in direction 3; d_{13} is proportional to mechanical deformation field output amplitude in direction 1, when an electrical field is applied in direction 3 (important for actuation); and to electrical field output amplitude in direction 3, when a mechanical deformation is applied in direction 1 (important for sensing). Considering transducer shape and orientation of piezoelectric material, d_{13} should be as high as possible in the piezoelectric material selected, to increase actuation amplitude and enhance sensing capabilities.

- Frequency constants (kHz.mm), which define the transducer's natural frequencies of vibration (for disc shapes: N_p and N_t), depending on their shape and dimensions. Specifically for thin discs, radial and thickness natural modes of vibration have to be considered, if the diameter of the disc is higher than ten times the disc thickness. In this case the transducer natural frequency for the radial mode is obtained by dividing N_p by the disc diameter in millimetres. Similarly, the natural frequency of the thickness mode is calculated by dividing N_t by the transducer thickness in millimetres.

In this discussion it is important to note the response properties of a system operating in a frequency near its natural frequency of vibration, particularly, its higher response amplitudes and lower damping. Translating that to a PZT transducer working in one of its natural frequencies, it would present higher mechanical deformation output amplitudes for a certain electrical field imposed, i.e., it would present an amplified actuation, what would be beneficial. Also, it would present higher voltage output amplitudes for a certain mechanical deformation imposed with such frequency, i.e., it would present enhanced

sensing capabilities. This principle was explored in some of the applications of PZT transducers to conventional NDT&E. Probes, including PZT elements, were designed according to certain geometries and dimensions to operate near their natural frequencies of vibration.

However, when the reduced damping is considered, a loss of signal definition in time exists, specifically in the termination of the signal, with increased number of oscillations, or waves generated, with relation to what is desired and specified.

The piezoelectric material properties referred are dependent on the transducers geometry (shape and dimensions). Regarding the piezoelectric effect, since the PZT d_{33} is through the disc thickness, actuation and sensing capabilities of transducers are proportional to their thickness. With increasing thickness, the mechanical deformation output, from transducers, increases, for the same applied input electrical (voltage) signal, i.e., actuation is amplified. The opposite is also true, for the same mechanical deformation applied to transducers, the electrical signal outputted is enhanced with increasing transducer thickness, i.e., sensing capabilities are enhanced. However, the PZT transducer mechanical rigidity increases with thickness, being less deformable and then less sensitive. One advantage of increasing the transducer thickness would also be to increase the piezoelectric material quantity and then increase charge that the transducer can accumulate, without being depolarized. The voltage of the actuation signal could be increased and then actuation could be enhanced.

Furthermore, with the application of simple wire leads to feed the voltage to the transducer, in actuation, for a transducer with considerable dimensions, electrical fields (and consequently, mechanical deformation fields generated) might not be uniform. Electrical contact plates instead of wires could be used to diminish such problem. However, these would increase the overall transducer rigidity, constraining again its deformation and consequently its mechanical deformation output amplitude, i.e., its actuation and sensing capabilities. In sensing mode, mechanical deformations (from the specimen to which the transducer is bonded) are applied to the sensor through the contact surface in between it and the specimen. If the transducer presents a considerable

thickness, these deformations can be considered as local deformations and then the mechanical deformation field is far from uniform in the transducer.

In addition, transducers mass and rigidity (increasing with increased thickness) affect local characteristics of the combined structure plus transducers, around their position. This affects the wave propagation pattern, as a damage or a structure reinforcement would do. Such might lead to the generation of further wave reflections and localized variation of wave propagation velocities and consequently wavelength, possibly even leading to mode conversion. With increased rigidity, transducers are also responsible for considerable localized wave amplitude damping.

As a compromise between all stated considerations, PZTs with a thickness of 1mm were selected. To note that with a diameter of 8mm and consequently a diameter to thickness ratio lower than ten, the natural frequencies and modes of vibration do not have to be considered for the PZTs selected. The PZT material selected was Ceramtec's Sonox P502, known for its good working performance at high frequencies, with a wide range of known applications, and presenting a desirable high d_{13}.

4.3 - Number of Elements in the Array

To be able to inspect an entire component, the scans performed by a phased array must be repeated, with the wave front being steered into different directions in the component in each scan. Consequently, different time delays must be applied in between the actuation of consecutive array elements, in the different scans. To define the directions (and related time delays) that must be considered to enable the inspection of the entire component, the aperture of the generated wavefronts must be taken into account. The aperture angle is centred around the propagation direction of the wave front generated by the phased array. It defines the region where such propagating wave front will be effectively formed and then the useful inspection region for each scan direction considered.

Such aperture ($\Delta\alpha$) is dependent on the total length of the phased array (l) - the phased array pitch and number of elements in the array (n) - and on the excited Lamb wave wavelength (λ) [132]:

$$\Delta\alpha \simeq 0.886\frac{\lambda}{l} \simeq 0.866\frac{\lambda}{n.\ pitch}\ (rad) \tag{4.2}$$

This relation is valid for all angles of the propagation direction of the array generated wavefront (in an isotropic plate), particularly for angles approaching the perpendicular to the linear array. It is predicted that due to the influence of the array elements into the excitation/propagation of the wavefronts, these will present lower amplitudes (decreasing inspection capability) and will be more spread in space when their propagation direction approaches the direction of the array (increasing the aperture in those directions). Then the aperture calculated according to Eq. 4.2, can be regarded as the minimum aperture. If such value is considered as the angle interval to be established in between consecutive inspection directions, it will be guaranteed that the entire component can be inspected. Simultaneously, the overlap of inspection regions will be promoted and inspection capabilities will be enhanced.

Theoretically, constructive interference in between generated waves from different transducers in the array is augmented (the amplitude of generated wavefronts is increased), when the number of generated waves and then the number of transducers is increased in the array. However, the wavefronts to be generated will be more spread in space in those conditions. As it can be observed from the above equation, such results, in fact, in a lower aperture of the array. As a compromise, it was decided to implement an array with seven elements.

4.4 - Actuation Waveform Analysis

As mentioned earlier, the dispersive behaviour of Lamb waves must also be considered in the selection of the actuation waveform. As a consequence of that behaviour, the actuation signal should be centered as much as possible on a single frequency. If not, multiple waves, with different frequencies and, consequently, propagation velocities, will be generated and will propagate in the plate. This promotes wave interference and

increases significantly the complexity of the wave pattern and corresponding sensed signals, being considerably more difficult to assess.

The generation signal should not be too long in time, not to promote overlaps between actuation and sensing. Furthermore, when a PZT is applied as an actuator, it can only be used as a sensor after actuation is completed. By that time, the generated waves already propagated to a certain distance. If a damage was encountered before half of that distance (since damage reflections have the same propagation velocity as actuated waves), damage reflections would not be sensed by that particular PZT. By increasing the duration of the actuation signal, the area not inspected by the actuator PZT increases. The conclusion that can be retrieved from this aspect is also that there is always a region around the actuator PZTs that cannot be inspected.

Naturally, for a pulse-echo technique it would be important to have an instantaneous or quasi-instantaneous actuation, such as an impulse, square or ramp waveform. These actuation signals would be well defined in time, with a high frequency and then potentially generating waves with smaller wavelengths, more prone to be affected by the existence of smaller damages. The application of these smaller wavelengths would result in a clear detection of potential damage reflections and then improved damage detectability and minimization of detectable damage dimensions. However, these types of signals excite a broad band of frequencies, with their frequency spectrum being spread by a broad frequency range, with the negative effect referred before of exciting multiple waves with different frequencies and propagation velocities.

Those are the types of actuation signals applied previously in conventional NDT&E to generate dispersive, scattering, bulk body waves. The use of these actuation signal waveforms, and their negative effects, is one more reason that justifies the application of those techniques only locally and through the thickness of the component under inspection, for successful damage detection. Other reasons are: the nature of application of such techniques, external to the surface of the component to be inspected; the type of waves selected (body waves), with related referred behaviour and which present considerable wave propagation amplitude damping. Besides their local application, sensor signals have to be heavily filtered. Localized application and sensor signal

filtering are implemented so that noise interference and complexity of sensor signals is sufficiently reduced. The objective is to enable feasible sensor signal assessment and the detection of waves in it and particularly, possible reflections from potential defects, i.e., to achieve a sufficient SNR for consequent successful application of the inspection method.

Considering the importance of the actuation frequency to be centered in a single value, a sinusoidal signal could be selected. The frequency is perfectly set, however lobes appear in the harmonic frequencies as can be observed in the function frequency spectrum.

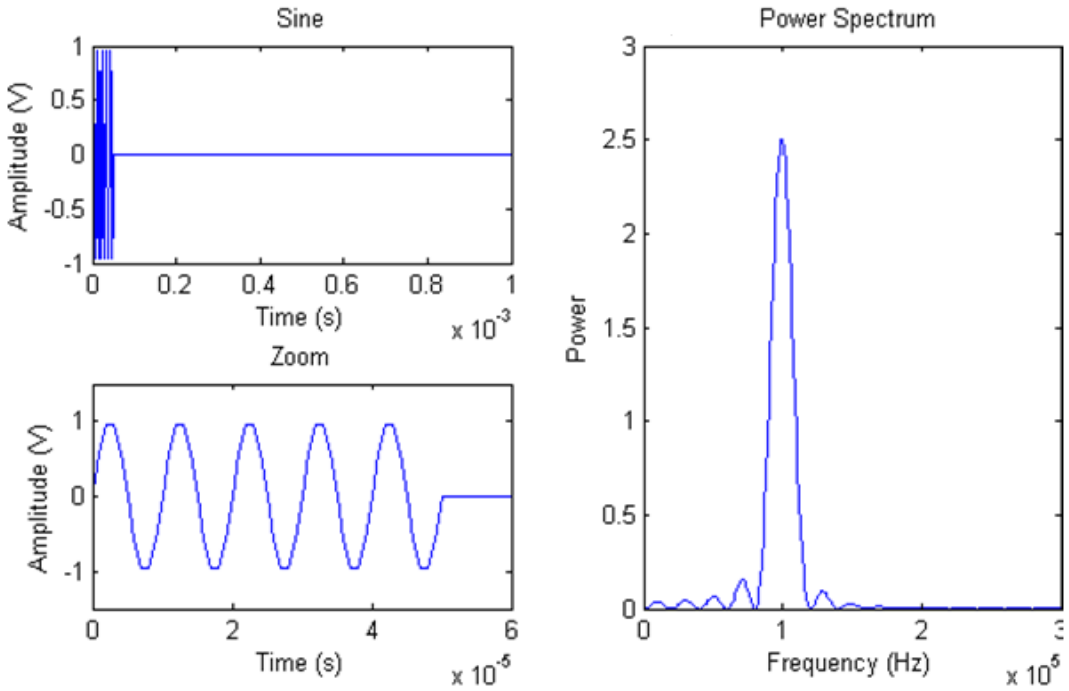

Figure 4.5: Sinusoidal actuation wave.

To center the function frequency spectrum on a single value, the sinusoidal function could be modulated by multiplying it by a second sinusoid of lower frequency – similarly to a Hann modulating window. As an example, the next function could be defined, with the modulating sine having a frequency ten times smaller, i.e., with the application of five sinusoids in the interior of the modulation window.

$$f(t) = A\sin(2\ \pi\ f\ t)\ \sin\left(\frac{2\ \pi\ f}{10}t\right) \tag{4.3}$$

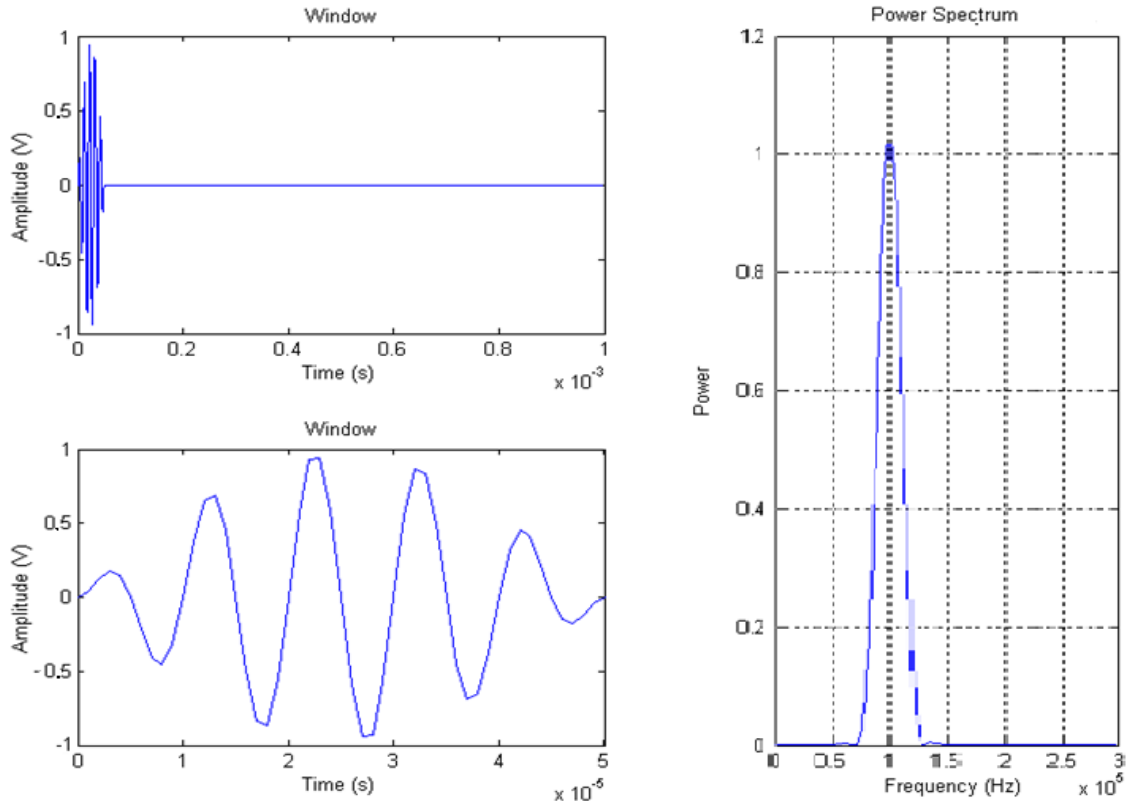

Figure 4.6: Time and frequency analysis of Eq. 4.3.

A better definition in time and, as expected, in frequency were observed, with lobes disappearing from the frequency spectrum of this signal. Several different modulation windows with different ratios between the inner sine and window frequencies were tested. When the number of the inner sine wavelengths is increased, the peak observed in the signal frequency spectrum becomes more narrow (smaller frequency bandwidth), with its amplitude being increased at the cost of appearing lobes. It was concluded that the optimum actuation signal would consist in an inner sine train of five wavelengths, modulated by a sine window, with the resulting function being smoothed in its beginning/end.

Considering the actuation frequency of 245kHz (inner sine frequency), the actuation signal will have a total duration in time of 20.41µs. According to what was referred before and considering that the S_0 waves of that frequency present a propagation velocity of 5390m/s, in the considered aluminum plate, a distance of 55mm around the PZT transducers (phased array) will not be inspected.

4.5 - Linear Phased Array Numerical Simulations

To better understand the beamforming process of the linear array and to assess the generation of side lobes, a simple code in MATLAB® was developed to implement trivial numerical simulations. In this study a square plate with 600mm side length was simulated with a single planar layer mesh of 600x600 nodes (spacing of 1mm). An interface window – Fig. 4.7 - was programmed to enable the user to:

- create the actuation waveform - specifically based in a Hann windowed sine waveform, the user can select the maximum amplitude and the inner and window frequencies;
- establish the wave propagation velocities by introducing the frequency of excitation times the thickness of the plate – the code has embedded a matrix to represent the dispersion curves presented in Fig. 3.3, for an aluminum plate, and considering the propagation velocities calculated in page 77;
- set a predetermined damping coefficient for the wave propagation (i.e. amplitude attenuation factor), assuming that such attenuation occurs exponentially with the wave travelled distance;
- select the number of actuators to apply and their respective positions in the plate – what enables the application of this code, in the future, to simulate arrays with different configurations than the linear. In this simple code, the actuators were assumed to be simple nodes in the mesh;
- define the angle of the propagation direction of the wavefront to generate, with the code calculating internally the required time delays to introduce in between consecutive actuations; or introduce explicitly the time delays in between the different consecutive actuations, enabling also the simulation of the generation of curved wavefronts.

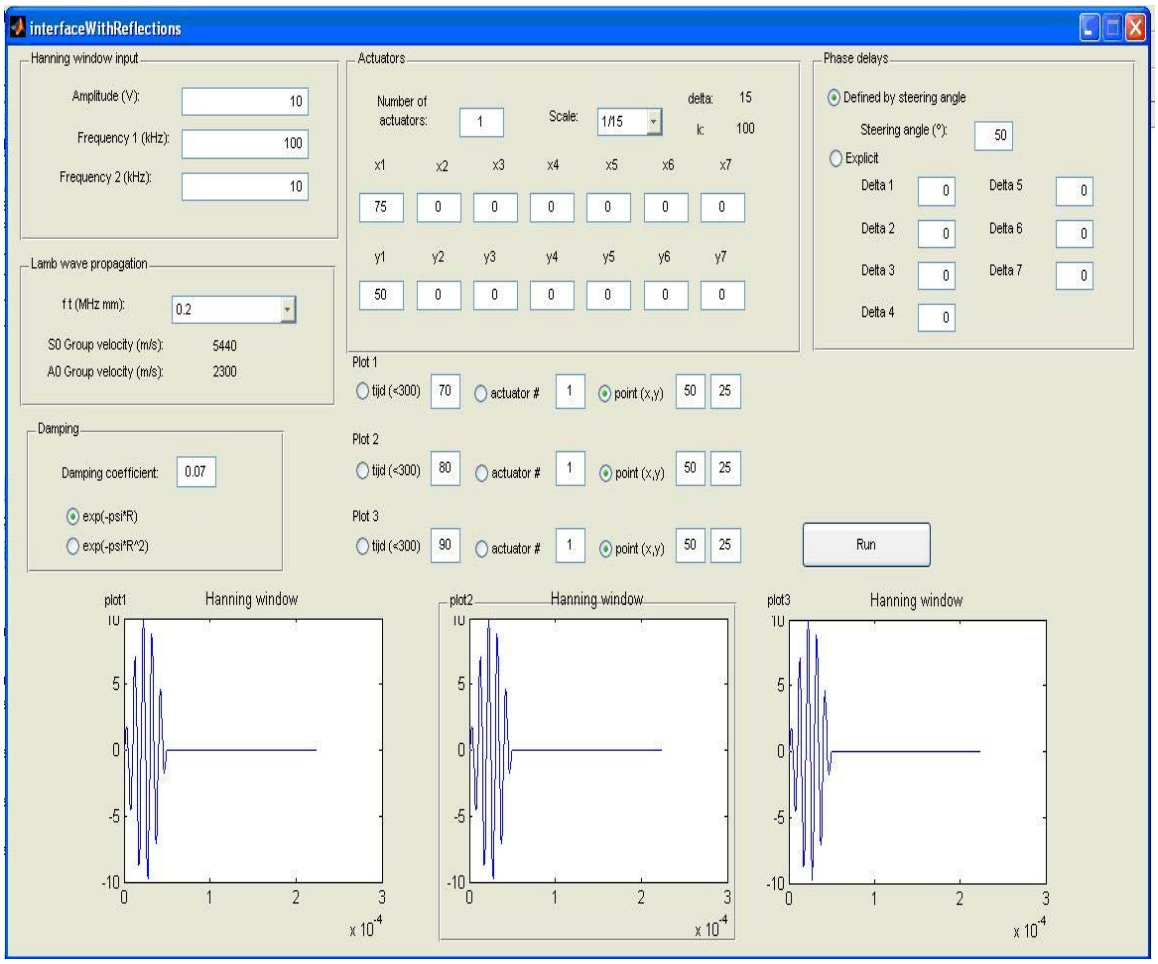

Figure 4.7: Interface window.

A time step of 100ns is established. For each time step, the code calculates for each node the amplitude of the excited waves by each actuator, considering the waveform selected and the damping determined by the user, the calculated propagation velocity, the different actuator positions and the time delays applied - either calculated by the code to achieve the propagation of a wavefront into a determined direction (angle), or introduced by the user. The resulting amplitudes, in each node, due to the propagation of the generated waves by each actuator, are then summed. The results for a 90º and 60º propagation direction are presented in Fig. 4.8. The constructive interference in between the different excited waves, i.e., the beamforming process and resulting wavefronts can be clearly observed.

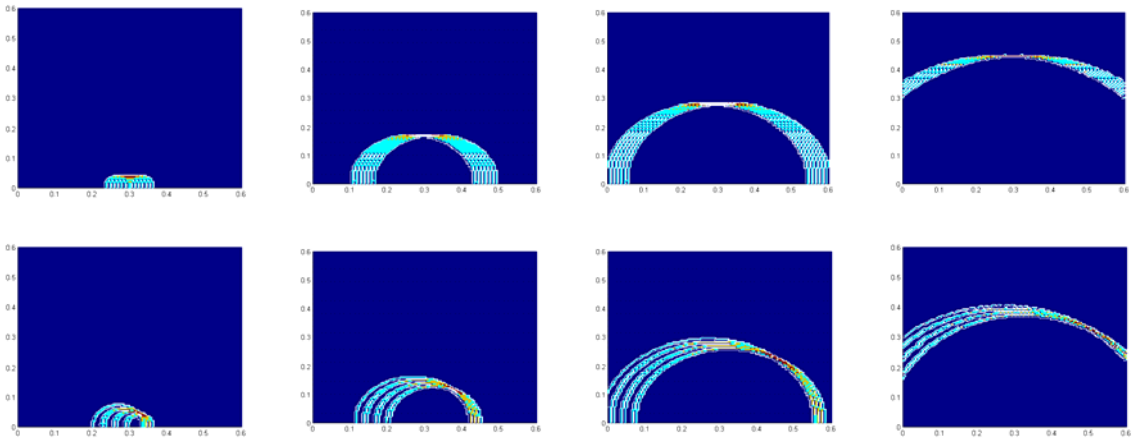

Figure 4.8: 90º and 60º beamforming simulation.

Through these simulations the condition expressed by Eq. 4.1 was verified, with the existence of side lobes when that condition is not enforced. The dependency of the wavefront aperture angle to the wavelengths being generated and the length of the phased array (determined by the number of actuators specified and their relative distance – pitch of the array) was verified. It was also observed that such aperture angle is approximately constant for all wavefront propagation directions in the plate.

4.6 - Development of the Actuation System

Regarding the phased array actuation system, a configuration based on a master circuit controlling the phased activation of different slave circuits was implemented. Each slave circuit, when activated by the master, generates the actuation signal to one PZT transducer in the array. The master circuit consists of a simple Micro Controller Unit (MCU). The MCU was selected considering its processor frequency, the output frequency it is capable of and number of output pins. The number of output pins limits the maximum number of slave channels that one MCU is able to control – however, two MCUs can be connected to communicate with each other, in order to expand the number of channels to control. The processing and maximum MCU output frequencies determine the minimum time delays that it is capable to apply for phased activation of the slave channels. A Texas Instruments (TI) MSP430F2012 [133] MCU with 16MHz of processing frequency, 4MHz of output frequency and two output ports, with eight and

two pins respectively, was selected. For the selection of the minimum time delay that the MCU would be able to apply, in this case 250ns (corresponding to an output frequency of 4MHz), a simple exercise was followed. The time delay to be applied in between consecutive actuations (Δt) – corresponding to the inverse of output frequency (f_{out}) - is equal to the difference in distance travelled by the consecutive generated waves (Δd) divided by the activated waves' propagation velocity (V):

$$\Delta t = \frac{1}{f_{out}} = \frac{\Delta d}{V} \tag{4.4}$$

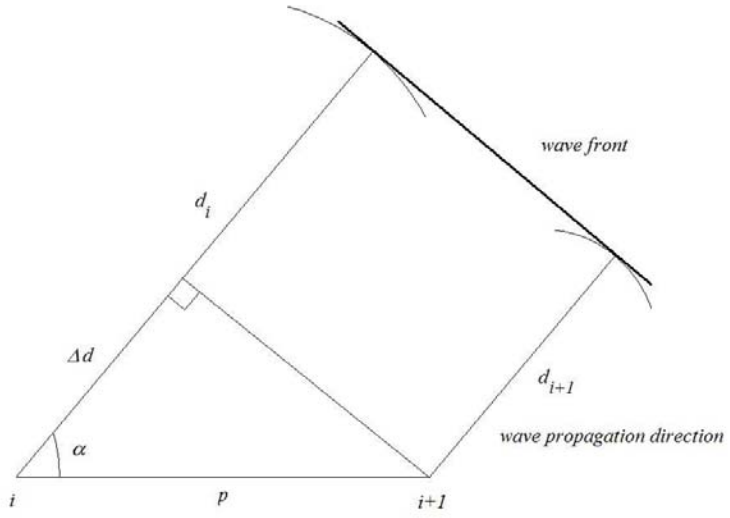

Figure 4.9: Phased array beamforming.

Through simple geometrical relations – depicted in Fig. 4.9 –, the difference in travelled distances can be related to the phased array pitch and the direction of propagation of the activated wavefront (α) by:

$$\cos\alpha = \frac{\Delta d}{pitch} \tag{4.5}$$

Combining the previous two equations:

$$\Delta t = \frac{pitch\,.\cos\propto}{V} \tag{4.6}$$

Knowing that for a wave:

$$V = \lambda . f_{wave} \tag{4.7}$$

Assuming that an optimized phased array is implemented such that its pitch is half of the wavelength of Lamb waves being generated:

$$\lambda = 2 \, . pitch \tag{4.8}$$

Replacing this equality in Eq. 4.7 and the result in Eq. 4.6, the following relations can be obtained:

$$\Delta t = \frac{\cos \propto}{2 f_{wave}} \quad \text{or} \quad f_{out} = \frac{2 f_{wave}}{\cos \propto} \tag{4.9}$$

To generate a wave front propagating in a direction perpendicular to the linear array, the master MCU must output simultaneously the activation signals to all slave circuits, without any delays applied in between actuations. Such means that the MCU must output all pins simultaneously, what is not problematic. The smallest, non zero, time delays to be applied, correspond to scanning directions (to wavefront propagation directions) closest to that normal direction. If it is desirable to inspect the entire component, for the different inspected regions in different scans to be contiguous, the different inspection directions must be spaced by no more than the array aperture. To achieve such, the scanning directions, closest to the normal of the linear array, to be selected, will be separated from that normal by the aperture angle. It is then necessary to calculate a minimum aperture that will correspond to the minimum time delays that the master will be able to apply. Eq. 4.2 can be simplified by assuming an optimized phased array, i.e., Eq. 4.8, resulting in:

$$\Delta \alpha \simeq \frac{2 \text{ x } 0.886}{n} \ (rad) \tag{4.10}$$

Considering the application of a phased array with a maximum number of seven elements, the array aperture is calculated to be 0.2476rad, or 14.19º. Considering a little superposition of adjacent inspection regions (for safety), the closest angle to 90º will then be 77º. With Eq. 4.9, the maximum wave frequency that can be applied in the inspection

method for the output frequency of the master MCU of 4MHz, will then be 450kHz. Such value is higher than the upper limit of 400kHz established for the actuation frequency to apply in this system.

It must be noted that the processing frequency of the MCU is also important for the correct implementation of the method, since the error in time between the desired time for output and the time at which such output occurs in reality, is in the worse situation 20% of its clock period (then 12.5ns) - usually below 10% of the clock period (6.25ns).

Furthermore, the TI MSP430F2012 MCU (with a 16 bit RISC architecture) was selected due to its extremely low cost, being a low power unit and due to the fact that it can be programmed effortlessly in ASSEMBLY, or C, by being attached to a USB development tool (MSP EZ430F201x) [134] - Fig. 4.10. This tool consists of a programming board capable to erase, translate and upload the code to the MCU. The MCU is attached and communicates with the board by a Spy By Wire interface (while it can also be used with a JTAG interface), while the kit is connected to a computer through a USB port. Such enables the use of the TI IAR Embedded Workbench [135] to develop the codes and program the MCU. After it is programmed, the MCU can be detached from the programming board and powered and used independently with the stored code. This MCU presents also 2KB of EEPROM CPU memory, 256B of flash memory and 128B of RAM. This is more than sufficient to store the simple codes to implement the SHM system (both for master and slave channels).

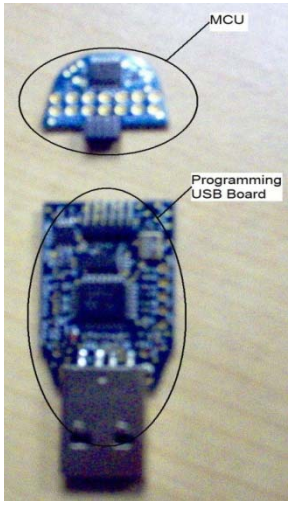

Figure 4.10: MCU and USB programming board.

According to the aperture determined for the array of 14.19º, and as referred, for safety reasons, the maximum angle interval in between consecutive directions of inspection was established to be 13º. The inspection direction angles, or the angles at which is intended that the wavefronts will propagate were selected to be 6º, 19º, 32º, 45º, 58º, 70º, 80º, 90º and the symmetric directions with relation to the normal of the array. Angles are measured anti-clockwise with relation to the direction of the linear array, from the right. With the selection of these directions some overlap in between the regions to inspect is promoted. Particularly, the 6º direction was selected to enable the inspection of the region laterally adjacent to the phased array, while avoiding the destructive interference of the PZT elements in the array to the propagation of the wavefront in the array direction.

With the selected inspection angles, knowing the propagation velocity of the S_0 waves (and wavefronts) to generate and the linear phased array pitch, the corresponding time delays to be introduced in each scan (for each propagation direction angle) were determined. These delays were then implemented in the developed code to use in the master MCU.

For the design of the slave circuits, for the actuation of each PZT in the array, it was also considered a MCU to generate the digital signal corresponding to the actuation waveform (the bit trail). One of the main advantages of the use of such MCU is that, as in the case of setting the time delays for the different scans through the use of the master MCU, it can be programmed so that the actuation signal waveform can be modified, particularly regarding its frequency. Such will enable the application of the inspection technique to different materials in the future. The MCUs used in the slave channels were similar to the one used for the master circuit. The number of pins was more than sufficient – from the available 10 pins, five pins are needed at the most, one for input from the master, two to output the inner sine function and the modulating window digital signals and between one to three pins to control output switches (depending on the configuration selected by the user). With the designed and implemented technique to generate the actuation signal, the MCU is capable to generate signals with frequencies up to 2MHz (half of its maximum achievable output frequency of 4MHz). The small errors in time introduced in the signal output are related to the MCU processor frequency, as it was the case for the master MCU.

To explore all capabilities of these MCUs, it is required the direct access and control of their registers and for that, MCUs had to be programmed in ASSEMBLY. The slave MCUs, after receiving the activation signal from the master (in one of their pins), generate and output the bit trail (with a voltage between 0 and 4V) in two different pins, one for the generation of the inner sine function (with the actuation frequency) and the other to generate the Hann modulation window. These signals are passed in a developed Digital to Analog (D2A) circuit, based on a Sallen-Key filtering technique – Fig. 4.11.

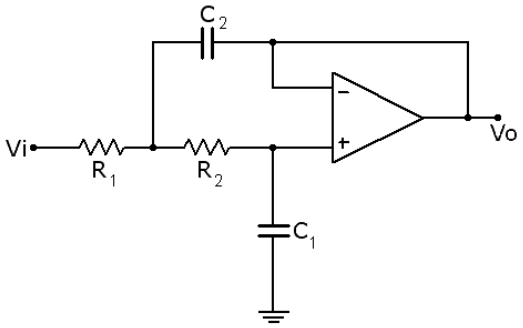

Figure 4.11: Sallen-Key filter.

This circuit consists on amplifier based filters to create the analog waveform, i.e., to create the sine wave output, from a corresponding square wave input (bit trail outputted by the MCU) of the same frequency. Two identical circuits were used for the inner sine wave and for the modulating window. The filters can be centered, by design, in any desired frequency of actuation, by changing uniquely the associated resistors:

$$C_2 = 2C_1 \quad and \quad R_1 = R_2 = \frac{1}{8.8856\ f\ .\ C_1} \tag{4.11}$$

In this case C_1 was selected to be 0.001μF, with R_1 being 459Ω for the inner sine (with a frequency of 245kHz) and 4594Ω for the modulating window (with a frequency ten times smaller).

As for the amplifiers, National Semiconductor LM6172 [136] were selected. These present a 100MHz unity gain bandwidth (i.e. a frequency range up to 100MHz with a unity gain), much broader than the actuation frequency range considered (up to 400kHz, without the need of amplification gains higher than 10). They also present a high slew

rate capability of 3000V/μs (high speed), with low distortion, low power consumption and high output current (average of 50mA/channel and maximum of 130mA in a single channel). These amplifiers can be used in either a positive or dual voltage mode (power supplies from 0 to 5V or ±18V), with a maximum differential input voltage of ±10V. In the D2A module, since the input and output signals are always positive, the amplifiers are used in their positive voltage mode (with the output signals presenting the same voltage range as the input signals). Their capability of being used in a dual voltage mode will be important for the final amplification of the circuit (output to the PZTs).

These filters were tested with the use of a bread board. An output resistor of 220Ω was used in the output of both filtering circuits for output impedance match (simulating an output load). The power supply bypassing circuit presented in Fig. 4.12 was also implemented, according to what is stated in the application notes for these amplifiers [136]. This power supply bypassing circuit is important to maintain the stability of the low power supply (impedance) to the amplifiers in their entire working frequency band.

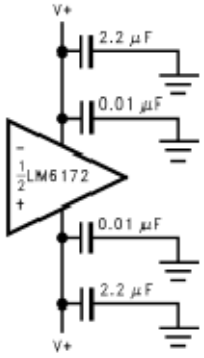

Figure 4.12: Power supply bypassing circuit [136].

The wide usable frequency band of the amplifiers means that errors introduced in time and frequency are considerably small (1/100MHz or 10ns in time). Furthermore, circuits used in both filters, for the generation of the inner sine and modulating window, were exactly the same (with the exception of frequency tuning resistors applied). Any delays in generation of those signals were then the same and the resultant waveform was not affected, except for possibly an initial delay in its output (not verified in experiments).

When working in the design frequencies these filters introduced an error in the generated analog signal of less than 1% in time, frequency and amplitude. These filtering

circuits were also tested by changing the frequency of the square wave input from 50kHz to 400kHz, with a step of 50kHz. Due to their design, it was verified that the error introduced by the filters never exceeded 10%, in terms of the output analog signal frequency. If wanted, this error can be decreased to the previous 1% error, by tuning the filter to the desired frequency (input signal frequency, equal to frequency of actuation), i.e., by calculating, selecting and introducing new resistors into the filters. Tests were performed, by modifying the filter resistors and tuning their frequency to values in the range previously referred (50kHz to 400kHz with a step of 50kHz). The maximum error of 1% was verified.

The two output signals from the D2A module (filters) present voltages between 0 and 4V. The inner sine corresponding signal must then be subtracted by 2V to be centered around zero. Afterwards, both sine and window signals are multiplied by a low noise, low distortion, high speed analog multiplier – Analog Devices AD734 [137]. This multiplier accepts differential input signals up to 20V peak to peak and is capable of output voltage swings in the range of ±10V, with 450V/μs of slew rate and a settling time under 200ns to achieve full amplitude signal output with an error of 0.1%. The multiplier has a 200MHz unity gain bandwidth and a working frequency range that goes beyond 40MHz. Particularly, when working with signal frequencies up to 10MHz, it is capable of full amplitude swings with an error in amplitude and time inferior to 0.1%. The error introduced in time, for the frequency range considered for the application of the phased array is less than 30ns. The multiplier circuit is depicted in Fig. 4.13.

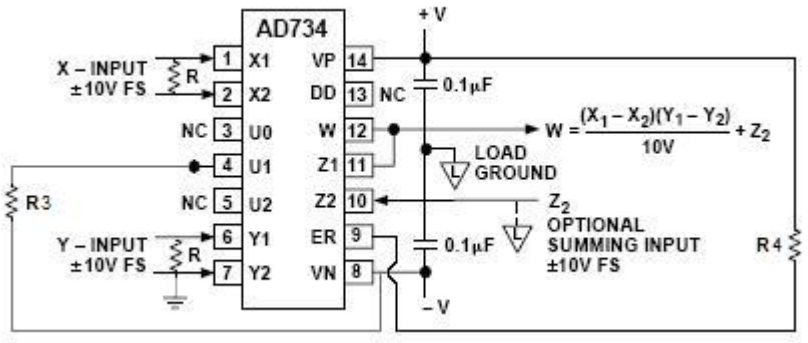

Figure 4.13: Analog multiplier circuit.

In this circuit, the inner sine corresponding signal is inputted in pin 1 of the multiplier and subtracted by 2V (inputted in pin 2, generated by an external power supply – also used to power the entire system with the different voltages: 4V, +18V and -18V). The modulation window signal is inputted in pin 6. To achieve a good stability of input signals, reducing noise and interference (cross talk), 51kΩ resistors were introduced in between pins 1 and 2, and 6 and 7. R_3 and R_4 are resistors used to set the amplitude of the output signal. These were experimentally tuned to achieve a voltage output range of ±4V, being determined as 137kΩ and 300kΩ, respectively. The multiplier output is already the final actuation signal waveform (Hann window modulated sine), correct in time and frequency, and only with an amplitude inferior to what might be desired.

The multiplier output is then amplified to the desired voltage range output, by a simple amplifying circuit – Fig. 4.14.

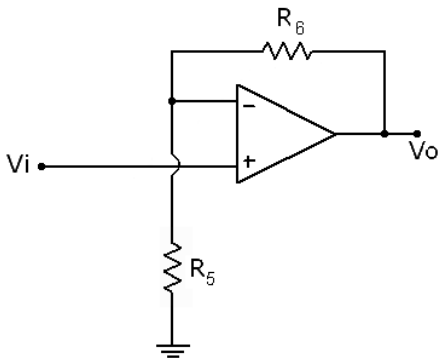

Figure 4.14: Amplifier circuit.

With:

$$V_o = V_i \frac{R_5 + R_6}{R_5} \tag{4.12}$$

An amplifier similar to the ones used in the filters (D2A module) was employed, with the use of the same power supply bypassing circuit (for stabilization and circuit protection). Since the amplitude of generated waves (their imposed mechanical deformation) is proportional to the amplitude of the actuation signal, such voltage output range should be as broad as possible, as long as the voltage peaks do not damage the actuator PZTs. In this case it was verified that the applied PZTs accepted the maximum

output voltage range that such amplifier is capable to output (±18V). The voltage range of the output signal from the multiplier (input to the amplifying circuit) was then experimentally verified with the use of the bread board. To reduce the effects of signal amplitude loss (in the real circuits), R_5 and R_6 were also tuned experimentally. To achieve the maximum voltage output range from this amplifier circuit R_5 and R_6 were determined to be 180Ω and 805Ω, respectively. To achieve good stability in the output signal from the amplifier, a 270Ω impedance matching resistor - also determined experimentally - was added at its output. The effect of this output resistor was extremely important for the stability of the output signal in the entire voltage output range, but particularly when the amplifier is used as a sink (negative output voltages).

Just before being directed to the slave channel corresponding single actuator PZT in the array, the actuation signal is passed by a low on resistance (5Ω) switch – ADG452 [138]. The switch is capable of working with 100mA of continuous current and up to 2A of transient current, what is more than sufficient regarding the current levels involved. The low on resistance of the switch means that the through voltage drop is also low.

The switch is controlled by a digital signal from the slave circuit MCU and is capable of analog inputs and outputs with amplitudes of 44V peak to peak. The switch admissible working frequency bandwidth for the passing analog signal is well in excess of 5MHz. To avoid the introduction of errors due to the required time for on-off operation of the switch (around 200ns maximum - 5MHz on-off frequency capable -, and around 60 to 70ns typically), it is closed before actuation, accounting for the required on time and it is opened just after actuation. This means that the MCU sends a signal to close the switch immediately after receiving the trigger signal from the master MCU and (some time) before it starts to output the digital signals, corresponding to the inner sine and modulation window actuation signals, to the D2A module. By doing so, the time in between closing the switch and starting to output the digital signals is experimentally determined, so that the influence on the actuation signal by the transient glitches, introduced by the switch (closing, in operation), is avoided. Also, since the different slave actuation channels are independent, there is no cross talk in between them and therefore no interference from those switch operation transient glitches from one slave channel to another.

The MCU sends then the order to open the switch after actuation, at a certain time after finishing the output of the digital signals. Such delay is also determined experimentally, to account for the time delays introduced by the D2A, multiplier and amplifying circuits; and to diminish the interference of the switch introduced transient glitches, when opening, into the actuation signal itself. Although such glitches will exist and interfere with the PZT actuator and consequently cause the random generation of waves (considered as introduced noise, with undetermined and broad frequencies and then propagation velocities and wavelengths), such will only happen after actuation and this setback was decreased as much as possible, with the selection of the referred switch.

This switch is only closed during actuation and afterwards flushes the remaining low actuation signal noise from the slave actuation circuit to ground. This is performed to protect the electronic components in the slave circuit, by avoiding the damaging accumulation of remaining swinging currents and voltages in it (noise after actuation). This switch is introduced to solve the usual impedance mismatch problems in between actuator and signal acquisition circuits when the PZT transducers are used as sensors. As in this case, the actuation circuits usually present relatively low output impedances (around 50 to 75Ω) to enable higher output voltages, frequencies, slew rates and lower settling times. However, the data acquisition, or voltage reader, presents desirably much higher input impedances, also to enhance acquisition precision. When a PZT transducer, working as a sensor, is connected simultaneously to both systems, a great part of its signal (current) will be lost (will escape) to ground through the actuation circuit, due to its lower impedance than the acquisition system - in the present actuation circuit it would flow to the output amplifier, working as a sink. The amplitudes of the acquired signals, presented by the voltage reader, will then be considerably decreased. Experiments were performed to compare the performance of the system (amplitude of acquired signal) with and without the use/operation of the output switch (with the switch always closed/on). Amplitudes of the acquired signal were increased in more than 600% with the use of the switch.

Some of the tests being performed to the components of the phased actuation system, using a bread board are depicted in Fig. 4.15.

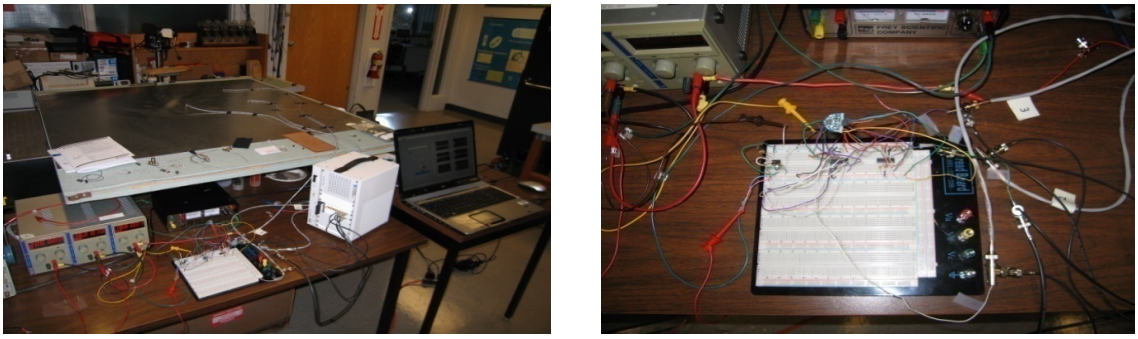

Figure 4.15: Components of the phased actuation circuit being tested.

The slave circuit experimental (non miniaturized prototype) board (and system diagram), with DIP (through hole) larger electronic components is depicted in Fig. 4.16.

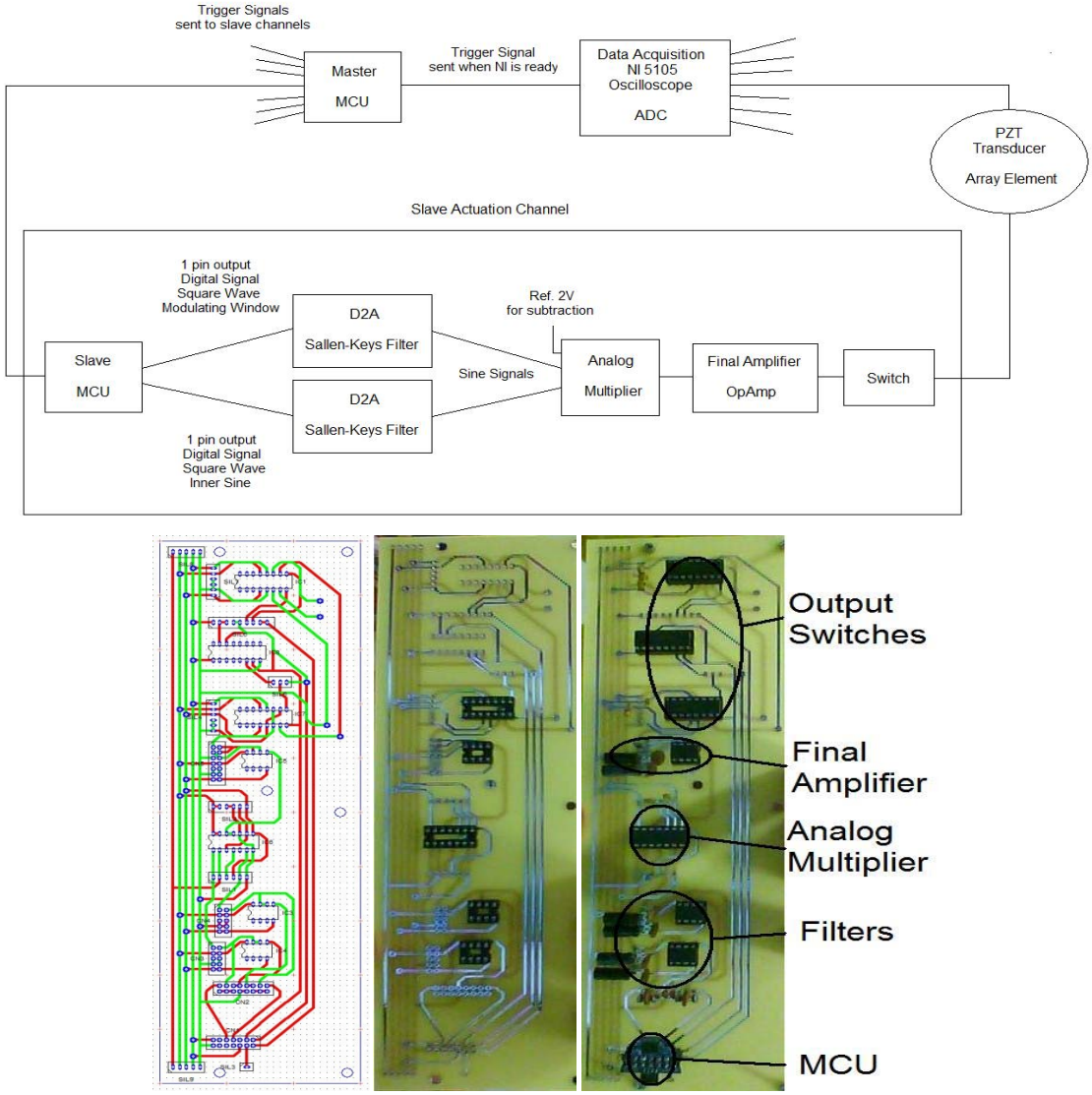

Figure 4.16: Slave circuit.

Chapter 5

Phased Array SHM Experiments

In these experiments the same equipment used previously in the tests performed for the development of a PZT network SHM system [4] was employed. Besides the NI PXI-5421 (single output channel) actuation board, a NI PXI-5105, 8 channels with simultaneous sampling oscilloscope board was used for acquisition of the array sensors signals. This oscilloscope is capable of a sampling rate of 60MS/s with 12 Bit resolution. Furthermore, in this board, the signal acquisition voltage range can be selected, depending on the intended application, from ±25mV to ±15V. This board has an internal memory of 128MB and when it is connected to a computer, it enables data transfer in real time, i.e., while executing data acquisition. With the data transfer rates possible, the internal memory in the board revealed to be sufficient, considering simultaneous acquisition of the 8 channels with the maximum sampling frequency and considering an imposed minimum recording time. The minimum recording time considered corresponds to a S_0 wave propagating in a 2m squared plate at 5500m/s and travelling four times the diagonal of such plate.

The two boards (NI PXI-5421 and NI PXI-5105) were mounted in a NI PXI-1033 chassis connected to a Laptop using a PCI-Express card slot. The chassis and PCI-Express card were carefully selected not to limit the performance of either the boards, specifically in terms of synchronising clock performance for the two boards and allowable maximum data transfer rates. Besides the use of the oscilloscope board to acquire the phased array sensors signals, this system (complete NI system) is used to save the test data (sensor signals, etc); for data post processing (application of filters, etc); to implement the damage detection algorithms; and to control and synchronize the operation of the entire SHM system, particularly in between the developed phased array actuation system and the NI system (particularly regarding the oscilloscope/acquisition and the laptop). In the experiments, for the phased array system, the NI PXI-5421 (single output

channel) actuation board was only used for synchronization purposes, to send a digital activation signal to the phased actuation system (to the master circuit), to start the actuation of the phased array. Such was done when the NI system and particularly the acquisition board is prepared to acquire the sensor data. This is enabled by the fact that both NI PXI-5421 and NI PXI-5105 boards are synchronized by the NI PXI-1033 chassis. The oscilloscope is then ready to start the readings, being triggered (with data being saved just after) by the actuation signals sent to the PZT transducers in the array.

As for software, initially NI SIGNAL EXPRESS® was used for a rapid assessment of system performance on signal generation (from each slave board and collectively for the determination of the precision at which time delays are introduced by the master and the subsequent beamforming process); precise activation of desirable Lamb waves and wavefronts; sensing and sensor signal acquisition, etc. This software is extremely user friendly. It has a visual interface that permits to manage and monitor in real time and in a simple and automatic manner the activation signal to the phased array actuation system and sensor signals acquisition and data recording. It also presents some simple but useful data post-processing capabilities for an initial assessment, such as: filters, spectrum analysers, switches, conditional decision making, triggers, mathematical signal operations, etc.

Afterwards, the control of the operation of the phased array SHM system, the synchronization of the boards, activation of the phased actuation system, sensor signal acquisition, data post-processing and the implementation of damage detection algorithms were performed in LABVIEW®. With this objective the previously developed software/code for the PZT network SHM system was adapted for the phased array system (actuation, sensing and damage detection algorithms). The resulting modules were then combined with the ones for the PZT network, forming a fully developed system to be used with networks or phased arrays, or a combination of both. As before the Virtual Instruments (VI) were graphically coded to control the NI boards; to create the front panel of the instruments and the system, for user interface – so that the user can setup and control inspection execution, save data, see inspection results, etc; and through the embedment of MATLAB® codes, to apply data post-processing (filters, etc) and the damage detection algorithms.

The experiments started by testing the slave circuits to verify the generation of the actuation signal waveform, specifically its correct amplitude and frequency, and to assess the introduced errors in time. The complete actuation system, depicted in Fig. 5.1, was then tested to verify the correct generation of the wave front and the influence of the previously referred errors (and relative errors in between the different channels).

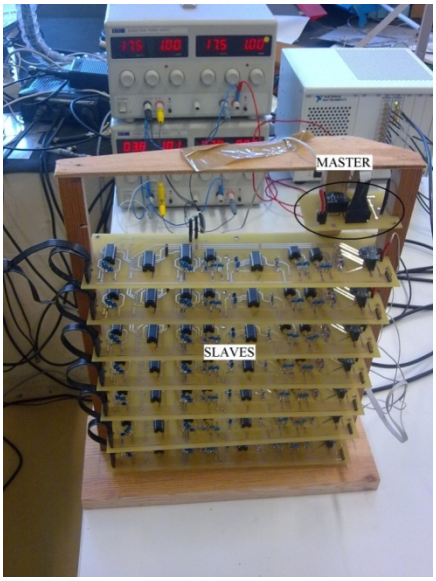

Figure 5.1: Phased array actuation system.

Initially the outputs from all slave circuits were directly connected to the data acquisition system. The delays introduced by the master circuit were confirmed and the errors in the beamforming process were verified. In Fig. 5.2, the output signals from the different slave channels are presented for a null time delay, i.e., when all slave circuits are activated by the master circuit simultaneously, to facilitate the verification of errors. A zoom is presented for the figure, around the highest peak of the actuation waveforms.

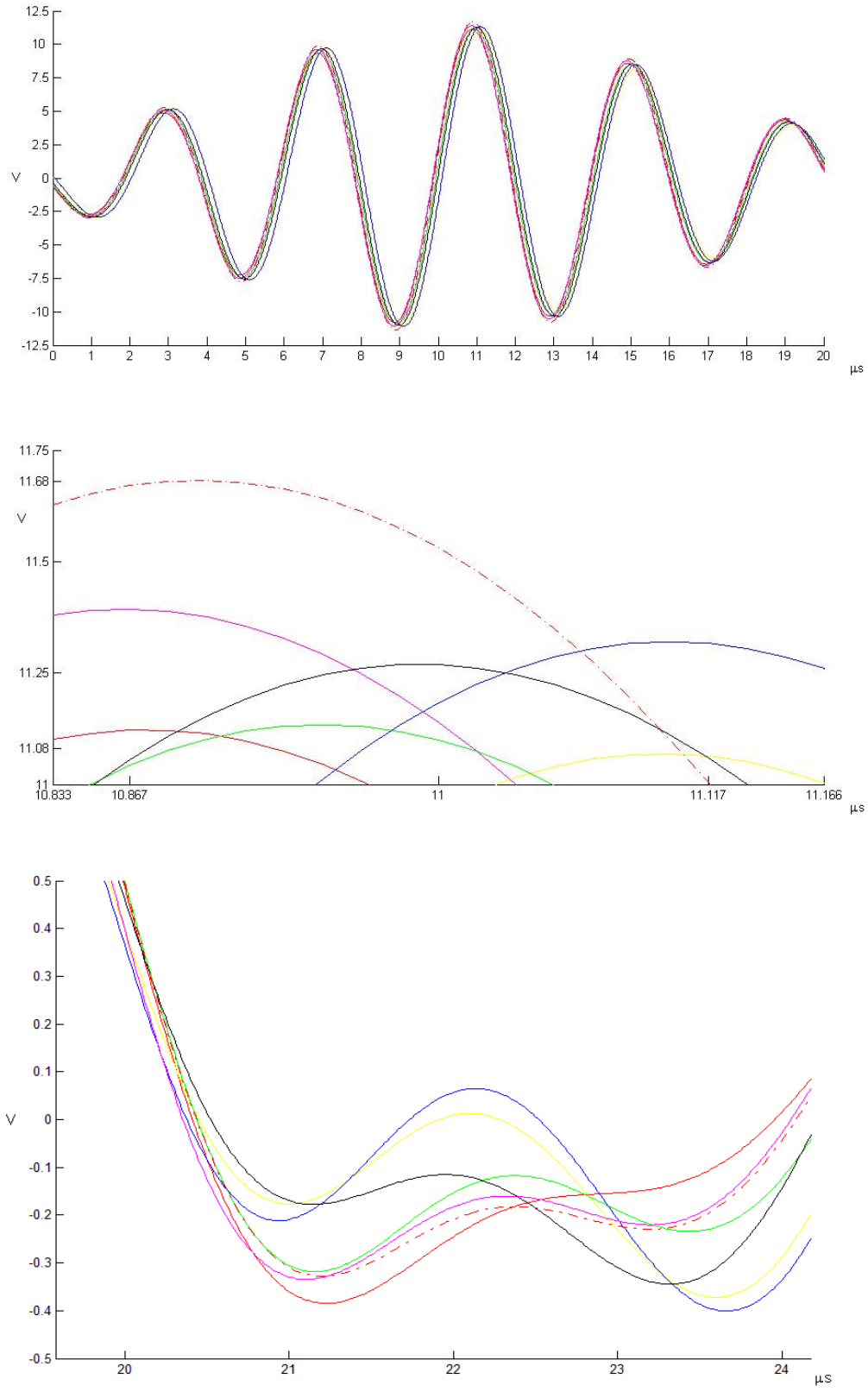

Figure 5.2: Actuation signals from the different slave circuits.

In the analysis of all generated signals, the maximum detected differences in amplitude were of 610mV, corresponding to a relative error in amplitude of 5.5%. The time differences observed for the highest peaks were of 250ns, corresponding to relative errors in time and in frequency of 2.5% (with relation to actuation frequency, i.e., inner sine period and frequency). Such errors will result in that the wave front generated will be spread through 1.3mm in its direction of propagation, considering the 245kHz frequency of actuation and the corresponding propagation velocity (of the S_0 waves/wavefronts). Do not mistake this wave front spread with the wave front width in the direction perpendicular to its propagation, or aperture. Comparing that value with the (S_0) wavelength excited, an error of 6.25% is determined in space.

Furthermore, the influence of the transient glitches introduced by the final switch opening (in operation), in the actuation was also verified and is depicted for the different array transducers/elements in the last graph from the previous figure – Fig. 5.2. As may be observed, the introduced glitches have an amplitude inferior to 4% of the maximum actuation signal amplitude, for each individual and independent slave actuation channel – and array element/transducer. As mentioned in the end of 4.6, these glitches will have as a consequence the generation of additional waves, to be considered as noise for the implementation of the system. The small relative amplitude of the glitches indicates that the relative amplitude of those additional waves will be small, when compared to the amplitude of the generated wavefront. Furthermore, being in a broad band of undetermined frequencies, those glitches will have as a consequence, the generation of highly dispersive and fortunately scattered waves. The relative amplitude of these waves is even smaller when compared to the generated wavefront considering the intrinsic constructive interference of the different generated waves to form such wavefront (beamforming).

With these promising results the linear PZT phased array was implemented in a square aluminum plate 1.5mx1.5m. The array was applied near and parallel to one of the edges of the plate, in its middle – Fig. 5.3.

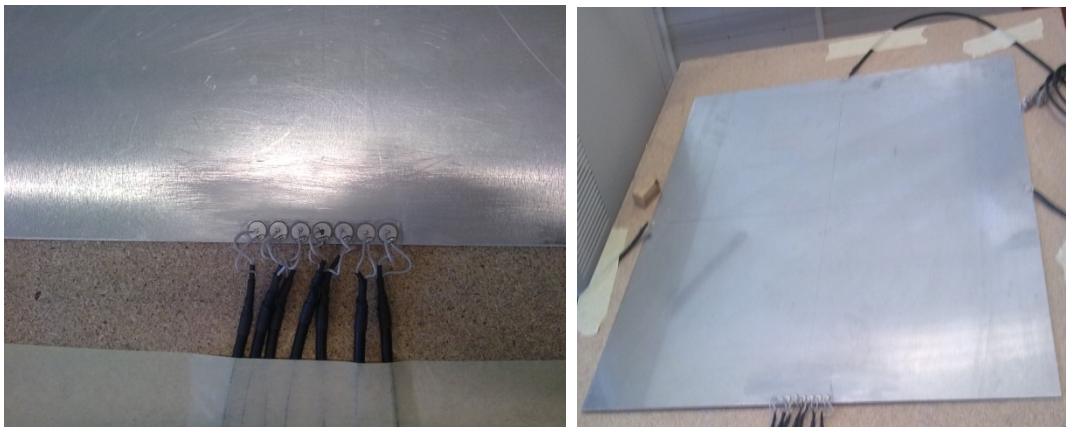

Figure 5.3: Linear PZT phased array applied to an aluminum plate.

The first experiments executed after the implementation of the PZT array were focused in the verification of the correct generation of wavefronts, their propagation directions, amplitudes and apertures. For these initial experiments a network of three PZT transducers was also used. These PZTs were bonded near the other three plate edges (also in the middle), with relation to the phased array. The wavefront was generated and steered to various directions in the plate and, besides the sensor signals from the PZT array, the network sensors' signals were also acquired. The time delays introduced by the master circuit were modified in these tests, to steer the wavefronts to the network PZT sensors and into their adjacent directions. From these experiments, it was concluded that the wavefronts were successfully generated and steered; their wavelength and frequency were also confirmed.

Through the wavefront Time of Flight, between generation and arrival to each one of the network sensors, the propagating velocity of the S_0 wave fronts was confirmed with the initially calculated values from dispersion curves.

The aperture of the array was then confirmed through the scans in which the generated wavefront was steered to propagate in directions adjacent to the ones including the network sensors. For each scan direction, the amplitudes of the resulting acquired signals for each PZT in the network were recorded – the amplitude of the wavefront and the amplitudes of the previous and trailing waves with relation to the wavefront (arriving at the network transducers before and after the wavefront, due to the actuation signal

morphology). In Fig. 5.4, the results for the scans performed in directions close to 45º are presented.

For the generation of these scan figures, a quadrangular, single layer mesh, with a spacing of 5mm, was applied to the plate. An array of 300 x 300 (for the 1.5m x 1.5m plate) was created, corresponding each of its positions to one point in the mesh – the point in the first line and first column corresponds to the left corner in the boundary closer to the phased array, with the columns representing the points in a direction parallel to the phased array. The amplitude values were then used to populate this matrix. For an easier representation, such amplitudes, of the wavefront and remaining waves, were staggered in space, corresponding to the distances determined through the waves (and wavefront) propagation velocity and the relative time intervals in between them, in the considered network sensor signal (their arrival at the sensor). Those amplitudes were then introduced in the matrix positions corresponding to the points in the mesh in the scan (wavefront propagation) direction considered. This process was executed for all scans performed in directions adjacent and including the considered network PZT, and for all three network PZTs. The figures are then generated by plotting the matrix and embedded values.

In the scan results presented in Fig. 5.4, it can be seen in red the highest amplitude values recorded. These values correspond to the amplitudes recorded for the arrival of the wavefront, while the remaining colors correspond to the waves arriving before and after the wavefront, with smaller amplitudes.

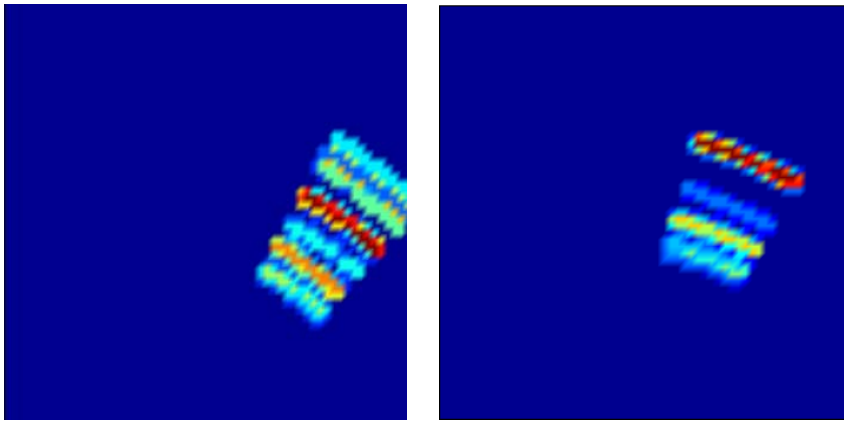

Figure 5.4: Verification of wavefront aperture.

Finally the amplitudes of the network sensors' signals corresponding to the propagating wavefronts generated by the phased array were assessed – Fig. 5.5. A simple experiment was also executed with all the slave actuation channels deactivated except the one corresponding to the PZT in the array closest to a particular network sensor. This was done to decrease the interference from the remaining PZTs in the array into the generated wave (by the only active PZT), particularly considering its propagation direction connecting the actuator PZT in the array and the network sensor selected. This experiment was repeated for all the three network sensors and the amplitudes of their signals corresponding to the propagating wave were also analyzed. These amplitudes were then compared to the amplitudes acquired for the wave front generated by the phased array. It was verified that the sensed amplitudes for the wave front were ten times higher than the ones obtained for the single wave generation.

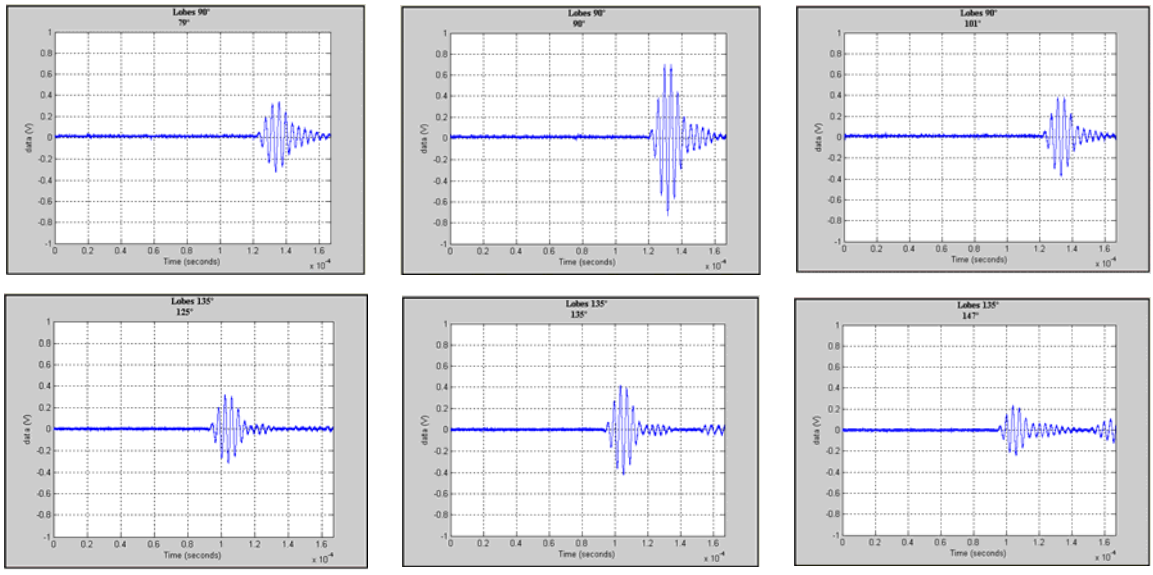

Figure 5.5: Wavefront amplitude detected by network PZTs.

As expected, the wavefront amplitude is higher for propagation directions approaching the perpendicular of the array orientation.

5.1 - Damage Detection Algorithms

Regarding the damage detection algorithms, two different approaches were followed concurrently. The first was based in the application of the phased array sensing principle referred in the literature review, which is applied by the majority of works in this field. In this approach, since the inspection direction is known, the phased array sensor signals are shifted in time for the corresponding relative time delays. Afterwards, the signals are added, with the resulting signal being searched for a potential damage reflection. With this procedure, incoming reflection waves in the inspection direction will be enhanced, increasing SNR. After encountering a potential damage reflection – damage detection -, its Time of Flight is retrieved from the sensor signals (time between the wavefront generation and detection of such reflection). Knowing the wave propagation velocity (equal for generated wave/wavefront and reflections), the total distance travelled by the generated and reflected waves is calculated. The distance between the phased array and damage is then determined, as half of the total distance travelled by the generated and reflection waves. Knowing the inspection direction, damage location is then determined. The disadvantage of this approach is that it is based on the approximation that the incoming damage reflection to the phased array is a (linear) wavefront and not a curved wave, as it is in reality. This approximation gives acceptable results for the determination of damage location, when the damage is sufficiently far from the array and the section of its reflected wave arriving to the phased array is approximately linear. However, when damages are close to the array, damage location is not accurate enough.

This approach can be used with either a single or a phased array actuation and can be applied in a supervised or unsupervised method. In the supervised approach, the (potential damage) reflections are searched for directly in the sensor signals obtained from scans for the current health condition of the component being inspected. There is no need in this mode of previously saved signals for a reference state (undamaged or with known damages, to monitor new damages and damage growth) and then no subtractions or comparisons are done. Since no subtractions are performed, the current signals to be analyzed will present all reflections from boundaries and other intrinsic geometric or

material discontinuities in the component. To distinguish a potential damage reflection from these reflections a supervised approach is required.

In the unsupervised approach, with the execution of subtractions between current and reference signals, potential damage reflections are enhanced (with relation to the disappearing boundary reflections) and easier to detect in the sensor signals. Besides this, the unsupervised method presents advantages towards a more global automation of the damage detection process.

To refer that the application of the supervised approach, depending on the direct detection of potential damage reflections in the current sensor signals, requires such reflections to present considerable amplitudes in order to be identified from the remaining noise in the signal (higher SNR). To achieve this, an increased actuation power and/or the enhancement of sensor signals (through the previously referred phased array sensing method) are required. To note that, due to this aspect, this approach will present better results when a phased array based scan/inspection is applied. In the previous development of transducer networks, due to the characteristic individual actuation, it was verified that the application of this method was not possible – low SNR -, with the reflections being less easily directly detected in the sensor signal analysis.

Either in the previous method or on the second one, to present next, to decrease the random influence of noise in sensor signals and since the execution of one scan takes less than 1ms, it was decided to repeat consecutively (fifty times) the execution of the same inspection scan (with the wavefront propagating in the same direction, i.e., the same inspection direction/region). This was performed for each and all scans executed (for the entire component, considering all inspection directions), both for the reference and actual health conditions, saving all corresponding sensor signals. After performing the multiple repeated scans, sensor signals corresponding to each transducer and for each scan direction are averaged, maximized and minimized for each and all times. Based in a Gaussian distribution approach new maximums and minimums corresponding to a 90% probability that the signal will be contained in such range, are determined, for all times. Signal bands are then obtained for all sensor signals corresponding to the actual and reference conditions of the component, for all scans, i.e., inspection directions.

Specifically for the unsupervised approach, the comparison of sensor signals for current and reference states, for each of the different scans (and for each sensor), is then based on the verification of when the current health state corresponding signal band differs from the reference band by more than 50% of its width.

In the damage detection procedure to be applied, all possible reflections are considered. Particularly in the unsupervised mode, all differences determined between actual and reference state corresponding sensor signal bands are used. These will include the potential damage reflections and false positives resulting from noise influence. To further contribute for the reduction of the influence of (random) noise and resulting false indications, the possible damage locations to be determined for each reflection, for each sensor signal and for each inspection scan (for every deployment of the array for the same and different directions of inspection, or directions of propagation of the wavefront) are superimposed – being equivalent to perform the intersection of all possible damage locations and forming a damage index. In this manner, it is predicted that the indication of damage positions will be enhanced with relation to false positives, since the probability of the intersection of the random false indications - resulting from (random) noise - to fall in the same position is reduced.

The second procedure was derived from the Time of Flight determination of damage reflections, considering the excited wavefront and the wave reflection generated by the damage (in this case considered as a curved circular wave propagating and not as a linear wavefront). The procedure is depicted in Fig. 5.6.

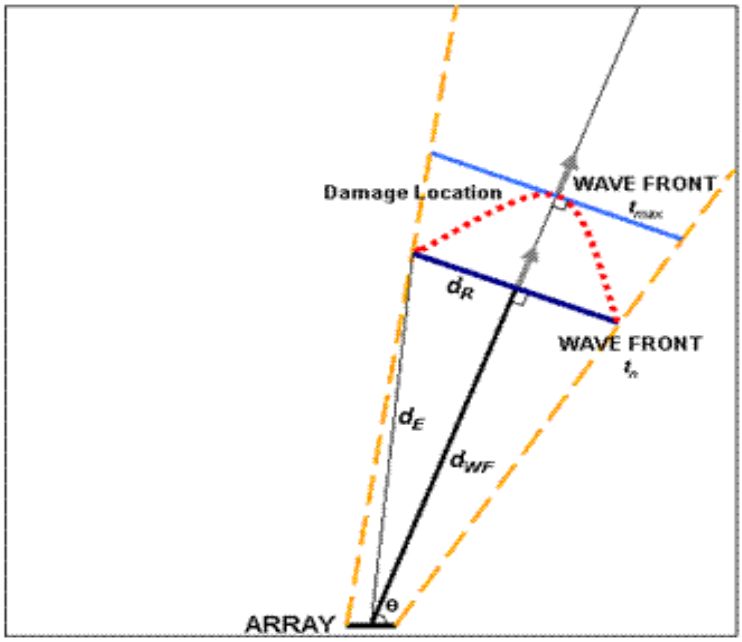

Figure 5.6: Developed damage location algorithm.

For each transducer in the array and for each scan (inspection direction) its sensed signal (band) is searched for potential damage reflections. In this procedure the ToF determined concurrently by the first method is also used. As referred previously, the ToF of all reflections are considered, in this case until the ToF of the reflection of the farthest boundary (corner) with relation to the phased array is reached - since the damage is contained in the component.

Since the signals from the individual sensors are considered in this method, although the phased actuation is applied, the reflections to be searched for will not be directly enhanced by the phased array sensing method. Since it will be prone to give better results with such expected smaller reflection amplitudes, it was considered the application of an unsupervised approach with this method, i.e., considering the comparison/subtraction to a baseline, or reference health state corresponding signals (obtained in previous scans and saved), and then determining the outliers.

In this damage detection technique, the known direction of propagation of the wavefront (predetermined by the phase delays), or the predetermined inspection direction is marked for each one of the sensors in the array, for the specific scan. All the Time of Flights considered are then related with the corresponding total traveled distance of the

activated wavefront and reflected wave. As referred before, damage distance, corresponding to half of the total traveled distance is determined and marked in the inspection direction lines for each and all PZTs - in Fig. 5.6, corresponding to the intersection point of the line representing the wavefront propagation direction and the line marked as wavefront at t_{max} (in light blue). Departing from each of those initial points and through the Time of Flight, parabolas are determined for each PZT. Each parabola is symmetric with relation to the inspection direction line passing through the corresponding transducer. It has its focus point in the corresponding transducer considered and its directrix parallel to the generated wavefront at a distance from the transducer corresponding to the Time of Flight previously determined – considering the known wavefront (wave) propagation velocity. The intersection of all the parabolas will determine (enhancing) the damage location, eliminating (or decreasing the relative importance of) the false indications.

In this process, the computational time required for the determination of the equations of the parabolas and their intersections is considerable. Furthermore, some potential imprecision in the determination of such equations must be accounted for. This results in a possible space imprecision in the determination of the parabolas, derived from errors in sensor signal time and consequent determination of ToF. If these errors are of enough magnitude, the different parabolas might not even generate any feasible intersection.

Considering these aspects and to decrease their potential negative effects, in the code created, the plate is meshed numerically (in a similar fashion as was performed before to obtain the scan results in Fig. 5.4). A quadrangular, single layer mesh is applied with a spacing of 5mm. An array of 300 x 300 (for the 1.5m x 1.5m plate) is created, corresponding each of its positions to one point in the mesh – the point in the first line and first column corresponds to the left corner in the boundary closer to the phased array, with the columns representing the points in a direction parallel to the phased array. In a first approach parabolas' equations are determined and a region of influence of 5mm is created around each parabola. For each parabola, each point in the mesh is verified if it falls in the region of influence of such parabola. If this condition is verified a unity value is introduced in the array, in the corresponding position. For the subsequently considered parabolas the unity values are added to the values already existing in the array in the

corresponding positions – superimposed results. The point in the mesh with higher final value (damage index) will correspond to the damage position. To decrease the processing time, only the points in the mesh in a region delimited by the inspection region (in between, or delimited by the dashed yellow lines in Fig. 5.6) and by the wavefront passing in the initially determined points (wavefront at t_{max} in Fig. 5.6, marked in light blue) are considered. As referred before, the inspection region is determined by the aperture angle of the phased array, centered in the propagation direction of the corresponding scan. This first approach revealed to be still time consuming. In a second approach, the distance of each point in the mesh to the considered transducer in the phased array is determined and introduced in a new array created similarly as the one referred before. This process is repeated, with the generation of seven arrays, one for each transducer. A range of distances obtained from the predetermined damage distance, plus or minus 5mm, is established. It is then verified if each distance in each array falls in that range – for all potential damage distances and for all sensor and scans (considering that the different directions of inspection were selected to promote a slight superposition of the different corresponding inspection regions). If this condition is verified a unity value is introduced in the array, in the corresponding position and the subsequent process referred for the first approach is then executed. In the end, all the values in the resultant, final matrix are divided by the highest value, becoming then a percentage, proportional to the highest (equal to one in the position corresponding to the highest value) and lowest probability of damage existing in such region. This is the approach that was used in the end, since it enabled a considerable reduction of processing time.

With this method the determination of damage location is performed with a precision of 5mm, i.e., it will be contained in a circle region with 5mm of diameter, around the determined point in the mesh (related with the mesh spacing).

5.2 - Damage Detection Experiments

The phased array system was then experimentally tested in the 1.5m x 1.5m x 2mm aluminum plate, subject to different boundary conditions, ranging from totally supported (to increase Lamb waves propagation damping), to simply supported and riveted in the

boundaries. The experimental setup is presented in Fig. 5.7. The experiments were conducted firstly in a laboratory setting and afterwards in an aircraft maintenance hangar, with no surrounding noise control and limited temperature control. Experiments were performed with the introduction (cumulatively) of surface and through the thickness circular holes and cuts (with different orientations), with a maximum dimension of 1mm, to simulate damage – Fig. 5.8. Damages were not inflicted around the phased array, respecting the non inspected distance, previously referred in Section 4.4, of 55mm.

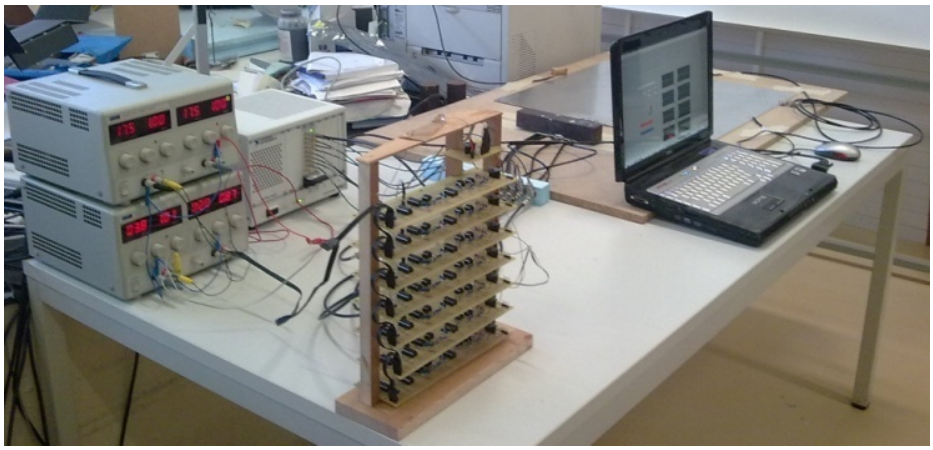

Figure 5.7: Phased array experimental setup.

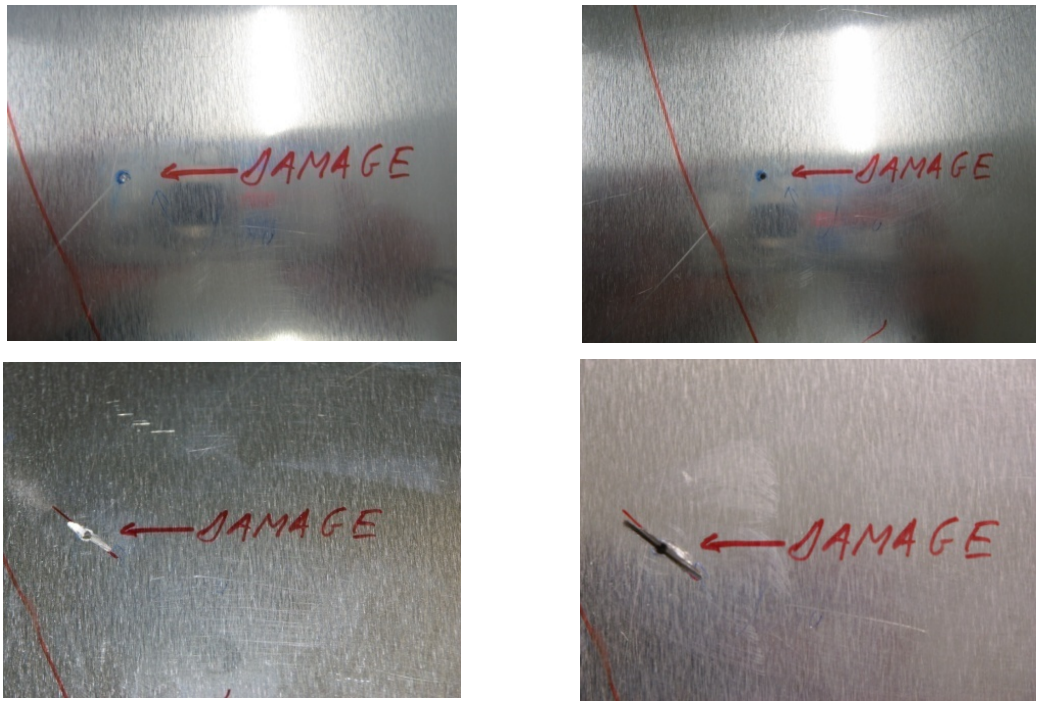

Figure 5.8: Plate's inflicted damage types.

A total of 46 damages were introduced cumulatively in the aluminum plate. From these, 17 damages were simulated by through the thickness holes, 7 damages by surface holes, 9 damages by surface cuts - 3 oriented in a radial direction considering the center as the phased array, 2 oriented perpendicular to the local radial direction, 1 at 45º from the local radial direction and 3 randomly oriented, at an angle (around 30º and 60º) with the local radial direction - and 13 damages by through the thickness cuts - 5 oriented in a radial direction considering the center as the phased array, 2 oriented perpendicular to the local radial direction, 2 at 45º from the local radial direction and 4 randomly oriented, at an angle with the local radial direction). The aluminum plate is presented in Fig. 5.9, after all the tests performed (scans/damage detection), i.e., with all inflicted damages (after all damages were applied cumulatively). The position of the phased array is depicted, as it is the positions of the inflicted damages.

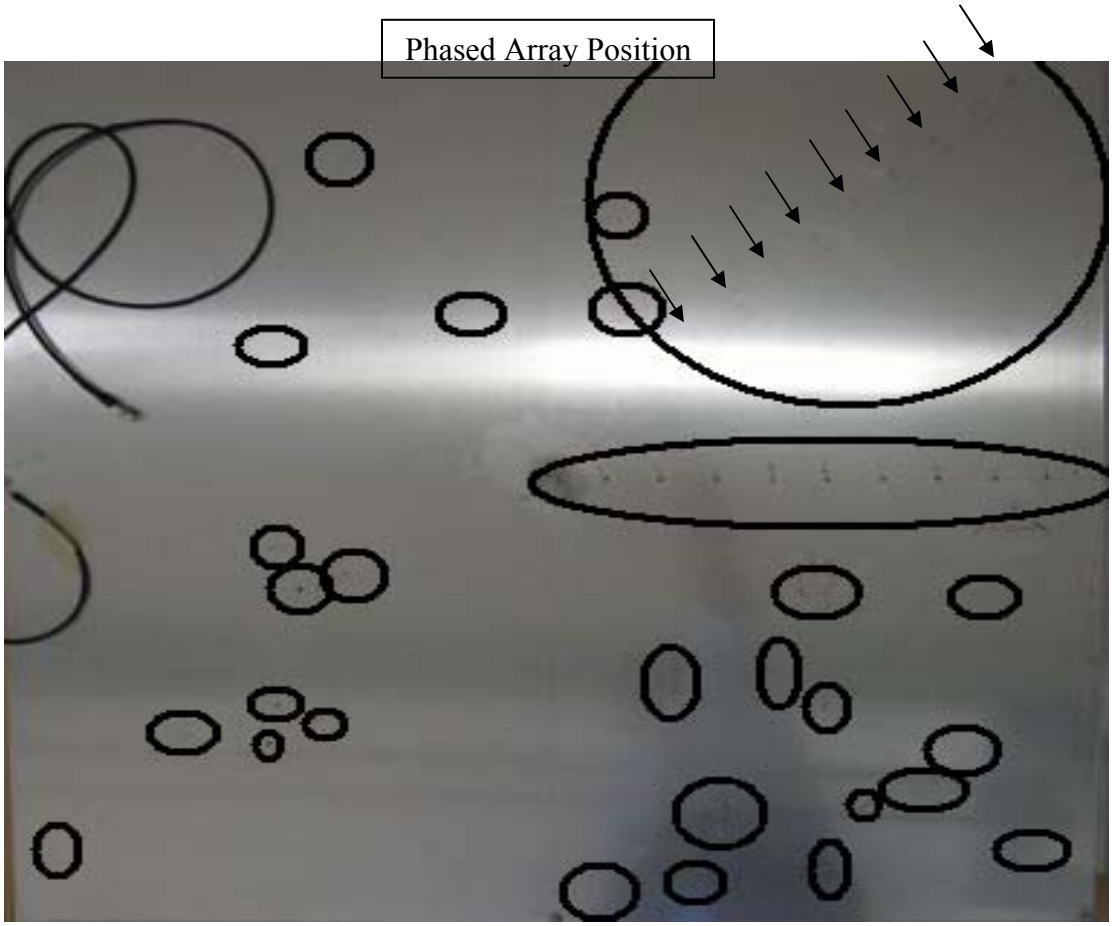

Figure 5.9: Aluminum plate with all, cumulatively, introduced damages (positions).

The simulated damages were successfully detected, with the only exceptions being damages created behind other damages previously introduced, i.e., in the same radial direction, with relation to the phased array (originating in the phased array) and also 60% of the cuts aligned with wavefront propagation directions, since their thickness was inferior to 1mm.

The software for automated inspection previously developed for networks [4, 5] (in LABVIEW®, with embedded MATLAB® codes for signal processing and to implement the damage detection algorithms) was adapted for the phased array system. Subsequently the software for networks and the software for phased arrays were integrated as two modules of an inspection software that can be applied for both network and phased array configurations. The user interface windows developed for the application of the phased array system are presented in the following figures.

In Fig. 5.10, the setup window is presented. Through this interface the user informs the code of the sampling rate used; the number of peaks in the actuation wave; the S_0 velocity; the phased array aperture angle to define the inspection region in each scan; the plate dimensions; and the location in the plate of the phased array (transducers). Since this is a test code, the user can also introduce the position of the inflicted damage to be compared afterwards with the detected damage position determined by the system.

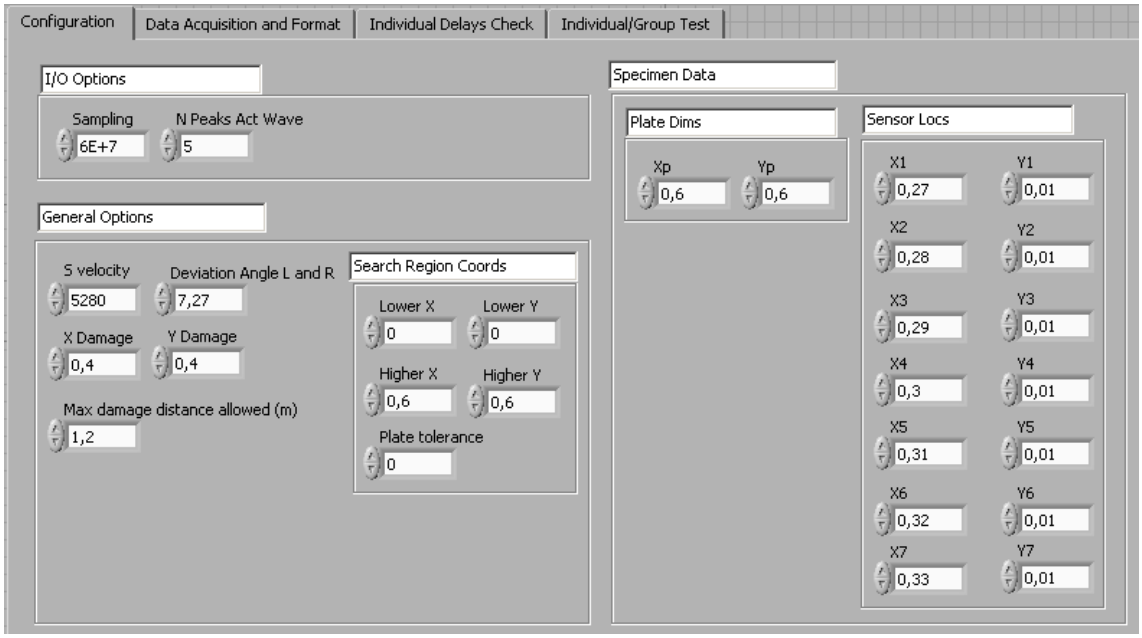

Figure 5.10: Setup window.

In the data acquisition window, presented in Fig. 5.11, the user defines the folder to save the data, or optionally where the baseline data was saved. The number of scans to be performed, to inspect the entire plate, and the number of repetitions to be performed for each scan are also introduced by the user, accordingly to what was set in the actuation system and specifically in the master MCU code. The frequency of actuation is introduced and the delay time between consecutive scans is set. This delay time should be introduced by the user, accounting for enough time in between consecutive scans to allow for the damping of all propagation waves and reflections generated from the previous scan. Furthermore, the user can select to apply a band-pass filter to the sensor signals acquired (centered in the inputted actuation frequency), before data post-processing. In this window the trigger signal for the phased array actuation system is presented, as the actuation and sensor signals, in real time.

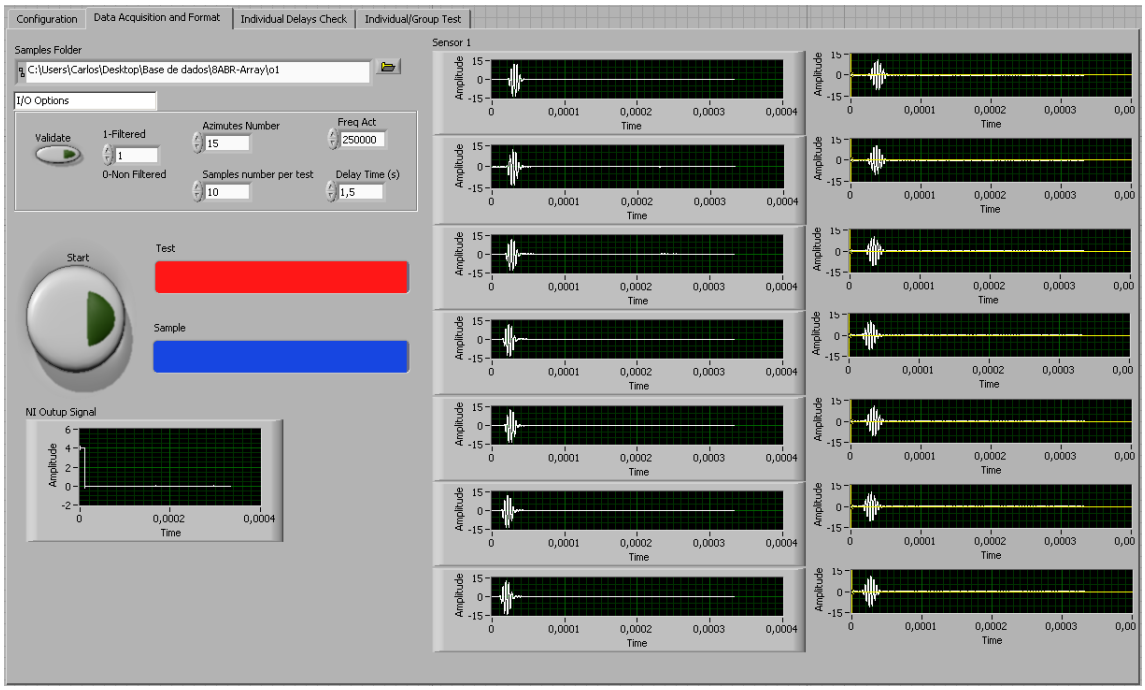

Figure 5.11: Phased array data acquisition window.

To enable the user to verify the delays introduced by the generation system in the phased actuation and the corresponding inspection direction, a window was also created with that objective – Fig. 5.12. This is based on the detection of the actuation peaks for each transducer.

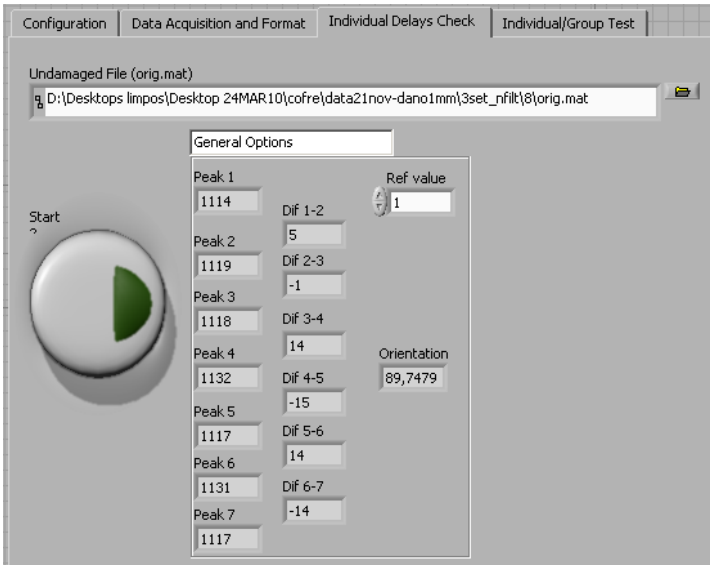

Figure 5.12: Phased array delays verification window.

A window was then created for the user to set and trigger the inspection system – Fig. 5.13. In this window the user can define the mesh spacing and possible post processing algorithms to be applied. The folders to save data in the different steps of the data post processing procedure are established by the user, including the folder where the final results will be saved.

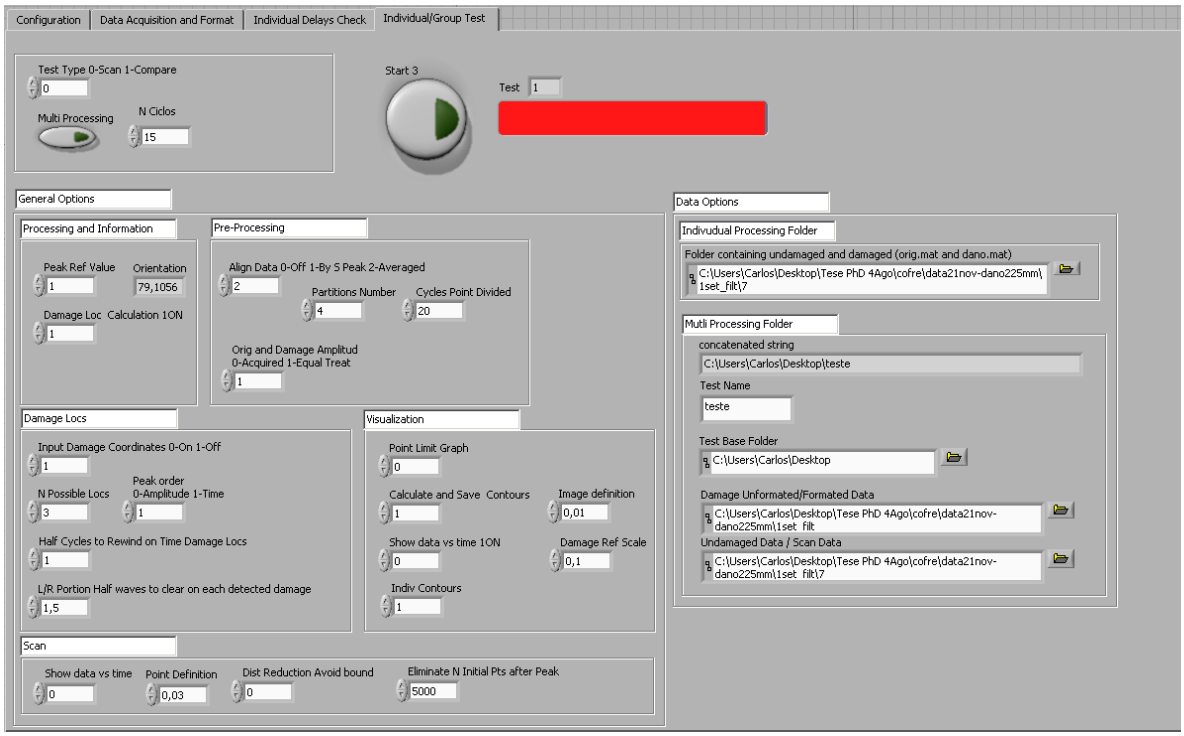

Figure 5.13: Phased array damage location window.

A typical results window from the code is shown in Fig. 5.14. In this plot the superimposed solution (tomography based) is presented to the user – as the plot of the resultant, final matrix described and obtained through the method explained in the end of section 5.1. In this particular case an existing through the thickness circular hole of 0.5mm in diameter was enlarged to 1mm in diameter (in the position in the plate presented as dark red in the plot). In these plots the most probable region where damage exists appears in dark red and the lowest probable areas in dark blue, passing by light red, orange, yellow, green and light blue. This result is presented to prove the capability of the system to monitor damage growth (in steps inferior to 1mm), since the baseline used, i.e., the reference health condition of the plate considered for comparison/subtraction was for an existing damage of 0.5mm, then enlarged by another 0.5mm.

In Fig. 5.14, it is also presented the results given by the code – obtained from the values of the final matrix -, representing the six areas with highest probability of damage existence (normalized to one, by the damage index/probability of the most probable area). In these results, the coordinate system's origin is positioned in the center of the phased array, with the X axis being parallel to the array direction (pointing to the right side in the figure) and the Y axis being perpendicular to the array (pointing upwards).

In this plot, the remaining colors represent the consideration by the system of false positives, due to noise (interfering more, usually, with boundary and other damage reflections), and also due to the intrinsic and inevitable generation of other waves (with smaller amplitude) than the wavefront and corresponding generated reflections in the damage (where mode conversion could also happen). Those additional waves/wavefronts include S_0 wavefronts of smaller amplitude, with relation to the main wavefront (being generated and propagating before and after such wavefront, due to the actuation signal morphology), with the same propagation direction and velocity; and include also A_0 waves and wavefronts (different mode - first anti-symmetric Lamb wave mode), propagating with different velocities and then in different directions than the S_0 wavefronts. The existence of other S_0 waves/wavefronts (propagating just before and after the main wavefront) and corresponding damage reflections will be responsible for the determination of different ToFs and then for shifting the determined damage position along the inspection direction. The existing A_0 waves/wavefronts (propagating in

different directions and with different propagation velocities) will be responsible for the determination of damage positions in directions apart from the inspection direction.

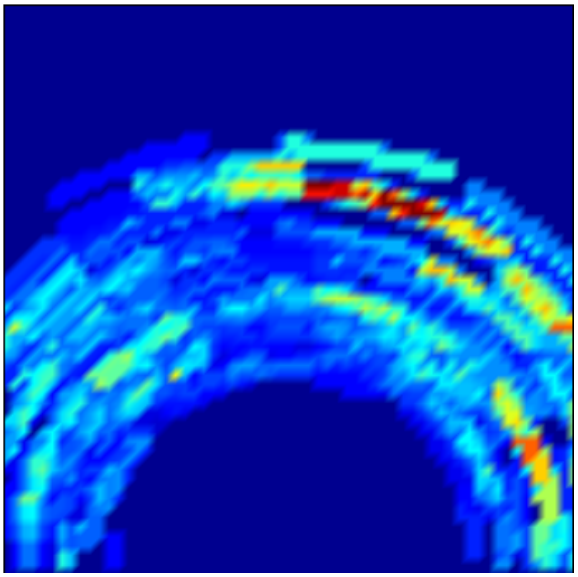

X (m)	Y (m)	Probability
0.26	1.05	1
0.22	1.07	0.82
0.625	0.3	0.6
0.72	0.72	0.55
0.55	0.9	0.5
0.5	0.8	0.45

Figure 5.14: Damage location contour output.

Chapter 6

Conclusions

During this work a linear phased array for damage detection in plate like or shell like structures was developed. The implemented phased array was based on disc shaped PZT transducers for the excitation of Lamb waves. Specifically, this SHM system was based on the first symmetric mode (S_0) of Lamb waves. The most important advantages and simultaneously the main difficulties in the application of the S_0 mode that were surpassed with this work are related with its high propagation velocity. The advantages are that, with the application of this wave mode and its high propagation velocity, this wave and its reflection suffer a small interference from lower propagating waves (modes). Furthermore, due to their deformation pattern they are more prone to detect any types of damage in the components, being easier to deal with, while presenting small amplitude propagation damping. Regarding obstacles that were overcome, due to such high propagation velocity, difficulties emerge in the generation of wavefronts resulting from the constructive interference of waves generated by the single actuators in the array and particularly in the precise establishment of the small time delays required for the phased actuation. One other difficulty is related with the small amplitude of damage reflected waves. This negative aspect is diminished by the use of the phased array and beamforming, increasing the amplitude of actuation and then the amplitude and SNR of reflections. Furthermore, with the application of a phased array, an entire component can be inspected by performing several scans in which the inspection direction is defined and changed from scan to scan. In this manner the inspection region is delimited for each scan, resulting in an intensification of inspection effort in such a region, decreasing simultaneously the complexity and increasing the precision of the inspection process. Also in the actuation of Lamb waves, their dispersive behaviour, i.e., the dependency of their propagation velocity to their frequency, must be accounted for. This means that the

actuation signal waveform must excite one single frequency, to obtain a wave with a particular frequency, propagating with a unique velocity.

To achieve the final objective of developing such a phased array SHM system, conventional NDT&E ultrasound systems were studied and the need for their replacement and implementation of SHM to aircraft structures was established. With the requirements established for such an SHM system, techniques under research were briefly referred. Afterwards, Lamb waves propagation behaviour was derived and carefully analyzed. With the obtained dispersion curves and tuning the system for the excitation of S_0 wavefronts, actuation frequency and actuation signal, the propagation velocity for the S_0 Lamb waves (and wavefront) and the dimensions of the PZT transducers to be used were determined for a representative aluminum plate, 2mm thick.

A dedicated actuation system, required for the phased generation of the waves and wavefront was developed. This system is based on a master MCU circuit, controlling the phased activation of slave channels. The master MCU has programmed the time delays to be applied for the phased activation for each and all scan (directions) to be implemented. Furthermore, in that code the number of scans and scan repetitions are also determined. The slave circuits/channels, connected to each PZT in the array, generate the correct actuation signal waveform. In these circuits, an output switch was applied to match the impedance of actuation and acquisition systems, what is a usual problem in the current existing systems. With the use of such switch, measured wave amplitudes were increased significantly.

The final actuation system was tested. The correct determined inspection directions and the array aperture were verified. The actuation system presented errors inferior to 6% and 3%, respectively in the relative amplitude and time (and frequency) of excited waves and wavefront generation.

Finally, experiments were performed with the application of the phased array SHM system. An aluminum plate 1.5m x 1.5m x 2mm was used, as representative of most aircraft structural components – since these can be divide in the majority of cases into plate like or low curvature like shells. The plate was subject to different boundary conditions ranging from totally supported (to increase Lamb waves propagation

damping), to simply supported and riveted in the boundaries. The experiments were conducted firstly in a laboratory setting and afterwards in an aircraft maintenance hangar, with no surrounding noise control and limited temperature control.

Experiments were performed with the introduction (cumulatively) of surface and through the thickness circular holes and cuts (with different orientations), with a maximum dimension of 1mm, to simulate damage. The simulated damages were successfully detected. The only exceptions were damages created behind other damages previously introduced, i.e., in the same radial direction, with relation to the phased array (originating in the phased array). To refer also that cuts aligned with wavefront propagation directions were more difficult to detect, since their thickness was inferior to 1mm.

For the experimental setup, a NI acquisition equipment was used, particularly a NI PXI-5105, 8 channels with simultaneous sampling oscilloscope, and a LABVIEW® code (with embedded MATLAB® codes) was developed to implement the interface for the SHM system and the damage detection process. This code performs signal processing and applies the developed damage detection algorithms in an automatic manner.

6.1 - Future Work

Some of the future work being considered can be summarized in the following points:

- application of transducers in the opposite face of the plate with relation to the implemented phased array, to enhance the selective excitation of the Lamb wave modes and wavefronts. If the transducers are actuated in phase with the phased array, the S_0 mode will be enhanced, while if excited in opposite phase, the A_0 mode will be enhanced;
- execute experiments for damage detection and location with the introduction of riveted stringers in the plate. These experiments will be focused in the verification of the capabilities of the phased array SHM system to detect and locate damage beyond such structural reinforcements and rivet lines, with relation to the phased array position – this is an interesting aspect to consider, since the rivets and structural

reinforcements existing in typical aircraft structures will introduce damping and will scatter the waves, introducing considerable reflections in the wave propagation pattern;

- verify damage detection capabilities of the current system to detect and locate damages initiating in rivets and in between rivet lines, and connecting rivets;
- consider different array configurations, such as stars, crosses and circular arrays, and the application of curved, focusing wavefronts after the determination of damage location through the use of linear wavefronts. The curved wavefronts would then be focused in such region, further increasing their amplitude;
- develop dedicated data acquisition boards and wireless systems;
- perform experiments in orthotropic (composite) materials, considering that the properties of these materials and consequently the propagation velocities are dependent on the direction considered;
- apply a mixed phased array and network SHM system;
- integrate the PZT phased array with FBG networks – particularly interesting for the application to composite materials, since FBGs can be easily embedded during the manufacturing process of those materials, while presenting an extremely small weight, what is important for the application to aircraft;
- integrate this system with other SHM techniques, such as low frequency or vibration based SHM methods, enabling damage detection in structural elements such as stringers and other structural reinforcements;
- perform tests in real aircraft structures in operation;
- investigate the possibility to create smart rivets, by integrating active PZT elements with such connecting elements, reducing weight, the number of transducers required, protecting the transducer and increasing the transducer life through such integration, while facilitating their replacement and access to them;

- implement Neural Networks to learn with the present system and to apply, in the future, the damage detection and location method, in an effort to decrease the computational time and to increase the precision of the SHM system;
- implement algorithms to characterize damage after damage location – to determine damage dimensions, shape and orientation, enabling the application of Damage Prognosis (calculating damage growth/propagation rate) to determine the Remaining Useful Life (RUL) of the component for a certain, typical load spectrum.

Bibliography

[1] National Transportation Safety Board, "Aircraft Accident Report: Aloha Airlines, Flight 243, Boeing 737-200, N73711, near Maui, Hawaii, April 28, 1988", NTSB/AAR-89/03, Washington, DC, USA, 1989.

[2] http://aviation-safety.net/database/record.php?id=19850812-1, last accessed on August, 30th, 2010.

[3] http://www.ntsb.gov/pressrel/2002/020924.htm, last accessed on August, 30th, 2010.

[4] Rocha, B., Silva, C. and Suleman, A., "Structural Health Monitoring System using PZT Networks with Tuned Lamb Waves", Journal of Shock and Vibration, Vol. 17, pp. 1 - 19, 2010.

[5] Silva, C., "Lamb Wave Based Structural Health Monitoring of Aircraft Structures", Ph.D. Thesis, Department of Mechanical Engineering, University of Victoria, 2010.

[6] http://www.dot.state.mn.us/i35wbridge/, last accessed on August, 30th, 2010.

[7] http://www.century-of-flight.net/Aviation%20history/coming%20of%20age/De%20Havilland%20Comet.htm, last accessed on August, 30th, 2010.

[8] DOD (U.S.A. Department of Defence), "Airplane Damage Tolerance Requirements", MIL-A-83444, Washington D.C., USA, 1987.

[9] http://www.justnews.com/news/22476154/detail.html, last accessed on April, 24th, 2010.

[10] http://www.aviationtoday.com/regions/usa/Boeing-757-In-flight-Wing-Panel-Loss-Due-to-Metal-Fatigue_21670.html, last accessed on April, 24th, 2010.

[11] Walter, P., "The FAA's Aging Aircraft Non-Destructive Inspection Validation Center at Sandia National Laboratories: An Introduction", Materials Evaluation, Vol. 53 (7), pp. 799 – 802, 1995.

[12] http://www.bloomberg.com/apps/news?pid=20601081&sid=aos7pGU3n0B8, last accessed on August, 30th, 2010.

[13] Aging of U.S. Air Force Aircraft: Final Report, Committee on Aging of U.S. Air Force Aircraft, Commission on Engineering and Technical Systems, National Research Council, 2007.

[14] http://integrator.hanscom.af.mil/2007/March/03082007/03082007-14.htm, last accessed on August, 30th, 2010.

[15] http://www.lockheedmartin.com/news/press_releases/2007/1017ae_accademonstration.html, last accessed on August, 30th, 2010.

[16] Domke, B., "B787 Lessons Learnt", internal Airbus presentation, 2008.

[17] http://www.midas-ndt.co.uk/tt1.html, last accessed on August, 30th, 2010.

[18] Winfree, W. P., "New Non-Destructive Techniques for Inspection of Aircraft Structures", SPIE Proceedings, Vol. 2945, pp. 2 – 13, 1996.

[19] Rempt, R. D. and Broz, A., *NDE of Aging Aircraft, Airports and Aerospace Hardware*, Society of Photo-Optical Instrumentation Engineers Ed., Bellingham, Washington, USA, 1996.

[20] Achenbach, J.D., "Quantitative Non-Destructive Evaluation", International Journal of Solids and Structures, Vol. 37, pp. 13 – 27, 2000.

[21] Bical, D., "NDT Procedures Qualification Process", ATA NDT forum, Hartford, UK, 1995.

[22] Cheeke, J. D. N., *Fundamentals and Applications of Ultrasonic Waves*, CRC Press, Boca Raton, 2002.

[23] Kolsky, H., *Stress Waves in Solids*, Dover, New York, USA, 1963.

[24] Graff, K., *Wave Motion in Elastic Solids*, Ohio State University Press, Columbus, Ohio, 1975, reprinted by Dover Publications, New York, USA, 1991.

[25] ASME Boiler and Pressure Vessel Code, Section V, Non-Destructive Examination, "Ultrasonic Examination Methods for In-Service Inspection", Articles 4 and 5, pp. 77-137, Jul. 1995.

[26] Adler, L., Cook, K. V. and Simpson, W. A., "Ultrasonic Frequency Analysis", Chapter 1, *Research Techniques in Nondestructive Testing*, Vol. III, R. S. Sharpe, Academic Press Ed., London, UK, 1980.

[27] Silk, M. G., *Ultrasonic Transducers for Nondestructive Testing*, Adam Hilger Ltd., Bristol, UK, 1984.

[28] Shaikh, N., "Transducer and Techniques for Ultrasonic Non-Destructive Evaluation of Structural Plates", *Review in Progress in Quantitative Non-Destructive Evaluation*, Vol. 11, D. O. Thompson and D. E. Chimenti, Plenum Press Ed., pp. 1831 – 1835, New York, USA, 1992.

[29] http://www.olympus-ims.com/en/applications-and-solutions/introductory-ultrasonics/introduction-flaw-detection/, last accessed on August, 30th, 2010.

[30] Wurstenberg, H., Rotter, B., Klanke, H. and Harbecke, D., "Ultrasonic Phased Arrays for Non-Destructive Inspection", Materials Evaluation, Vol. 51 (7), pp. 669 – 671, Jun. 1993.

[31] Posakony, G. J., "Influence of the Pulser on the Ultrasonic Spectrum: The Results of an Experiment", Materials Evaluation, Vol. 43 (4), pp. 413 – 419, March 1985.

[32] Washington, A. B. G., "The Design of Ultrasonic Probes", British Journal of NDT, Vol. 3 (3), pp. 56 – 63, Sept. 1961.

[33] Silk, M. G. and Lidington, B. H., "A Preliminary Study of the Effect of Defect Shape and Roughness on Ultrasonic Size Estimation", Non-Destructive Testing, Vol. 8 (1), pp. 27 – 31, Feb. 1975.

[34] Silk, M. G., "Sizing Crack-like Defects by Ultrasonic Means", Chapter 2, *Research Techniques in Non-Destructive Testing*, R. S. Sharpe, Academic Press Ed., London, UK, 1977.

[35] Thompson, R. B., "Application of Elastic Wave Scattering Theory to the Detection and Characterization of Flaws in Structural Materials", Wave Propagation in Inhomogeneous Media and Ultrasonic Non-Destructive Evaluation, AMD-Vol. 62, pp. 61 – 73, ASME – American Society of Mechanical Engineers, New York, USA, 1984.

[36] Song, S. J. and Schmeer, L., "An Ultrasonic Time-of-Flight Equivalent Flaw Sizing Method", Research in Non-Destructive Evaluation, Vol. 4, pp. 1 – 18, 1992.

[37] Williams, S. and Mudge, P. J., "Statistical Aspects of Defect Evaluation using Ultrasonics", NDT International, Vol. 18 (3), pp. 123 – 131, 1985.

[38] Serabian, S., "Frequency and Grain Size Dependence of Ultrasonic Attenuation in Polycrystalline Materials", British Journal of Non-Destructive Testing, Vol. 22 (2), pp. 69 – 77, March 1980.

[39] Farrar, C. R., Lieven, N. A. J. and Bement, M. T., "An Introduction to Damage Prognosis", Inman, D. J., Farrar, C. R., Lopes Jr., V., Steffen Jr., V., *Damage Prognosis for Aerospace, Civil and Mechanical Systems*, Chapter 1, pp. 1 – 12, John Wiley & Sons Ed., Chichester, USA, 2005.

[40] Montalvão, D., Maia, N. M. M. and Ribeiro, A. M. R., "A Review of Vibration-Based Structural Health Monitoring with Special Emphasis on Composite Materials", The Shock and Vibration Digest, Vol. 38 (4), pp. 295 – 324, 2006.

[41] Rocha, B., Silva, C. P. and Suleman, A., "Vibration-Based Health Monitoring of Aircraft Structures", 3rd European Workshop on Structural Health Monitoring, Granada, Spain, 2006.

[42] Fritzen, C. P., "Vibration-Based Structural Health Monitoring – Concepts and Applications", Proceedings of VI DAMAS - Damage Assessment of Structures, 2005.

[43] Park, G., Sohn, H., Farrar, C. R. and Inman, D. J., "Overview of Piezoelectric Impedance-Based Health Monitoring and Path Forward", The Shock and Vibration Digest, Vol. 35 (6), pp. 451 – 463, 2003.

[44] Peairs, D. M., Park, G. and Inman, D. J., "Improving Accessibility of the Impedance-Based Structural Health Monitoring Method", Journal of Intelligent Material Systems and Structures, Vol. 15 (2), pp. 129 – 140, 2004.

[45] Spanos, P. D., Failla, G., Santini, A. and Pappatico, M., "Damage Detection in Euler-Bernoulli Beams via Spatial Wavelet Analysis", Structural Control & Health Monitoring, Vol. 13 (1), pp. 472 – 487, Jan. – Feb. 2006.

[46] Miller, R. K. and McIntire, P., *Non-Destructive Testing Handbook*, Vol. 5, *Acoustic Emission Testing*, American Society for Non-Destructive Testing, Columbus, Ohio, USA, 1987.

[47] Pollock, A. A., "Acoustic Emission Inspection", Metals Handbook, 9th Ed., Vol. 17, ASM International, pp. 278 – 294, 1989.

[48] Gorman, M., "Plate Wave Acoustic Emission", Journal of the Acoustic Society of America, Vol. 90 (1), pp. 358 – 364, Jul. 1991.

[49] Ziola, S. and Gorman, M., "Source Location in Thin Plates using Cross Correlation", Journal of the Acoustic Society of America, Vol. 90 (5), pp. 2551 – 2556, Nov. 1991.

[50] Pullin, R., Holford, K. M. and Baxter, M. G., "Modal Analysis of Acoustic Emission Signals from Artificial and Fatigue Crack Sources in Aerospace Grade Steel", Proceedings of VI DAMAS – Damage Assessment of Structures, 2005.

[51] Hock, V., McInerney, M., Morefield, S., Majumdar, A. and Carlyle, J., "Investigating Fundamental Mechanics of Microcracks in Concrete using Acoustic Signature Modelling", Proceedings of VI DAMAS – Damage Assessment of Structures, 2005.

[52] Luo, Y., Zhao, G. Q., Gu, J. Z., Zhu, J. G., Gong, R. R. and Liu, Z. T., "New Method of Planar Location of Acoustic Emission Source and its Application", Structural Health Monitoring, pp. 953 - 960, 2005.

[53] ASME Boiler & Pressure Vessel Code, Section V, Non-Destructive Examination, *Acoustic Emission Examination for Metallic Vessels During Pressure Testing*, Article 12, pp. 233 – 250, 1995.

[54] ASME Boiler & Pressure Vessel Code, Section V, Non-Destructive Examination, *Continuous Acoustic Emission Monitoring*, Article 13, pp. 251 – 271, 1995.

[55] ASME Boiler & Pressure Vessel Code, Section V, Non-Destructive Examination, *Acoustic Emission Examination for Fiber-Reinforced Plastic Vessels*, Article 11, pp. 207 – 232, 1995.

[56] Raghavan, A. and Cesnik, C. E. S., "Review of Guided-Wave Structural Health Monitoring", The Shock and Vibration Digest, Vol. 39 (2), pp. 91 – 114, 2007.

[57] Ye, L. and Su, Z., "Identification of Damage Using Lamb Waves", Lecture Notes in Applied and Computational Mechanics, Vol. 48, pp. 4 - 5, Springer Ed., 2009.

[58] Rayleigh, J. W. S.., "On Waves Propagated Along the Plane Surfaces of an Elastic Solid", Proceedings of the London Mathematical Society, London, UK, 1885.

[59] Lamb, H., "On Waves in an Elastic Plate", Proceedings of the Royal Society, Mathematical, Physical and Engineering Sciences, Vol. 93, pp. 114 – 128, 1917.

[60] Mindlin, R. D., "Waves and Vibrations in Isotropic, Elastic Plates", Structural Mechanics, pp. 199 – 232, 1960.

[61] Worlton, D. C., "Experimental Confirmation of Lamb Waves at Megacycle Frequencies", Journal of Applied Physics, Vol. 32, pp. 967 – 971, 1961.

[62] Frederick, C. L. and Worlton, D. C., "Ultrasonic Thickness Measurements with Lamb Waves", Journal of Non-Destructive Test, Vol. 20, pp. 51 – 55, 1962.

[63] Rose, J. L., "A Vision of Ultrasonic Guided Wave Inspection Potential", Proceedings of the 7th ASME NDE Topical Conference, NDE, Vol. 20, pp. 1 – 5, 2001.

[64] Dalton, R. P., Cawley, P. and Lowe, M. J., "The Potential of Guided Waves for Monitoring Large Areas of Metallic Aircraft Fuselage Structures", Journal of Non-Destructive Evaluation, Vol. 20 (1), 2001.

[65] Giurgiutiu, V. and Bao, J., "Embedded Ultrasonic Structural Radar with Piezoelectric Wafer Active Sensors for the NDE of Thin-Wall Structures", ASME International Mechanical Engineering Congress, New Orleans, USA, 2002.

[66] Rose, J. L., "Ultrasonic Waves in Solid Media", Cambridge University Press, New York, USA, 1999.

[67] Viktorov, I. A., "Rayleigh and Lamb Waves: Physical Theory and Applications", Plenum Press, New York, USA, 1967.

[68] Lee, B. C. and Staszewski, W. J., "Modelling of Lamb waves for Damage Detection in Metallic Structures: Part I - Wave Propagation", Smart Materials and Structures, Vol.12, pp. 804 – 814, 2003.

[69] Apetre, N., Ruzzene, M., Hanagud, S. and Gopalakrishman, S., "Nonlinear Spectral Methods for the Analysis of Wave Propagation", 49th AIAA/ASME/ASCE/AHS/ASC Structures, Structural Dynamics, and Materials, Schaumburg-IL, USA, 2008.

[70] Galan, J. M. and Abascal, R., "Boundary Element Solution for the Bidimensional Scattering of Guided Waves in Laminated Plates", Computers & Structures, Vol. 83 (10-11), pp. 740 - 757, 2005.

[71] Ostachowicz, W. M., "Damage Detection of Structures Using Spectral Finite Element Method", Computers and Structures, Vol. 86, pp. 454 – 462, 2008.

[72] Blaise, E. and Chang, F. K., "Built-in Diagnostic for Debonding in Sandwich Structures Under Extreme Temperature - II", Chang, F. K. (ed.), Proceedings of the 3rd International Workshop on Structural Health Monitoring, Stanford, CA, USA, September 12-14, 2001, pp. 154–163, CRC Press, Boca Raton, 2001

[73] Blaise, E. and Chang, F. K., "Built-in Damage Detection System for Sandwich Structures Under Cryogenic Temperatures", Proceedings of the SPIE, Vol. 4701, pp. 97–107, 2002.

[74] Konstantinidis, G., Drinkwater, B. W. and Wilcox, P. D., "The Temperature Stability of Guided Wave Structural Health Monitoring Systems", Smart Materials and Structures, Vol. 15, pp. 967 – 976, 2006.

[75] Nguyen, C. H., Pietrzko, S. and Buetikofer, R., "The Influence of Temperature and Bonding Thickness on the Actuation of a Cantilever Beam by PZT Patches", Smart Materials and Structures, Vol. 13, pp. 851 – 860, 2004.

[76] Zhao, X., Gao, H., Zhang, G., Ayhan, B., Yan, F., Kwan, C. and Rose, J.L., "Active Health Monitoring of an Aircraft Wing with Embedded Piezoelectric Sensor/Actuator Network: I. Defect Detection, Localization and Growth Monitoring", Smart Materials and Structures, Vol. 16, pp. 1208 – 1217, 2007.

[77] Monnier, T., "Lamb Wave-Based Impact Damage Monitoring of a Stiffened Aircraft Panel Using Piezoelectric Ttransducers", Journal of Intelligent Material Systems and Structures, Vol. 17, pp. 411 – 421, 2006.

[78] Lu, Y., Ye, L., Su, Z. and Huang, N., "Quantitative Evaluation of Crack Orientation in Aluminum Plates Based on Lamb Waves", Smart Materials and Structures, Vol. 16, pp. 1907 – 1914, 2007.

[79] Jin, J., Quek, S. T. and Wang, Q., “Design of Interdigital Transducers for Crack Detection in Plates”, Ultrasonics, Vol. 43, pp. 481 – 493, 2005.

[80] CeramTec AG Catalog - MF080007/D/GB/ 2.000/0807/echolot (3570)

[81] Bottai, G., Pollock, P. J., Behling, T. A., Giurgiutiu, V., Bland, S. M. and Joshi, S. P., “Damage Detection in Cryogenic Composites for Space Applications Using Piezoelectric Wafer Active Sensors”, 49th AIAA/ASME/ASCE/AHS/ASC Structures, Structural Dynamics, and Materials, Schaumburg-IL, USA, 2008.

[82] Giurgiutiu, V., Bao, J. and Zhao, W., “Piezoelectric Wafer Active Sensor Embedded Ultrasonics in Beams and Plates”, Experimental Mechanics, Vol. 43 (4), pp. 428 – 449, 2003.

[83] Worden, K. and Dulieu-Barton, J. M., "An Overview of Intelligent Fault Detection in Systems and Structures", Structural Health Monitoring, Vol. 3 (1), pp. 85 - 98, 2004.

[84] Nieuwenhuis, J. H., Neumann, J. J., Greve, D. W. and Oppenheim, I. J, "Generation and Detection of Guided Waves Using PZT Wafer Transducers", IEEE Ultrasonics, Ferroelectrics, and Frequency Control Society, Vol. 5 (11), pp. 2103 – 2111, 2005.

[85] Giurgiutiu, V., “Tuned Lamb Wave Excitation and Detection with Piezoelectric Wafer Active Sensors for Structural Health Monitoring”, Journal of Intelligent Material Systems and Structures, Vol. 16, pp. 291 - 305, 2005.

[86] Quek, S. T., Tua, P. S. and Jin, J., “Comparison of Plain Piezoceramics and Inter-Digital Transducer for Crack Detection in Plates”, Journal of Intelligent Material Systems and Structures, Vol. 18, pp. 949 – 961, 2007.

[87] Rogers, A., “Distributed Optical-Fibre Sensing”, Measurement Science and Technology, Vol. 10, pp. 75 – 99, 1999.

[88] Cheng, L. K., "High-speed Dense Channel Fiber Bragg Grating Sensor Array For Structural Health Monitoring", Proceedings of the International Conference on MEMS, NANO and Smart Systems, pp. 364 - 365, Banff, Alberta, Canada, July 2005.

[89] Betz, D. C., Thursby, G., Culshaw, B. and Staszewski, W. J., “Structural Damage Location with Fiber Bragg Grating Rosettes and Lamb Waves”, Structural Health Monitoring: An International Journal, Vol. 6 (4), pp. 299 – 308, 2007.

[90] Hongo, A., Kojima, S. and Komatsuzaki, S., “Applications of Fiber Bragg Grating Sensors and High-Speed Interrogation Techniques”, Structural Control and Health Monitoring, Vol. 12, pp. 269 – 282, 2005.

[91] Frieden, J., Cugnoni, J., Botsis, J., Gmür, T. and Coric, D., “High-Speed Internal Strain Measurements in Composite Structures Under Dynamic Load Using Embedded FBG Sensors”, Composite Structures, Vol. 92 (8), pp. 1905 – 1912, 2010.

[92] Majumder, M., Gangopadhyay, T. K., Chakraborty, A. K., Dasgupta, K. and Bhattacharya, D. K., “Fibre Bragg Gratings in Structural Health Monitoring — Present Status and Applications”, Sensors and Actuators, Vol. A147, pp. 150 – 164, 2008.

[93] Takeda, N., Okabe, Y., Kuwahara, J., Kojima, S. and Ogisu, T., "Development of Smart Composite Structures with Small-Diameter Fiber Bragg Grating Sensors for Damage Detection: Quantitative Evaluation of Delamination Length in CFRP Laminates Using Lamb Wave Sensing", Composites Science and Technology, Vol. 65, pp. 2575 – 2587, 2005.

[94] Lam, P-M., Lau, K-T., Ling, H-Y., Su, Z. and Tam, H-Y., "Acousto-Ultrasonic Sensing for Delaminated GFRP Composites Using an Embedded FBG Sensor", Optics and Lasers in Engineering, Vol. 47, pp. 1049 – 1055, 2009.

[95] Li, F., Murayama, H., Kageyama, K. and Shira, T., "Guided Wave and Damage Detection in Composite Laminates Using Different Fiber Optic Sensors", Sensors, Vol. 9, pp. 4005 – 4021, 2009.

[96] Kwun, H., Light, G. M., Kim, S. Y. and Spinks, R. L., "Magnetostrictive Sensor for Active Health Monitoring in Structures", Proceedings of the SPIE, Vol. 4702, pp. 282 – 288, 2002.

[97] Varadan, V. K., "Nanotechnology, MEMS and NEMS and Their Applications to Smart Systems and Devices", Proceedings of the SPIE, Vol. 5062, pp. 20 – 43, 2003.

[98] Neumann, J. J., Greve, D. W., Oppenheim, I.J., "Comparison of Piezoresistive and Capacitive Ultrasonic Transducers", Proceedings of the SPIE, Vol. 5391, pp. 230 – 238, 2004.

[99] Giurgiutiu, V. and Cuc, A., "Embedded Non-Destructive Evaluation for Structural Health Monitoring, Damage Detection, and Failure Prevention", The Shock and Vibration Digest, Vol. 37 (2), pp. 83 – 105, 2005.

[100] Wang, L. and Yuan, F.G., "Group Velocity and Characteristic Wave Curves of Lamb Waves in Composites: Modelling and Experiments", Composites Science and Technology, Vol. 67, pp. 1370 – 1384, 2007.

[101] Rose, J. L., Pilarski, A. and Ditri, J. J., "An Approach to Guided Wave Mode Selection for Inspection of Laminated Plate", Journal of Reinforced Plastics and Composites, Vol.12, pp. 536 – 544, 1993.

[102] Su, Z. and Ye, L., "Selective Generation of Lamb Wave Modes and Their Propagation Characteristics in Defective Composite Laminates", Proceedings of the Institution of Mechanical Engineers, Part L - Journal of Materials: Design and Applications, Vol.218, pp. 95 – 110, 2004.

[103] Wilcox, P. D., Lowe, M. J. S. and Cawley, P., "Mode and Transducer Selection for Long Range Lamb Wave Inspection", Journal of Intelligent Material Systems and Structures, Vol. 12 (8), pp. 553 - 565, 2001.

[104] Chakrabarty, K., Iyengar, S. S., Ai, H. and Cho, E., "Grid Coverage for Surveillance and Target Location in Distributed Sensor Networks", IEEE Transactions on Computers, Vol. 51, pp. 1448 – 1453, 2002.

[105] Staszewski, W. J. and Worden, K., "Overview of Optimal Sensor Location Methods for Damage Detection", Rao, V.S. (ed.), Proceedings of the 8th SPIE Symposium on Smart Structures and Materials (Conference on Modelling, Signal Processing and Control of Smart Structures), Vol. 4326, pp. 179 – 187, Newport Beach, CA, USA, 2001.

[106] http://www.accellent.com/engineering_tools/measurement_tools.shtml, last accessed on August, 30th, 2010.

[107] http://sine.ni.com/nips/cds/view/p/lang/en/nid/208649, last accessed on August, 30th, 2010.

[108] Bao, J., "Lamb Wave Generation and Detection with Piezoelectric Wafer Active Sensors", Ph.D. Thesis, College of Engineering and Information Technology, University of South Carolina, 2003.

[109] Purekar, A. S., "Piezoelectric Phased Array Acousto-Ultrasonic Interrogation of Damage in Thin Plates", Ph.D. Thesis, University of Maryland, College Park, 2006.

[110] Pena J., Perez C., Martinez-Onab R., Gomez-Ullatec Y., Espinosa F., and Kawiecki G., "Phased Array Transducers for Damage Detection in Aircraft Structures ", SPIE, 2005.

[111] Malinowski, P., Wandowski, T., Trendafilova, I. and Ostachowicz, W., "A Phased Array-Based Method for Damage Detection and Localization in Thin Plates", Structural Health Monitoring, Vol. 31, pp. 611 – 628, 2009.

[112] Salas, K. I. and Cesnik, C. E. S., "Guided Wave Experimentation Using CLoVER Transducers for Structural Health Monitoring", 49th AIAA/ASME/ASCE/AHS/ASC Structures, Structural Dynamics, and Materials, Schaumburg-IL, USA, 2008.

[113] Michaels, J. E. and Michaels, T.E., "Guided Wave Signal Processing and Image Fusion for In Situ Damage Localization in Plates", Wave Motion, Vol. 44, pp. 482 – 492, 2007.

[114] Sedlak, P., Hirose, Y., Khan, S. A., Enoki, M. and Sikula, J., "New Automatic Localization Technique of Acoustic Emission Signals in Thin Metal Plates", Ultrasonics, Vol. 49, pp. 254 – 262, 2009.

[115] Sohn, H., Park, H. W., Law, K. H. and Farrar, C.R., "Combination of a Time Reversal Process and a Consecutive Outlier Analysis for Baseline-Free Damage Diagnosis", Journal of Intelligent Material Systems and Structures, Vol. 18, pp. 335 – 346, 2007.

[116] Xu, B. and Giurgiutiu, V., "Single Mode Tuning Effects on Lamb Wave Time Reversal with Piezoelectric Wafer Active Sensors for Structural Health Monitoring", Journal of Non-Destructive Evaluation, Vol. 26, pp. 123 – 134, 2007.

[117] Gomez-Ullate, Y., Espinosa, F., Reynolds, P. and Mould, J., "Selective Excitation of Lamb Wave Modes in Thin Aluminium Plates using Bonded Piezoceramics: FEM Modelling and Measurements", Poster 205, ECNDT, 2006.

[118] Gao, W., Glorieux, C. and Thoen, J., "Laser Ultrasonic Study of Lamb Waves: Determination of the Thickness and Velocities on a Thin Plate", International Journal of Engineering Science, Vol. 41, pp. 219 – 228, 2003.

[119] Paget, C. A., Grondel, S., Levin, K. and Delebarre, C., "Damage Assessment in Composites by Lamb Waves and Wavelet Coefficients", Smart Materials and Structures, Vol. 12, pp. 393 – 402, 2003.

[120] Yuan, S., Liang, D., Shi, L., Zhao, X., Wu, J., Li, G. and Qiu, L., "Recent Pogress on Distributed Structural Health Monitoring Research at NUAA", Journal of Intelligent Material Systems and Structures, Vol. 19, pp. 373 – 386, 2008.

[121] Rizzo, P. and di Scalea, F.L., "Feature Extraction for Defect Detection in Strands by Guided Ultrasonic Waves", Structural Health Monitoring: An International Journal, Vol. 5 (3), pp. 297 – 308, 2006.

[122] Chang, F. K., Markmiller, F. C., Ihn, J. B. and Cheng, K.Y., "A Potential Link from Damage Diagnostics to Health Prognostics of Composites Through Built-in Sensors", Journal of Vibration and Acoustics, Vol. 129, pp. 718 - 729, 2007.

[123] Garg, A. K., Mahapatra, D. R., Suresh, S., Gopalakrishnan, S. and Omkar, S. N., "Estimation of Composite Damage Model Parameters Using Spectral Finite Element and Neural Network", Composites Science and Technology, Vol. 64, pp. 2477 – 2493, 2004.

[124] Ihn, J. B. and Chang, F. K., "Pitch-Catch Active Sensing Methods in Structural Health Monitoring for Aircraft Structures", Structural Health Monitoring: An International Journal, Vol. 7 (1), pp. 5 – 19, 2008.

[125] Raghavan, A. and Cesnik, C. E. S., "Effects of Elevated Temperature on Guided-Wave Structural Health Monitoring", Journal of Intelligent Material Systems and Structures, Vol. 19, pp. 1383 – 1398, 2008.

[126] Wang, L. and Yuan, F.G., "Damage Identification in a Composite Plate Using Pre-Stack Reverse-Time Migration Technique", Journal of Intelligent Material Systems and Structures, Vol. 12, pp. 469 – 482, 2001.

[127] Yu, L., Santoni-Bottai, G., Xu, B., Liu, W. and Giurgiutiu, V., "Piezoelectric Wafer Active Sensors for In Situ Ultrasonic-Guided Wave SHM", Fatigue & Fracture of Engineering Materials & Structures, 2008.

[128] Quaegebeur, N., Micheau, P., Masson, P. and Maslouhi, A., "Structural Health Monitoring Strategy for Detection of Interlaminar Delamination in Composite Plates", Smart Materials and Structures, Vol. 19 (8), 2010.

[129] Masson, P. and Halkyard, C. R., "The Use of Time Domain Localized Structural Intensity for Damage Characterization", Smart Materials and Structures, Vol. 19 (3), 2010.

[130] Wang, D., Ye, L., Lu, Y. and Li, F., "A Damage Diagnostic Imaging Algorithm Based on the Quantitative Comparison of Lamb Wave Signals", Smart Materials and Structures, Vol. 19 (6), 2010.

[131] Sohn, H. and Lee, S. J., "Lamb Wave Tuning Curve Calibration for Surface-Bonded Piezoelectric Transducers", Smart Materials and Structures, Vol. 19 (1), 2010.

[132] Giurgiutiu, V., "Structural Health Monitoring with Piezoelectric Wafer Active Sensors", Elsevier Academic Press, Boston, USA, 2008.

[133] http://focus.ti.com/docs/prod/folders/print/msp430f2012.html, last accessed on August, 30th, 2010.

[134] http://focus.ti.com/docs/toolsw/folders/print/ez430-f2013.html, last accessed on August, 30th, 2010.

[135] http://focus.ti.com/docs/toolsw/folders/print/iar-kickstart.html, last accessed on August, 30th, 2010.

[136] http://www.national.com/mpf/LM/LM6172.html#Overview, last accessed on August, 30th, 2010.

[137] http://www.analog.com/en/other-products/analog-multipliersdividers/ad734/products/product.html, last accessed on August, 30th, 2010.

[138] http://www.analog.com/en/switchesmultiplexers/analog-switches/adg452/products/product.html, last accessed on August, 30th, 2010.